VNIVERSITAT DE VALÈNCIA

Facultad de Física
Departamento de Física Aplicada

Development of a polarimetric based optical biosensor using a free standing porous membrane

TESIS DOCTORAL

Presentada por:

Jesús Álvarez Álvarez

Dirigida por:

Daniel Hill
Juan P. Martínez Pastor

Valencia, Julio de 2013

Table of Contents

1. Introduction

Biosensors are analytical devices used for the detection of a biological analyte. They consist of a biological receptor molecule combined with a physical or physiochemical transduction mechanism [1]. The increase in the number of applications of these devices is leading to greater standardization of equipment, types of biomolecules and test processes. Current areas of application of biosensors include Point of Care Testing, Home Diagnostics, Environmental Monitoring, Process Industry and Security and Biodefense.

The evaluation of the performance of the biosensors relies on the following criteria: sensitivity, operational and linear concentration range, detection limits, selectivity, steady-state and transient response times, reproducibility, stability and long lifetime [2]. Other aspects such as cost of test, ease of use, time of analysis including all the steps required for sample preparation are also often taken into account.

One way to classify biosensors relates to their transduction mode, such as electrochemical, piezoelectric, optical or gravimetric transduction [3]. The most common are the first three (Fig. 1.1).

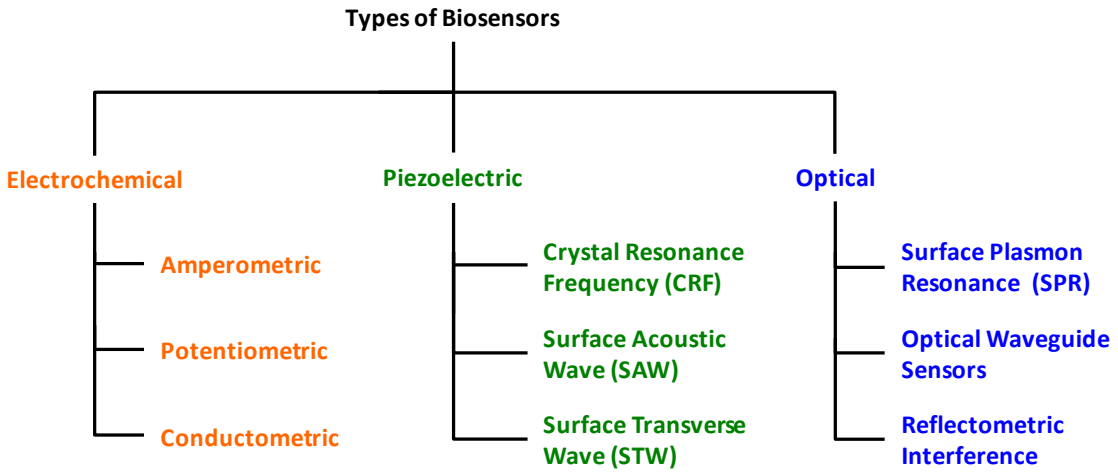

Figure 1.1 Different type of biosensors classified according to their transduction mechanism.

Electrochemical biosensors provide direct conversion of a biological recognition event to an electronic signal. Based on a bioelectrochemical receptor, which serves as the transduction element, the reaction under investigation either generates a measurable current (amperometric), a measurable potential (potentiometric) or a change in the conductive properties (conductometric) of the medium between the electrodes [4]:

- Amperometric devices are types of electrochemical sensors that continuously measure the current resulting from the oxidation or reduction of an electroactive species in a biochemical reaction [5, 6].
- Potentiometric devices measure the accumulation of a charge potential at the working electrode compared to the reference electrode in an electrochemical cell when zero or no significant current flows between them [7, 8].
- Conductometric devices measure the ability of an analyte (e.g. electrolyte solutions) or a medium (e.g. nanowires) to conduct an electrical current between electrodes or reference nodes. This approach directly monitors the changes in conductance of an electrode as a result of the immobilization of e.g. enzymes, complementary antibody-antigen pairs, etc. onto the electrode surface [9, 10].

Piezoelectric sensors are designed around the driving of piezoelectric crystals with an alternating potential so that they produce a standing wave at a characteristic frequency. This frequency is highly dependent on the elastic properties of the crystal, such that if a crystal is coated with a biological recognition element the binding of a target analyte to a receptor will produce a change in the resonance frequency, which gives a binding signal [11, 12].

Optical sensors are described in Section 1.1.

1.1 Optical Biosensors

Among the different types of biosensor technologies, optical biosensors offer several advantages over the others, since they are non-invasive/safe, label-free and can offer multi-dimensional and highly sensitive multiplexed detection. Label-free optical biosensors are based on measuring the refractive index of the surrounding media which is modified by the presence of the target analytes [13, 14]. With a proper design, label-free optical biosensor can combine a high sensitivity to changes in the refractive index of an outer medium with the possibility of being fabricated with nanometer to micron sized dimensions, which leads to an added advantage of a need for only small sample and reagent volumes, the latter generally forming a large proportion of an assay cost [15].

Different technologies of optical biosensing like surface plasmon resonance (SPR) [16, 17], optical waveguides [18] or thin-films [19] have been successfully incorporated in

lab-on-chip solutions becoming well established analysis methods in chemistry and biology.

1.1.1 Surface Plasmon Resonance (SPR)

Surface plasmon resonance is the technology that has found most commercial success being one of the most widely employed label-free techniques for the determination of many types of interactions [20, 21].

SPR biosensors are based on the detection of changes to the refractive index of an environment via the coupling of a light wave to the surface plasmons it excites (Fig. 1.2.a). A surface plasmon is an oscillation of free electrons that propagates along the surface of a conductor, typically a thin film of metal, such as silver or gold. In SPR both the wavelength and the angle of light at which coupling occurs are characteristic of the particular metal and the environment of its surface. The coupling is observed by measuring the amount of light reflected by the metal surface. All the light at most wavelengths is reflected, except at the resonant wavelength where almost all the light is absorbed (Fig. 1.2.b). Any change in the refractive index of the environment within the range of the plasmons field causes a change in the wavelength of the resonance wavelength.

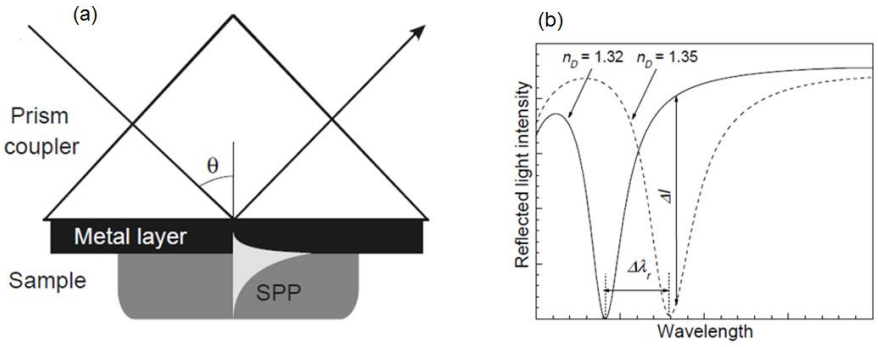

Figure 1.2 (a) Configuration based on a prism coupler to excite the surface plasmons. (b) Reflected light intensity as a function of wavelength for two refractive indices of the sample [22].

1.1.2 Localized Surface Plasmon Resonance (LSPR)

Localized surface plasmons are charge density oscillations confined in one or more dimensions and so found within metallic nanoparticles and metallic nanostructures. The excitation of these localized surface plasmons by an incident light where resonance occurs results in a high degree of light scattering which translates to an

absorption band in the transmittance spectrum and an enhancement of the local electromagnetic field [23]. The localized surface plasmon resonance wavelength is highly dependent on the composition, size, shape and refractive index environment of the nanoparticles [24, 25]. Due to that property the LSPR phenomenon can be used for developing chemical and biological sensors based on measuring the resonance wavelength with simple transmission spectroscopy. The resonance wavelength is exquisitely sensitive to the refractive index of the nanoparticles environment (Fig. 1.3) and so by measuring it in real-time it is possible to detect molecular binding events [26].

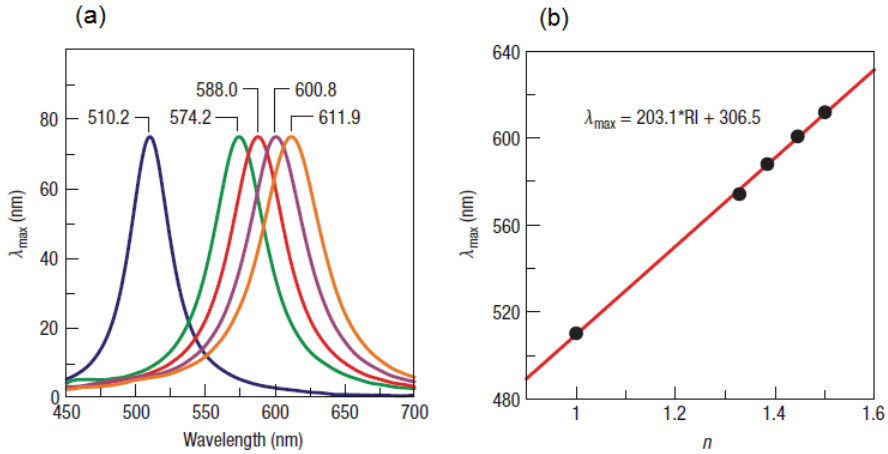

Figure 1.3 (a) Scattering spectra from a single nanoparticle in various solvent environments (left to right): nitrogen, methanol, propanol-1-ol, chloroform and benzene. (b) Linear relationship between the solvent refractive index n and the LSPR λ_{max} [24].

1.1.3 Optical Waveguides

In the quest for label free lab-on-a-chip systems with lower limits of detection an alternative optical biosensing technology to SPR and LSPR biosensors, based on dielectric structures [27] has arisen. Optical waveguides are dielectric structures that guide electromagnetic waves in the optical spectrum. Common types of optical waveguides include optical fibers and waveguides made in planar technology. Integrated photonic devices based on planar technologies are achieving significant advantages as biosensors due to its compatibility with mature silicon microprocessing technologies and materials which have permitted a high development of different structures that acts biosensors with high-throughput arrays on single-chip for simultaneous detection of multiple analytes [28, 29].

Although light is mostly confined within the core of the optical waveguide, through suitable design part of it can be allowed to extend through the medium surrounding the waveguide. Any variation in the refractive index of the medium surrounding the waveguide will be translated into a variation of the effective index of the waveguide. Among the different configurations used for detection of effective index variation, devices based on the Mach-Zehnder interferometer (MZI) have shown highly sensitive results for bulk refractive index sensing as well as biosensing applications [30, 31]. In a MZI, the phase shift given by the difference in the effective index difference between the sensing arm and the reference arm is transformed in an intensity modulation at the output of the MZI [32].

Using the same physical principle based on the variation in the effective index of the waveguide produced by a change in the refractive index of the surrounding media biosensing devices have been developed based on microring resonators [33]. Microring resonators offer the advantage of reducing the device size by orders of magnitude, thus reducing the amount of analyte needed for analyte detection as well as the possibility of integrating hundreds of devices into a lab-on-a-chip microsystem. In this way detection limits down to the femtomolar range for proteins have been achieved in an array configuration of 32 sensors monitored simultaneously [34].

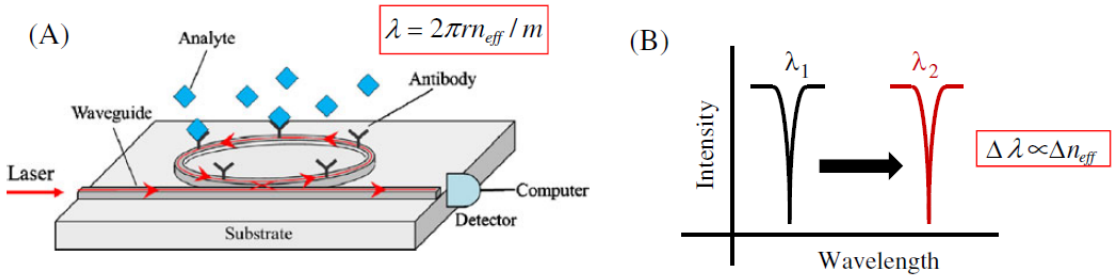

Figure 1.4 Illustration of a ring resonator biosensor that detects the binding of analyte to the surface. A tunable laser is coupled to the ring resonator. When the laser is in resonance with the resonant mode in the resonator, a spectral dip is shown at the detector to indicate the spectral position. (b) The resonant mode shifts in response to the local RI change induced by the molecular binding [35].

1.1.4 Reflectometric sensors

Reflectometric optical sensors are based on the method called Reflectometric Interference Spectroscopy (RIfS) where interference spectroscopy is used to record the reflectance spectra at thin transparent films [36]. Within the reflectance spectra a

Fabry-Perot interference pattern is observed due to the interference of the two reflected waves at the two interfaces of the thin film.

Within biosensing affinity reactions of biomolecules at the sensor surface lead to the formation of a biological layer from bound analytes with the increase in the thickness of the thin film leading to a shift of the interference pattern to higher wavelengths. The absolute thickness of the layer can however only be derived from the reflectance pattern after thorough characterization of the whole optical system [37].

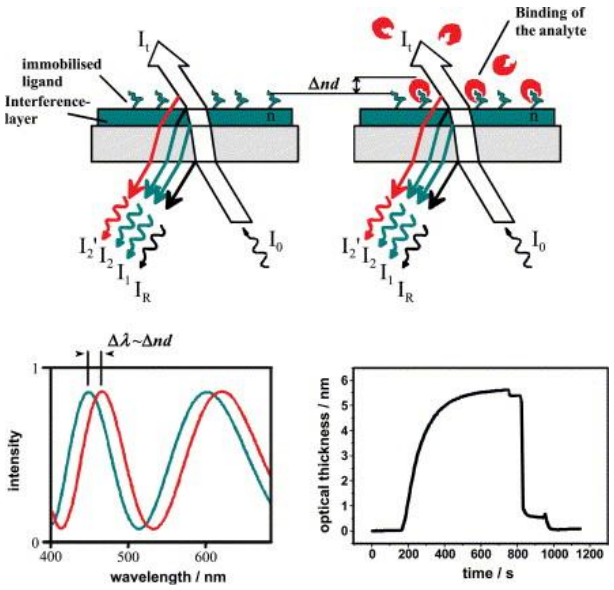

Figure 1.5 Principle of Reflectometric Interference Spectroscopy (RiFS). The optical thickness is obtained from the redshift produced in the reflection spectrum of a thin film layer [37].

Based on the RIfS method, multiplexed devices have been developed by using a silicon substrate with top layer of multi-strata thermally grown silicon dioxide (SiO_2) which acts as the interferometric layer. Illuminating the array with a tunable laser and measuring the reflected light at the different wavelengths with a CCD camera it is possible to monitor in parallel the binding events that take place in the individual elements of the array [38].

Several studies have been done towards improving the performance of the RIfS method focusing on using the internal area of the interference film for sensing binding events [39]. In this way, a greater surface area can be exploited for increased immobilization of bioreceptor molecules in the area of optical interrogation.

For this purpose, one approach has been based on the use of SU-8 nanopillars as the interferometric layer. This approach improves the sensitivity in comparison with a

single layer and also permits straightforward analyte infiltration and liquid trapping [40, 41]. The sensitivity is enhanced because the periodic array of nanopillars increases the effective sensing surface area for biosensing.

Other approaches for increasing the internal surface area of the interference film are based on the use of porous materials and these will be presented on Section 1.2.

1.2 Porous Materials for Optical Biosensing

For biosensing applications porous materials like porous silicon (PSi) or porous alumina (AAO) are mainly used as their surface areas are considerably larger than those of planar biosensors which results in higher sensitivities and so lower detection limits [42]. Among the large variety of optical biosensors based on porous materials the simplest devices are the reflectometric sensors that consist of an interferometer porous layer of a few microns thickness (Fig. 1.6). Binding of an analyte to the corresponding bioreceptor, previously immobilized on the pore walls, results in a change in the refractive index of that layer which is detected as a corresponding shift in the interference pattern [43]. Both porous silicon and porous alumina have been used this approach for biosensor devices based on the RiFS method [44-47].

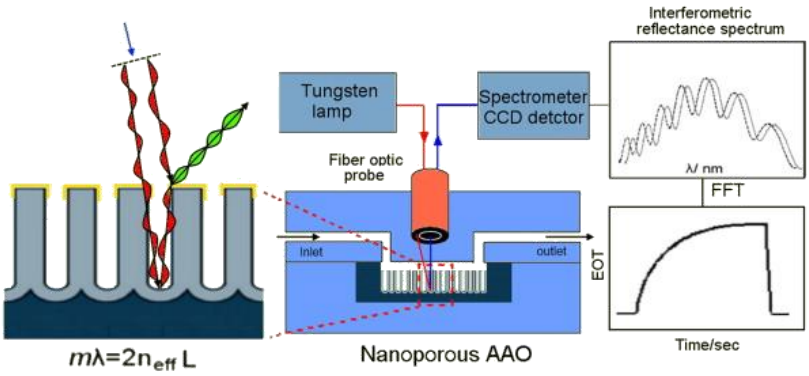

Figure 1.6 Schematic of a RIfS detection system when using a porous layer as the interferometer layer. The interaction of light with the pore structures generates a Fabry–Perot interference pattern and the shift of fringe pattern as a result of binding molecules or cells on the surface of the pores [47].

Another group of optical biosensors based on porous materials have used multilayer structures that exhibit a high reflectivity in a well defined wavelength range such as Bragg mirrors [48] or rugate filters [49, 50]. These devices usually exhibit higher sensitivities due to the enhancement of the light-matter interaction produced by the multiple reflections of light within the multilayer [51]. When a defect layer is

introduced inside the multilayer structure with a different width or a different porosity from the porous layers constituting the multilayer, a microcavity is built. Such a device enables to obtain very narrow resonances that are highly confined inside the microcavity and thus are very sensitive to any variation in refractive index induced by the presence of target biomolecules in this defect-layer [52] (Fig. 1.7).

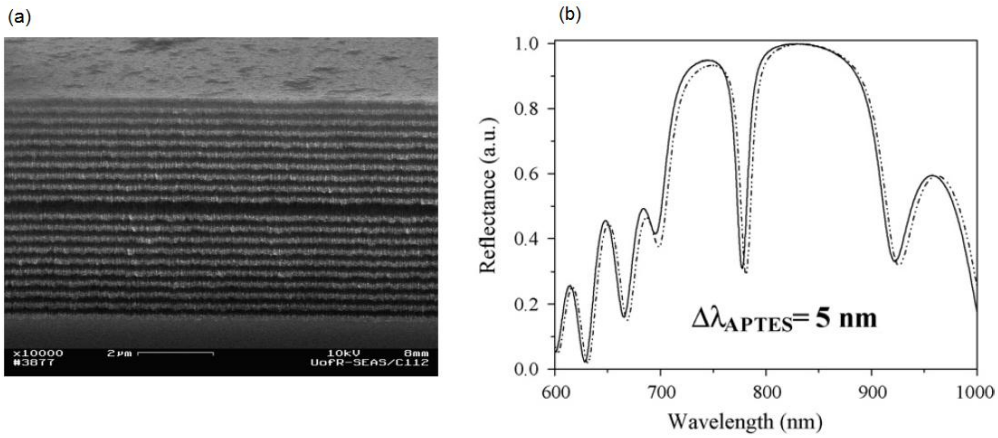

Figure 1.7 (a) SEM cross section image of a typical multilayer structure with a defect layer that acts as a microcavity [53]. (b) Typical reflectance spectrum of the as a microcavity. A blueshift is observed in the reflectance spectrum after the silanization of the pores surface [54].

As an alternative to the previously described biosensors based on porous monolayer or multilayers, planar waveguides made in porous materials have also been proposed [55, 56]. They consist of a thin waveguiding layer of medium porosity material on top of a highly porous layer substrate whose refractive index is lower than the waveguiding layer. As explained in Section 1.1.3 planar waveguides support light modes propagating within the waveguide parallel to the surface.

A typical configuration used for measuring the refractive index variations produced by the infiltration of the molecules in the pores of the porous waveguide uses a coupling prism for monitoring the variation in the coupling angle [55].

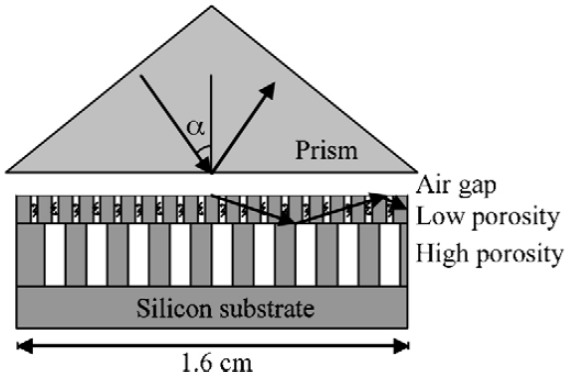

Figure 1.8 Porous waveguide consisting of a medium porosity on the top of a high porosity substrate. A prism is used to couple light at a specific angle into the waveguide which is modified when the analytes get into the pores. [Rong2008].

1.3 Publications

The first published paper entitled "Birefringent porous silicon membranes for optical sensing" presents the results of the investigation on free standing silicon membranes prepared from p-type (110) surface oriented silicon as a material for optical biosensing. The birefringence and sensitivity of this type of porous membrane is theoretically simulated using the Bruggeman model which is extended to incorporate the influence that silicon oxidation has on both birefringence and sensitivity. Using this extended theoretical model a good agreement is found between the measured sensitivity values and the theoretical ones. The final section of this chapter describes the development of a statistical model for characterizing the main depolarization sources responsible of the differences found between the measured transmittance spectra and the theoretical ones. These depolarization sources were mainly the resolution of the spectrometer used, the variations in the porous membrane thickness and the light scattering produced by the pores. The main contribution to the whole depolarization process was found to be the light scattering which increases dramatically with the sample thickness causing an increase in the standard deviation of the measured birefringence values.

The second publication, "Highly-sensitive anisotropic Porous Silicon based optical sensors", reports on the modeling, fabrication and characterization of PSi membranes from both (110) and (100) silicon was reported. Based on the Bruggeman model the theoretical birefringence and sensitivity was obtained as a function of the porosity and wavelength, with both values have a maximum shown for porosities around 0.5. The

impact that the oxidation of pore walls has on birefringence and sensitivity was also studied theoretically. Thereafter a set of PSi samples from different oriented substrates fabricated and characterized. Porous silicon made from (110) shown to be higher values of birefringence than the ones obtained from a (100) surface oriented silicon. Due to the highest birefringence, also the better sensitivity is found in the (110) samples, measuring a value as high as 1407 nm/RIU at a wavelength of 1500 nm.

The third publication, "Phase sensitive detection for optical sensing with porous silicon", addresses the development of a highly sensitive optical sensor by combining a phase retardation measurement readout scheme for measuring the optical anisotropy, at a wavelength of 1500 nm, with mesoporous silicon membranes fabricated from medium doped n-type (100) surface oriented silicon. These mesoporous membranes with 50 nm pore size are suitable for biosensing applications since they allow the infiltration of the target analytes inside the pores. Birefringence measurements show that the measured birefringence values decrease with sample thickness due to decreasing number of pores that grow in the <113> directions. Subsequent sensing experiments carried out using membranes with thicknesses from 10 to 60 μm showed that the amount of depolarized light increases with sample thickness resulting in a poorer resolution of birefringence measurements. Thus, the lowest detection limit obtained was 6.25×10^{-6} refractive index units, from a 10 μm thick membrane. The thermooptic coefficient of that membrane was measured in an aqueous environment and found to be 8×10^{-4} rad/°C.

In the fourth publication, "Real-time polarimetric optical sensor using macroporous alumina membranes", we report on the first demonstration of real-time highly sensitive optical sensing using free standing alumina membranes of 200 nm pore diameter. In comparison with the previously studied porous silicon membranes, these macroporous alumina membranes not only allow the infiltration of biomolecules but also present flow-through properties so that analytes can be delivered fast to bioreceptors placed on the surface of the pores throughout their length. The birefringence measurements of this type of membrane at wavelengths of 1500 nm, 980 nm and 808 nm show a decrease at shorter wavelengths where depolarization caused by light scattering becomes more significant. The volumetric sensing experiments performed at the same wavelengths demonstrated detection limits of in the range of 10^{-6} refractive index units. The lowest detection limit was 5.2×10^{-6} refractive index units measured at a wavelength of 980 nm which demonstrates the

possibility of developing low-cost multiplexed devices through the use of silicon CCD detectors.

The last publication, "Real-time polarimetric biosensing using macroporous alumina membranes", describes the immobilization of the allergen protein β-Lactoglobulin by means of functionalizing the alumina membrane pores surface with an epoxysilane. The specific binding response produced by the recognition of the rabbit anti-β-lactoglobulin antibody by the immobilized protein is then measured in real-time by the developed porous alumina based optical biosensor microsystem. The binding response from the recognition between this first antibody and a secondary antibody anti-rabbit IgG was then also measured in real-time demonstrating the biosensing capabilities of the free-standing membrane when its birefringence is measured using an polarimetric setup.

1.4 References

[1] A. Brecht, G. Gauglitz, "Optical probes and transducers" Biosensors & Bioelectronics Vol. 10(9-10), pp. 923-936 (1995).

[2] D. R. Thevenot, K. Tóth, R. A. Durst and G. S. Wilson "Electrochemical Biosensors: Recommended Definitions and Classification" Pure Appl. Chem., Vol. 71(12) pp. 2333-2348 (1999).

[3] A. Sassolas, B.D. Leca-Bouvier, L.J. Blum, "DNA Biosensors and Microarrays" Chemical Reviews, Vol. 108(1), pp. 109-139 (2008).

[4] A. Chaubey, B.D. Malhotra, "Mediated biosensors" Biosensors & Bioelectronics Vol. 17(6-7), pp. 441-456 (2002).

[5] B. Eggins, "Chemical sensors and biosensors. Analytical Techniques in the Sciences". John Wiley & Sons, West Sussex, (2002).

[6] J. Wang, "Amperometric biosensors for clinical and therapeutic drug monitoring: a review", Journal of Pharmaceutical and Biomedical Analysis, Vol. 19(1–2) pp. 47-53 (1999).

[7] A.A. Karyakin, M. Vuki, L.V. Lukachova, E.E. Karyakina, A.V. Orlov, G.P. Karpachova, J. Wang "Processible polyaniline as an advanced potentiometric pH transducer" Analytical Chemistry, Vol. 71(13), pp. 2534-2540 (1999).

[8] P. D'Orazio, "Biosensors in clinical chemistry" Clinica Chimica Acta Vol. 334(1-2), pp. 41-69 (2003).

[9] A.A. Shulga, A.P. Soldatkin, A.V. Elskaya, S.V. Dzyadevich, S.V. Patskovsky, V.I. Strikha, "Thin-film conductometric biosensors for glucose and urea determination", Biosensors and Bioelectronics, Vol. 9(3), pp. 217-223 (1994).

[10] A. Steinschaden, D. Adamovic, G. Jobst, R. Glatz, G. Urban, "Miniaturised thin film conductometric biosensors with high dynamic range and high sensitivity", Sensors and Actuators B: Chemical, Vol. 44(1–3), pp. 365-369 (1997).

[11] R.C. Ebersole , Jeffrey A. Miller , John R. Moran , Michael D. Ward "Spontaneously formed functionally active avidin monolayers on metal surfaces: a strategy for immobilizing biological reagents and design of piezoelectric biosensors" J. Am. Chem. Soc., Vol. 112(8), pp. 3239-3241, (1990).

[12] Renee L. Bunde, Eric J. Jarvi, Jeffrey J. Rosentreter, Piezoelectric quartz crystal biosensors, Talanta, Volume 46, Issue 6, August 1998, Pages 1223-1236, ISSN 0039-9140, 10.1016/S0039-9140(97)00392-5.

[13] Fan, X.D.; White, I.M.; Shopoua, S.I.; Zhu, H.Y.; Suter, J.D.; Sun, Y.Z., "Sensitive optical biosensors for unlabeled targets: A review" Analytica Chimica Acta, Vol. 620(1-2), pp. 8-26 (2008).

[14] M.C. Estevez, M. Alvarez, L.M. Lechuga "Integrated optical devices for lab-on-a-chip biosensing applications" Laser & Photon. Rev. Vol. 6(4), pp. 463-487 (2012).

[15] D. Hill, "Advances in Nanophotonic Sensing Technologies During Three International Label-Free Lab-On-Chip Projects" BioNanoScience, Vol. 1, pp. 162-172 (2011).

[16] H.J. Lee, W.W. Alastair, R.M. Corn "Creating Advanced Multifunctional Biosensors with Surface Enzymatic Transformations", Langmuir Vol. 22(12), pp. 5241-5250 (2006).

[17] Y. Li, A.W. Wark, H.J Lee, R.M. Corn "Single-Nucleotide Polymorphism Genotyping by Nanoparticle-Enhanced Surface Plasmon Resonance Imaging Measurements of Surface Ligation Reactions" Analytical Chemistry, Vol. 78(9), pp. 3158-3164 (2006).

[18] J. Vörös, R. Graf, G.L. Kenausis, A. Bruinink, J. Mayer, M. Textor, E. Wintermantel, N.D. Spencer, "Feasibility study of an online toxicological sensor based on the optical waveguide technique", Biosensors and Bioelectronics, Vol. 15(9-10) pp. 423-429 (2000).

[19] J. Lu, C.M. Strohsahl, B.L. Miller, L.J. Rothberg "Reflective Interferometric Detection of Label-Free Oligonucleotides" Analytical Chemistry, Vol. 76(15), pp. 4416-4420 (2004).

[20] C. Williams, T.A. Addona "The integration of SPR biosensors with mass spectrometry: possible applications for proteome analysis" Trends in biotechnology, Vol. 18(2) pp. 45-48 (2000).

[21] J. Homola, "Surface plasmon resonance based sensors" Springer Vol. 4 (2006).

[22] J. Homola, H. Vaisocherová, J. Dostálek, M. Piliarik, "Multi-analyte surface plasmon resonance biosensing" Methods, 37(1), pp. 26-36 (2005).

[23] E. Hutter, J.H. Fendler "Exploitation of Localized Surface Plasmon Resonance" Adv. Mater. Vol. 16(19) pp. 1685-1706 (2004).

[24] J.N. Anker, W.P. Hall, O. Lyandres, N.C. Shah, J. Zhao, R.P. Van Duyne "Biosensing with plasmonic nanosensors", Nat. Mater. Vol. 7(6), pp. 442-453 (2008).

[25] K.A. Willets, R.P. Van Duyne "Localized surface plasmon resonance spectroscopy and sensing" Annu. Rev. Phys. Chem., Vol. 58, pp. 267-297 (2007).

[26] B. Sepúlveda, P.C. Angelomé, L.M. Lechuga, L.M. Liz-Marzán, "LSPR-based nanobiosensors" Nano Today, Vol. 4(3) pp. 244-251 (2009).

[27] G. Gauglitz "Direct optical sensors: principles and selected applications" Anal. Bioanal. Chem, Vol. 381(1) pp. 141-155 (2005).

[28] A.L. Washburn, R.C. Bailey "Photonics-on-a-chip: recent advances in integrated waveguides as enabling detection elements for real-world, lab-on-a-chip biosensing applications" Analyst, Vol. 136(2), pp. 227-236 (2011).

[29] J.T. Kirk, G.E. Fridley, J.W. Chamberlain, E.D. Christensen, M. Hochberg, D.M. Ratner "Multiplexed inkjet functionalization of silicon photonic biosensors" Lab on a Chip, Vol. 11(7), pp. 1372-1377 (2011).

[30] B. Luff, J. Wilkinson, J. Piehler, U. Hollenbach, J. Ingenhoff, and N. Fabricius, "Integrated Optical Mach-Zehnder Biosensor," J. Lightwave Technol. Vol. 16(4), pp. 583- (1998).

[31] F. Prieto, B. Sepúlveda, A. Calle, A. Llobera, C. Domínguez, A. Abad, A. Montoya, L.M. Lechuga "An integrated optical interferometric nanodevice based on silicon technology for biosensor applications" Nanotechnology, Vol. 14(8), pp. 907 (2003).

[32] R.G. Heideman, R.P.H. Kooyman, J. Greve, "Performance of a highly sensitive optical waveguide Mach-Zehnder interferometer immunosensor" Sensors and Actuators B: Chemical, Vol. 10(3), pp. 209-217 (2003).

[33] A. Yalcin, K.C. Popat, J.C. Aldridge, T.A. Desai, J. Hryniewicz, N. Chbouki, B.E. Little, O. King, V. Van, Sai Chu, D. Gill, M. Anthes-Washburn, M.S. Unlu, B.B. Goldberg, "Optical sensing of biomolecules using microring resonators" IEEE Journal of Selected Topics in Quantum Electronics, Vol. 12(1), pp. 148-155 (2006).

[34] M. Iqbal, M.A. Gleeson, B. Spaugh, F. Tybor, W.G. Gunn, M. Hochberg, L.C. Gunn, "Label-free biosensor arrays based on silicon ring resonators and high-speed optical scanning instrumentation" IEEE Journal of Selected Topics in Quantum Electronics, Vol. 16(3), pp. 654-661 (2010).

[35] Y. Sun, X. Fan, "Optical ring resonators for biochemical and chemical sensing" Analytical and bioanalytical chemistry, Vol. 399(1), pp. 205-211 (2011).

[36] A. Brecht, G. Gauglitz, W. Nahm, (1992). "Interferometric measurements used in chemical and biochemical sensors" Analysis, Vol. 20(3), pp. 135-140 (1992).

[37] G. Gauglitz, A. Brecht, G. Kraus, W. Mahm, "Chemical and biochemical sensors based on interferometry at thin (multi-) layers" Sensors and Actuators B: Chemical, Vol. 11(1), pp. 21-27 (1993).

[38] E. Özkumur, J.W. Needham, D.A. Bergstein, R. Gonzalez, M. Cabodi, J.M. Gershoni, B.B. Goldberg, M.S. Ünlü, "Label-free and dynamic detection of biomolecular interactions for high-throughput microarray applications" Proceedings of the National Academy of Sciences, Vol. 105(23), pp. 7988-7992 (2008).

[39] K.P.S. Dancil, D.P. Greiner, M.J. Sailor, "A porous silicon optical biosensor: detection of reversible binding of IgG to a protein A-modified surface" Journal of the American Chemical Society, Vol. 121(34), pp. 7925-7930 (1999).

[40] M. Holgado, C.A. Barrios, F.J. Ortega, F.J. Sanza, R. Casquel, M.F. Laguna, M.J. Bañuls, D. López-Romero, R. Puchades, A. Maquieira, "Label-free biosensing by means of periodic lattices of high aspect ratio SU-8 nano-pillars" Biosensors and Bioelectronics, Vol. 25(12), pp. 2553-2558 (2010).

[41] D. López-Romero, C.A. Barrios, M. Holgado, M.F. Laguna, R. Casquel, "High aspect-ratio SU-8 resist nano-pillar lattice by e-beam direct writing and its application for liquid trapping" Microelectronic Engineering, Vol. 87(4), pp. 663-667 (2010).

[42] T.D. Lazzara, I. Mey, C. Steinem, A. Janshoff, "Benefits and limitations of porous substrates as biosensors for protein adsorption" Analytical chemistry Vol. 83(14), pp. 5624-5630 (2011).

[43] V.S. Lin, K. Motesharei, K.S. Dancil, M.J. Sailor, M.R. Ghadiri, "A Porous Silicon-Based Optical Interferometric Biosensor" Science Vol. 278(5339), pp. 840-843 (1997).

[44] M.M. Orosco, C. Pacholski, M.J. Sailor "Real-time monitoring of enzyme activity in a mesoporous silicon double layer", Nature Nanotechnology Vol. 4, pp. 255-258 (2009).

[45] C.K. Tsang, T.L. Kelly, M.J. Sailor, Y.Y. Li, "Highly Stable Porous Silicon–Carbon Composites as Label-Free Optical Biosensors" ACS Nano Vol. 6, pp. 10546-10554, (2012).

[46] S.D. Alvarez, C.P. Li, C.E. Chiang, I.K. Schuller, M.J. Sailor, "A Label-Free Porous Alumina Interferometric Immunosensor" ACS Nano Vol. 3(10), pp. 3301-3307 (2009).

[47] T. Kumeria, M.D. Kurkuri, K.R. Diener, L. Parkinson, D. Losic, "Label-free reflectometric interference microchip biosensor based on nanoporous alumina for detection of circulating tumour cells" Biosensors and Bioelectronics, Vol. 35(1), pp. 167-173 (2012).

[48] I. Rendina, I. Rea, L. Rotiroti, L. De Stefano, "Porous silicon-based optical biosensors and biochips" Physica E: Low-dimensional Systems and Nanostructures, Vol. 38(1), pp. 188-192 (2007).

[49] J. Chapron, S.A. Alekseev, V. Lysenko, V.N. Zaitsev, D. Barbier, "Analysis of interaction between chemical agents and porous Si nanostructures using optical sensing properties of infra-red Rugate filters", Sensors and Actuators B: Chemical, Vol. 120(2) pp. 706-711 (2007).

[50] F. Cunin, T.A. Schmedake, J.R. Link, Y.Y. Li, J. Koh, S.N. Bhatia, M.J. Sailor, "Biomolecular screening with encoded porous-silicon photonic crystals" Nature materials, Vol. 1(1), pp. 39-41 (2002).

[51] H. Ouyang, C.C. Striemer, P.M. Fauchet, "Quantitative analysis of the sensitivity of porous silicon optical biosensors" Applied Physics Letters, Vol. 88(16), pp. 163108-163108 (2006).

[52] W. Theiß, "Optical properties of porous silicon" Surface Science Reports, Vol. 29(3), pp. 91-192 (1997).

[53] L.A. DeLouise, P.M. Kou, B.L. Miller, "Cross-correlation of optical microcavity biosensor response with immobilized enzyme activity. Insights into biosensor sensitivity" Analytical chemistry, Vol. 77(10), pp. 3222-3230 (2005).

[54] G. Palestino, R. Legros, V. Agarwal, E. Pérez, C. Gergely, "Functionalization of nanostructured porous silicon microcavities for glucose oxidase detection" Sensors and Actuators B: Chemical, Vol. 135(1), pp. 27-34 (2008).

[55] G. Rong, A. Najmaie, J.E. Sipe, S.M. Weiss, "Nanoscale porous silicon waveguide for label-free DNA sensing" Biosensors and Bioelectronics, Vol. 23(10), pp. 1572-1576 (2008).

[56]A. Yamaguchi, K. Hotta, N. Teramae "Optical Waveguide Sensor Based on a Porous Anodic Alumina/Aluminum Multilayer Film" Analytical Chemistry Vol. 81(1), pp. 105-111 (2009).

2. Summary

2.1 Experimental techniques

2.1.1 Fabrication

Porous silicon anodization

PSi is typically prepared by the electrochemical etching of silicon using HF dissolved in water or ethanol. Parameters such as pore size, porosity and layer thickness can be adjusted by correctly choosing the resistivity of the silicon wafer, the HF concentration and the etch time [1].

The mesoporous samples prepared from (110) surface oriented n-type Si with a resistivity of 0.01-0.001 Ω·cm had pore sizes around 50 nanometers, as shown in Fig. 2.1 (a). They were prepared by electrochemical etching using a solution composed of HF:Ethanol=3:7 by volume, considering an initial HF concentration of 48% and a current density of 25 mA/cm^2 .

The other set of mesoporous samples were prepared from (100) surface oriented p-type Si with resistivity of 0.01-0.001 01 Ω·cm. In this case the pore sizes were around 80 nanometers, as shown in Fig. 3.1 (b).

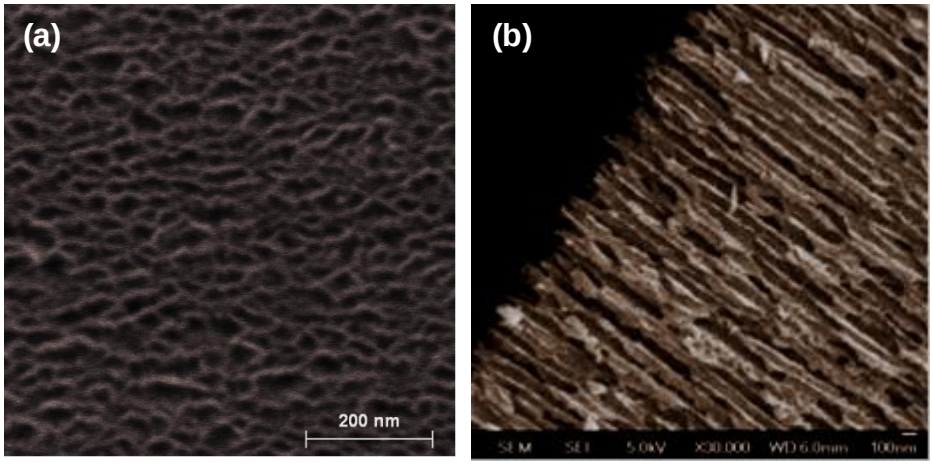

Figure 2.1 (a) Surface SEM image of one of the samples etched from (110) surface oriented silicon. Pore diameter is around 50 nm. (b) Cross section SEM image of one of the fabricated samples from (100) surface oriented silicon. Pore diameters are around 80 nm.

For subsequent optical characterization, porous membranes were detached from the bulk silicon layer that supports them by applying a strong current burst at the end of the etching, completely dissolving the bottom silicon layer that surrounds the etched area. With this procedure the membrane can be transferred to a support substrate [2].

Before optical characterization, the detached membranes were then thermally oxidized at 200 °C for 12 hours. This oxidation process has two purposes; first a thin silicon dioxide layer is formed on the pore walls so as to stabilize them, reducing the drift in effective refractive index. Secondly, the thin silicon dioxide layer increases the hydrophilicity of the samples [3] for improve microfluidic transport of liquids in the subsequent sensing experiments.

Membrane transfer to support structures

After oxidation, the free-standing membranes were transferred onto support structures using a 1 μm thick of PMMA (Poly(methyl methacrylate)) resist as the adhesion layer between the support structure and the free-standing membrane. The support structures used were typically aluminum, glass or silicon substrates square pieces of 15 by 15 millimeters with a hole performed in the center of the structure for the light and the analytes to pass through to the membranes.

Pore surface functionalization

The pore surfaces of the free standing membranes studied in this work were functionalized by a self-assembled epoxysilane monolayer. This monolayer was chemisorbed onto the pores walls through a reaction of alumina hydroxyl groups with the silane groups so that receptors biomolecules could be latter attached (Fig. 2.2).

In doing so, first the hydroxyl groups of the membranes surface were activated by an oxygen plasma treatment and then the membranes were immersed into a 1% solution (in volume) of (3-glycidoxypropyl) trimethoxy silane in dry toluene over night at room temperature. This was followed by a curing step at 80 °C under vacuum to ensure a high degree of coverage of the surface. Finally the membranes were rinsed with toluene and ethanol and dried under a stream of nitrogen in order to remove any physisorbed silane groups.

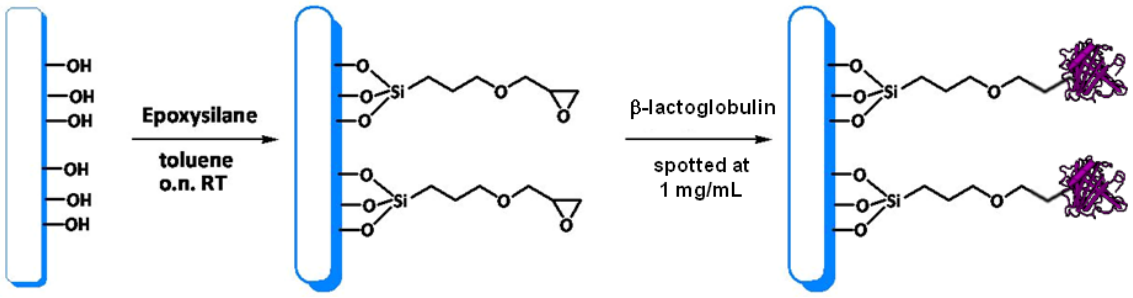

Figure 2.2 Formation of the epoxysilane monolayer on the pores surface by (3-glycidoxypropyl)trimethoxysilane and the following immobilization of β-lactoglobulin protein onto the resulting monolayer.

Bioreceptor immobilization

Once the free standing membranes had been functionalized and transferred to the supports the β-lactoglobulin protein bioreceptors were immobilized on the silanized surface, via spotting, through the linkage to the active surface epoxy groups. For this purpose a piezoelectric spotter SciFlexArrayer S5 from Scienion was used to spot ten microliters of β-lactoglobulin B protein at 1 mg/mL concentration on the functionalized membranes. Thereafter the spotted membranes were incubated at room temperature in a moisture chamber overnight and rinsed with PBS solution to remove unbound protein. The spotted membranes were then blocked by a BSA solution at 0.1 µg/mL concentration, washed again with PBS and dried under a nitrogen stream.

2.2.1 Optical characterization

The optical anisotropy of the porous free standing membranes was studied by analyzing the polarization change of the light transmitted through them. Two different polarimetric setups were employed to determine the birefringence of the free standing membranes and its sensitivity to refractive index changes. Those setups are explained in the two next subsections.

Polarization resolved transmittance measurements

The setup used for characterizing the porous membranes fabricated from (110) surface oriented silicon is depicted in Fig. 2.3. The output light from a tungsten halogen lamp is collimated and then polarized linearly at 45° with respect to the horizontal direction. The linearly polarized light passes through the anisotropic PSi sample which is oriented with its [001] and [1$\bar{1}$0] crystallographic directions parallel to

the vertical and horizontal directions, respectively. The lamp spot incident on the PSi samples had a diameter of 1.2 mm with a divergence of 1°. The components of light along the [001] and [1$\bar{1}$0] directions undergo a phase shift or retardation upon traversing the membrane given by:

$$\Delta\phi(\lambda) = \frac{2\pi}{\lambda} \cdot d \cdot \Delta n(\lambda) \tag{2.1}$$

where λ is the incident wavelength of light, d the PSi membrane thickness and $\Delta n(\lambda)$ its birefringence. The phase shift is then converted into an amplitude shift through traversing a second polarizer (usually called analyzer), and is then recorded by a spectrometer. To cover the transmission spectrum in the whole region of interest, from 600 to 1600 nm, the spectrometers used were an Ocean Optics NIR512 with a bandwidth of 3.1 nm and an Ocean Optics RedTide 650 with a bandwidth of 2 nm.

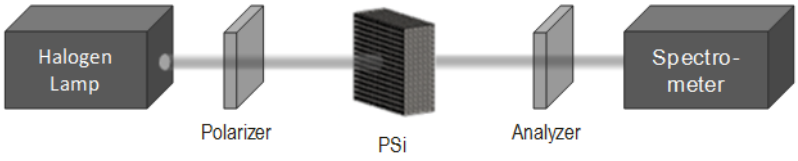

Figure 2.3 Scheme of the setup used for the optical characterization of the PSi membranes.

The normalized transmittance (light recorded in the parallel or cross direction divided by the sum of the light in the parallel and cross directions) for polarizers placed in parallel or crossed is given by:

$$T_{\parallel}(\lambda) = \cos^2\left(\Delta\phi(\lambda)/2\right) \tag{2.2}$$

$$T_{\perp}(\lambda) = \sin^2\left(\Delta\phi(\lambda)/2\right) \tag{2.3}$$

where $\Delta\phi(\lambda)$ is the phase retardation given by Eq. 2.1.

Phase retardation measurements

Optical birefringence can be measured by a wide variety of methods; the simplest one is based on the measurement of the transmitted light through a sample when it is placed between crossed polarizers [4]. Although this method is simple to implement a photoelastic modulator (PEM) can be used instead for greater measurement accuracy [5]. The optical setup with a PEM that was used for characterizing the optical

anisotropy of the porous silicon membranes fabricated from (100) surface oriented silicon as well as the macroporous alumina membranes is shown in Fig. 2.4.

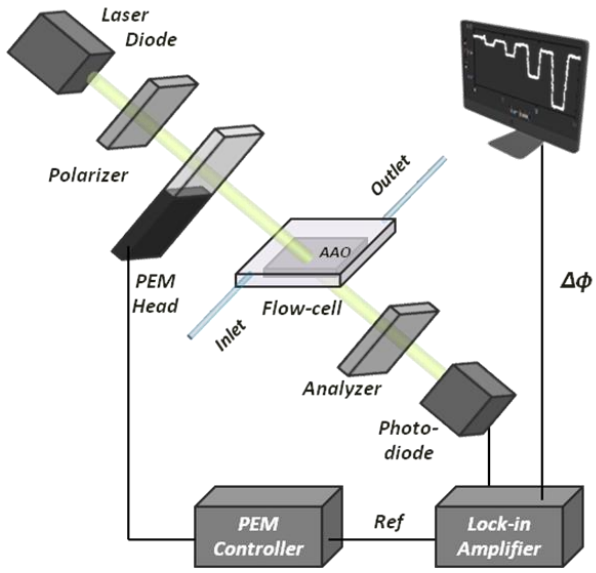

Figure 2.4 Polarimetric setup used for the optical anisotropy characterization of the free-standing membranes.

The output light from a laser diode is collimated and directed to a first linear polarizer. The linearly polarized light from the polarizer arrives at a photoelastic modulator (PEM; Hinds Instruments PEM-100) that modulates the light polarization. The modulated light is incident at 45º to the alumina membrane, which is mounted on a flow-cell. The light exiting the membrane, after passing a second polarizer, is detected by a photodiode which is connected to a lock-in amplifier. The lock-in amplifier (SR-830) demodulates the detected signal extracting the amplitudes of its first and second harmonics, which are related to the phase retardation $\Delta\phi$ between the ordinary and extraordinary components of the polarized light by [12]:

$$\Delta\phi = \arctan\left(\frac{V_{1f}}{V_{2f}} \cdot \frac{J_2(A_0)}{J_1(A_0)}\right) \tag{2.4}$$

where V_{1f} and V_{2f} are the amplitudes of the first and second harmonics of the modulated signal, $J_1(A_0)$ and $J_2(A_0)$ are the Bessel functions of first and second order respectively, and A_0 is the amplitude of the modulating signal (in radians).

This polarimetric measurement platform offers several advantages over other photonics platforms that rely on vertical interrogation mechanisms as it avoids a

complex coupling system thereby constituting a robust sensing platform minimizing alignment requirements for light coupling.

The resolution of the setup was tested by taking multiple measurements of a quartz sample with a known birefringence. The measured values had a Gaussian distribution with a standard deviation equal to 10^{-7} rad. By adopting the convention that the resolution is given by the standard deviation when the values have a Gaussian distribution, we obtain the resolution of our measurement system as 10^{-7} rad.

2.1.3 Fluidic platform

A layout of the flow-cell used for the flow-through sensing is depicted in Fig. 2.5. A free standing membrane mounted on a support structure is placed between two glass windows with inlet and an outlet ports. The inlet port is connected to a syringe pressure source which operates at 15 psi to deliver a constant flow.

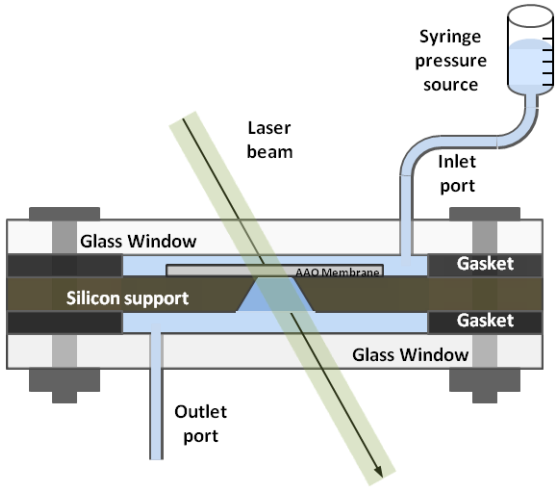

Figure 2.5 Scheme of the flow cell where a free standing membrane mounted on a silicon support is placed inside for letting the different liquids used in the sensing experiments to flow through the pores.

2.2 Results and discussion

2.2.1 Birefringent porous silicon membranes for optical sensing

Bulk silicon is an isotropic material due to its diamond cubic crystal structure, however PSi prepared from (110) Si surface oriented substrates presents a high anisotropy due to its pores having grown preferentially along the [100] and [010] crystallographic directions [6], as seen in Fig. 2.6. The orientation of the pores along those directions results in a difference in refractive index between the [001] and [1$\bar{1}$0] directions [7].

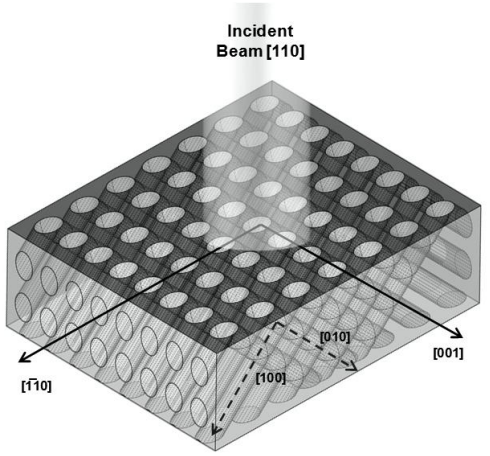

Figure 2.6 Scheme of an anisotropic PSi layer produced from a (110) surface oriented Si wafer.

Birefringence modeling and characterization

In accounting for the anisotropic microstructure of this type of PSi, the pores were modeled as ellipsoids of revolution with their axes of symmetry aligned along the [001] direction and the [1$\bar{1}$0] direction lying on the (110) surface plane. The screening efficiency of external electromagnetic fields inside the ellipsoids are described by depolarization factors, $L_{[001]}$ and $L_{[1\bar{1}0]}$, characterizing the optical properties of the PSi layer. Their values are given by [8, 9]:

$$L_{[1\bar{1}0]} = \frac{1}{1-\xi^2}\left(1-\xi\cdot\frac{\arcsin\left(\sqrt{1-\xi^2}\right)}{\sqrt{1-\xi^2}}\right) \tag{2.5}$$

$$L_{[001]} = \frac{1-L_{[1\bar{1}0]}}{2} \tag{2.6}$$

where $\xi=a/b$, being a and b the major and minor ellipse axes respectively. As the directions [100] and [010] form an angle of 50.77° with respect to the normal plane (110) [6], the ratio ξ has a value of 0.7746. Substituting this value into Eq. 2.5 and Ep. 2.6 depolarization factors of $L_{[001]}$ equal to 0.2938 and $L_{[1\bar{1}0]}$ equal to 0.4035 are obtained.

Among the several methods that can be used to estimate the birefringence of an anisotropic PSi layer the Bruggeman model [10] was chosen since for samples with porosities below 0.8 it provides more accurate predictions than the other methods [11, 12]. The only assumption made by this model is the static electric field condition, which is satisfied when the wavelength of light is much longer than the transverse pore size. As the fabricated samples have porosities below 0.8 and pore diameters smaller than 100 nm, fulfilling the static electric field condition. The Bruggeman model is described by Eq. 3.3:

$$\sum_i f_i \frac{n_i^2(\lambda) - n_{[001],[1\bar{1}0]}^2}{n_{[001],[1\bar{1}0]}^2 + L_{[001],[1\bar{1}0]} \cdot (n_i^2(\lambda) - n_{[001],[1\bar{1}0]}^2)} = 0 \tag{3.3}$$

where f_i is the volume fraction of the different materials that form the PSi membrane, $n_i(\lambda)$ their refractive indices, and $L_{[001]}$ and $L_{[1\bar{1}0]}$ the previously described depolarization factors. The unknown $n_{[001]}$ and $n_{[1\bar{1}0]}$ are the refractive indices along the main axes and are related to the birefringence by means of $\Delta n=n_{[001]}-n_{[1\bar{1}0]}$.

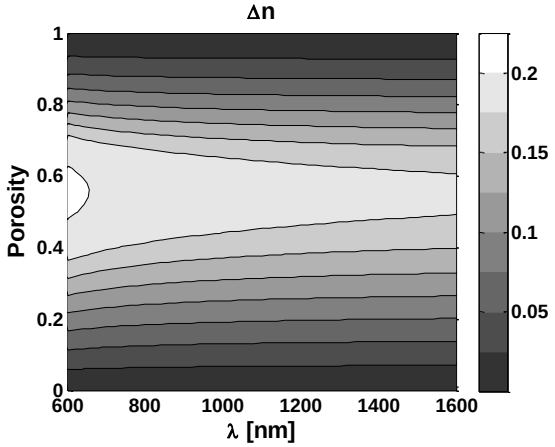

Figure 2.7 Birefringence computed using the Bruggeman model for a binary PSi layer (silicon and pores filled with air) as a function of wavelength and porosity.

Fig. 2.7 shows the theoretical birefringence obtained by solving Eq. 2.7 for wavelengths from 600 nm to 1600 nm and porosities ranging from 0 to 1. Two clear observations can be made. First, it can be noted that birefringence has a maximum for a porosity of 0.55. Secondly, it decreases with wavelength, following the behavior of refractive index for silicon.

After determining the theoretical birefringence of a porous membrane fabricated from (110) surface oriented silicon, using the experimental setup described in Section 2.1.2 the values of $T_{\perp}(\lambda)/T_{\parallel}(\lambda)$ versus wavelength for two PSi membranes with thicknesses of 30 µm and 64 µm were measured. The $T_{\perp}(\lambda)/T_{\parallel}(\lambda)$ spectra are shown in Fig. 2.8 (a). From the poles and zeros of the spectra the birefringence values were obtained and represented in Fig. 2.8 (b).

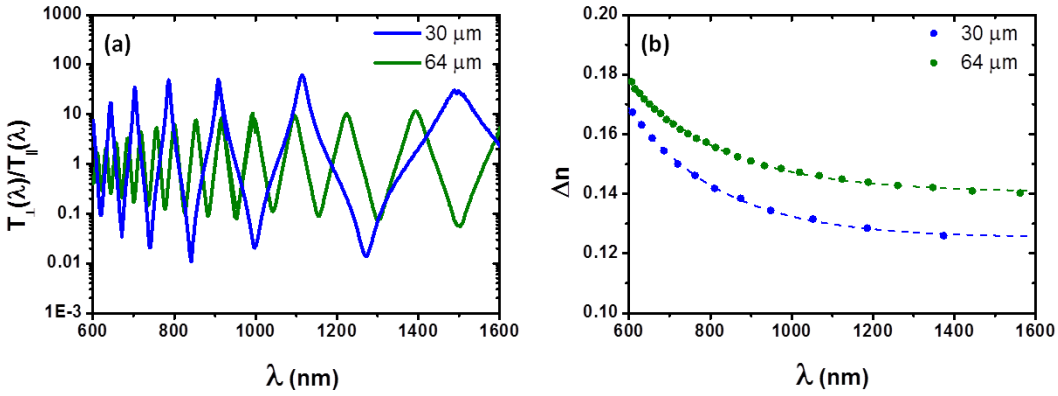

Figure 2.8 (a) Transmission spectra for a PSi sample with a thickness of 30 µm (blue line), and another with a thickness of 64 µm (green line). (b) Birefringence data obtained from the measured spectra (dots) and simulated curves using the Bruggeman model (dashed lines) for a 30 µm thick sample (blue), and a 64 µm thick sample (green).

Sensitivity

The sensitivity of the PSi membrane samples was determined by filling them with the different liquids such as ethanol and isopropanol and then measuring the shift produced in the transmission spectrum. To do this we placed a thermally treated PSi sample in a flow cell made from optical glass and then filled the cell with ethanol ($n_{Etha} \approx 1.36$) and isopropanol ($n_{Isop} \approx 1.377$). A few seconds after filling the flow cell with the liquids, the transmission spectra stabilized, indicating that the liquids had completely filled the pores. Fig. 2.9 (a) shows the values of $T_{\perp}(\lambda)/T_{\parallel}(\lambda)$ versus wavelength for a thermally oxidized PSi sample with a thickness of 30 µm when the

pores are empty (red line), when filled with isopropanol (green line) or ethanol (blue line). From this graph, the birefringence was obtained and is depicted in Fig. 2.9 (b).

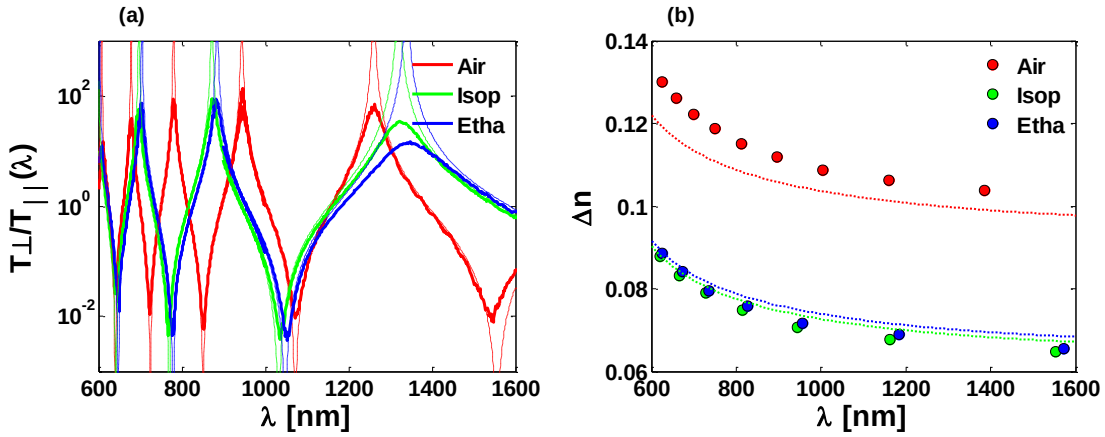

Figure 2.9 (a) Transmission spectra for empty pores (red line), pores completely filled with isopropanol (green line) and ethanol (blue line). Dashed lines represent the corresponding theoretical curves. (b) Birefringence data obtained from the measured spectra (dots) and simulated curves using the Bruggeman model (dashed lines) for air (red), isopropanol (green) and ethanol (blue).

A blue shift in the $T_\perp(\lambda)/T_{||}(\lambda)$ can be clearly seen in Fig. 2.9 (a) that is associated with the birefringence change seen in Fig. 2.9 (b). The birefringence change between the samples filled with isopropanol and filled with ethanol was obtained from the curves fitted to experimental birefringence values depicted in Fig. 2.9 (b). These values are $1.8\text{x}10^{-3}$, $1.1\text{x}10^{-3}$, and $0.98\text{x}10^{-3}$ for the wavelengths of 810, 1300 and 1500 nm respectively. For comparison, the values theoretically predicted for a silicon oxide volume fraction of 0.16 were $1.3\text{x}10^{-3}$ at 810 nm, and $1.2\text{x}10^{-3}$ at 1300 and 1500 nm. The model for estimating the optical sensitivity of a PSi membrane in a polarimetric scheme is thereby validated with the effect of silicon oxidation found to be a critical parameter.

Depolarization effects in porous silicon

Although poles and zeros (ideal theoretical curves shown in Fig. 2.9 (a) by dashed lines) are expected when $T_{||}(\lambda)$ and $T_\perp(\lambda)$ are respectively zero, we observed in Fig. 2.9 (a) that local maxima and minima values of 10^2 and 10^{-2} were measured, respectively.

Depolarization is known to be the cause of the difference between the ideal response and that measured [13]. The depolarization represents the degree of random

polarization that occurs during the measurement process. In the birefringence measurements of PSi membranes, we identified the three main sources of depolarization to be: (1) spectrometer bandwidth, (2) thickness variations in the PSi membrane across the light spot area and (3) light scattering produced by pores with a random spatial distribution:

(1) The spectrometer bandwidth affects the phase retardation in two different ways. First the quasi-monochromatic waves superimpose incoherently providing different phase retardation values for each wave. Secondly, since the PSi birefringence is wavelength dependent, light waves with different wavelengths have different birefringence.

(2) Phase retardation is a function of sample thickness and so thickness variations across the spot area will result in superimposing waves that see different thicknesses of the sample.

(3) Volume scattering in the inhomogeneous medium of PSi generates incoherent light which also contributes to the depolarization process [14].

We take into account the previously described effect by modeling the phase retardation as a stochastic process where the each of the light waves that pass through the porous silicon has a phase retardation given by:

$$\Delta\phi_s(\lambda) = \frac{2\pi}{\lambda+\Lambda}\cdot(d+\Gamma)\cdot\Delta n(\lambda+\Lambda)+\Psi \tag{2.8}$$

where Λ, Γ and Ψ are random variables with a Gaussian distribution whose most probable values are zero; and their standard deviation corresponds to the above described effects (1)-(3): Λ represents the variance in the wavelength due to the effect of the spectrometer bandwidth, Γ represents the irregularities in the porous silicon samples thickness and Ψ represents the contribution of the scattering to the depolarization process.

From Eq. 3.4 the normalized transmittance for the parallel and crossed polarizers is obtained be means of averaging an infinite (or high enough) number of light waves whose phase retardation is the random variable declared in Eq. 2.8. Those averaged transmittances can be thus calculated by the expressions:

$$T_{\parallel}(\lambda) = \lim_{N\to\infty}\left(\frac{1}{N}\sum_{1}^{N}\cos^2\left(\Delta\phi_s(\lambda)/2\right)\right) \tag{2.9}$$

$$T_{\perp}(\lambda) = \lim_{N\to\infty}\left(\frac{1}{N}\sum_{1}^{N}\sin^2\left(\Delta\phi_s(\lambda)/2\right)\right) \tag{2.10}$$

Using Eq. 2.9 and Eq. 2.10, the depolarization effect observed in the PSi membrane measurements were evaluated. Since the bandwidth of the spectrometer is known, and equal to 2 nm for 600-1000 nm and 3.1 nm for 1000-1600 nm, the standard deviation of the variables Γ and Ψ could be obtained by fitting calculated spectra from Eq. 2.9 and Eq. 2.10 to the measured spectrum. Fig. 2.10 (a) displays the $T_{\perp}(\lambda)/T_{\parallel}(\lambda)$ measured spectra and the simulated one from the previously described model for a 30 µm thickness sample. The best fitting between the experimental data and the simulation was obtained for standard deviations of Γ and Ψ equal to 100 nm and 0.13 rad, respectively. Fig. 2.10 (b) displays the measured and simulated spectra of a 64 µm thick PSi sample. In this case, the experimental data was fitted with standard deviations of Γ and Ψ of 100 nm and 0.3 rad, respectively. In other samples, the standard deviation of Γ was always found to be equal to 100 nm. However in the case of Ψ its standard deviation clearly increases with sample thickness.

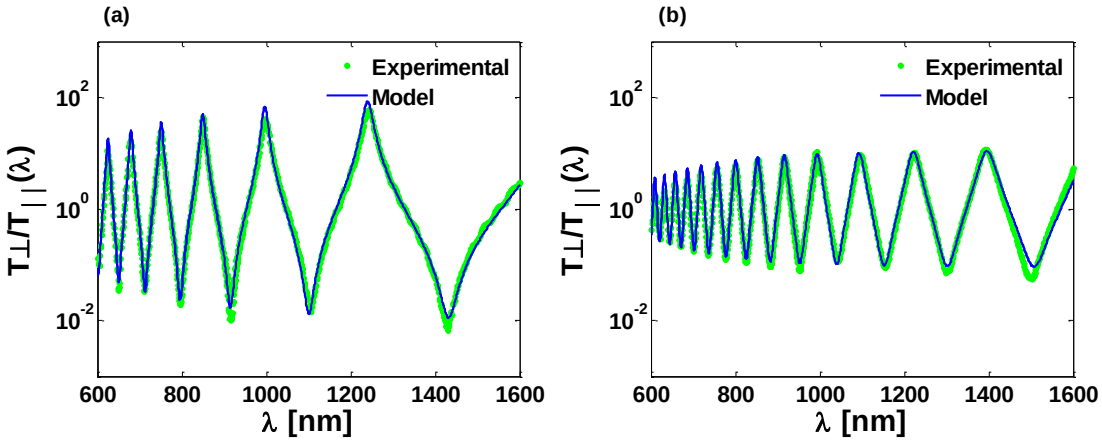

Figure 2.10 (a) Measured (green line) and fitted transmittance spectra (dotted blue line) for a PSi sample with a thickness of 30 µm (a) and a PSi sample with a thickness of 64 µm (b).

A consequence of the depolarization process is the spreading of the phase retardation given by Eq. 2.8. The uncertainties in the phase retardation produced by the depolarization is related to the resolution in the birefringence measurements of

the PSi samples. Theoretically, in an ideal system where there is no depolarization, the resolution of phase retardation (or birefringence) measurements is determined solely by the instrumentation limits. In reality since depolarization characterizes the randomness of the measurement process the resolution of phase retardation measurements is related to depolarization.

Fig. 2.11 shows the probability density function of the birefringence when the depolarization effect on the phase retardation is taken into account for the 30 µm and 64 µm samples, respectively. Comparing both graphs we can see that the main contribution to the total depolarization is that from light scattering by the pores which becomes more important for thicker samples, as expected. The depolarization process affects the measurement birefringence by increasing its standard deviation, which reduces the precision of the measured value.

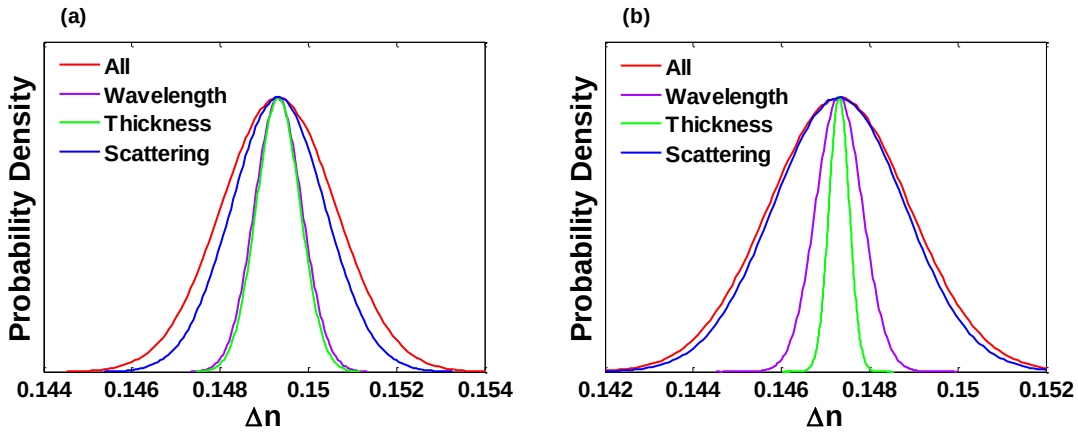

Figure 2.11 (a) Birefringence probability density functions in account for the three main factors that produces the depolarization for a 30 µm thick sample (a) and a 64 µm thick sample (b).

2.2.2 Phase-Sensitive Detection for Optical Sensing With Porous Silicon

Using the optical setup described in Section 2.1.2 the phase retardation of several porous silicon membranes fabricated from (100) surface oriented silicon was measured as a function of the membrane rotation angle. The first measurements were carried out in order to determine the birefringence of the different samples. After that, the phase retardation was measured when different solutions of water and ethanol filled the membranes pores. For this purpose the samples were immersed in an optical cuvette (mounted over the rotation stage) where the different solutions of water and ethanol were introduced. The detection limit (DL) of the system was also obtained and

lastly, the effect that temperature variation has over the PSi transducer performance was determined.

Birefringence

The birefringence of the membranes was obtained by fitting the measured phase retardation values to the theoretical values given by:

$$\Delta\phi = \frac{2\pi}{\lambda} d \cdot \Delta n \tag{2.11}$$

where λ is the light wavelength, d is the membrane thickness and Δn its birefringence. The birefringence of the fabricated mesoporous membranes is clearly related to the sensitivity, with membranes being more sensitive when they have greater birefringence.

The measured phase retardation values of the fabricated samples are shown in Fig. 2.12 where blue lines represent the theoretical values obtained from the fitting. Birefringence values of 0.06607, 0.04401 and 0.03712 were obtained for the 10, 30 and 60 µm samples, respectively. A clear decrease in birefringence values for thicker samples is seen.

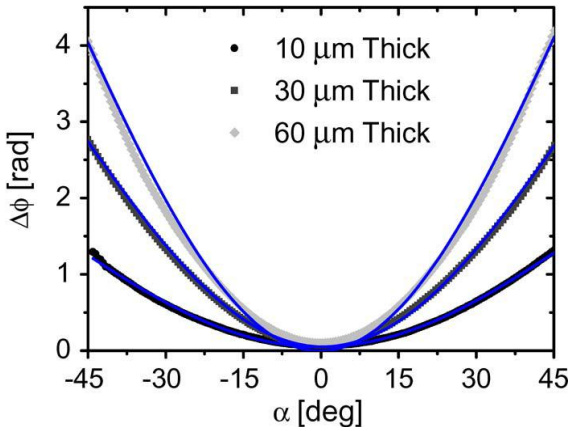

Figure 2.12 Phase retardation as a function of the sample rotation angle for samples with thicknesses of 10, 30 and 60 µm. Blue lines represent the theoretical values obtained from the fitting of Eq 3.7 to the experimental ones.

Sensitivity

One of the two key figures of merit for an optical transducer is the sensitivity of its optical response to given changes in the refractive index of its environment. In this section the sensitivities of the same three membranes from Fig. 2.12 are obtained by

measuring their phase retardations when immersed in liquids with different refractive indices. The liquids employed were water (n_{Water} = 1.328) and ethanol ($n_{Ethanol}$ = 1.354), as well as solutions of ethanol in water with concentrations of 50:50 and 75:25.

Results in air, water and ethanol for the 30 µm thick samples are shown in Fig. 2.13. Three clear annotations can be made: firstly, a reduction in the phase retardation is observed when the refractive index of the liquids that fill the samples increases. Secondly, both phase retardation and its derivative are greater for thicker samples, thus higher sensitivities are also expected. Thirdly, the change in the phase retardation and therefore sensitivity increases with the incidence angle.

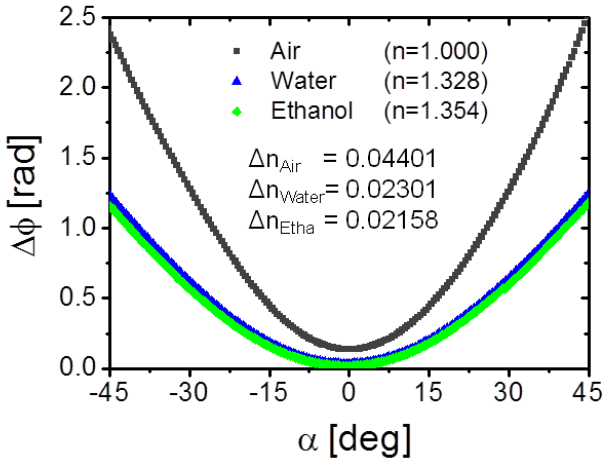

Figure 2.13 Phase retardation as a function of the light incidence angle for pores filled with air (gray line), water (blue line) and ethanol (green line) for a 30 µm thick sample.

Fixing the sample azimuthal rotation angle to 45° the phase retardation was measured when the samples were immersed in a solution of water:ethanol = 100:0, 25:75, 50:50 and 0:100. Fig. 2.14 shows the phase retardation change as a function of the solution refractive index showing a linear behavior between the liquids refractive index and the change in the phase retardation value. The phase retardation change was fitted to a linear function showing sensitivities of 1.6, 4 and 6 rad/RIU.

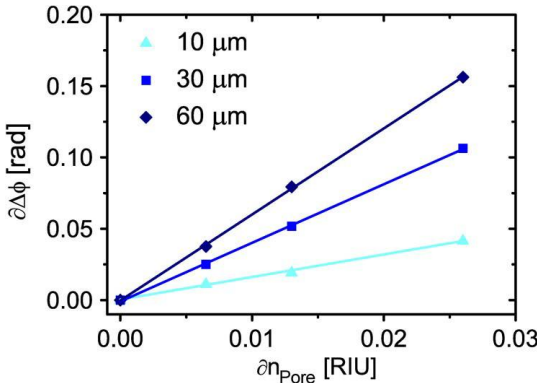

Figure 2.14 Phase retardation shifts for samples rotation angle of 45° as a function of the refractive index of the material that fills the pores for samples with thickness 10, 30 and 60 µm (dots). A solid line represents the linear fitting of the experimental data, showing sensitivities of 1.6 rad/RIU, 4 and 6 rad/RIU for the 10, 30 and 60 µm thick, respectively.

Detection limit

While the sensitivity gives an idea of the optical transducer performance, the usually more important figure of merit is the smallest refractive index change that it can respond to and be resolved, i.e., measure accurately, that is the detection limit (DL). The detection limits relates the sensitivity of the transducer to the resolution of the readout system by:

$$DL[RIU] = \frac{\sigma[rad]}{\partial\Delta\phi[rad/RIU]} \tag{2.12}$$

where σ is the measurement system resolution and $\partial\Delta\phi$ is the transducer sensitivity.

As previously reported [15, 16], light scattering in an inhomogeneous medium like PSi generates incoherent light which depolarizes the light thereby deteriorating the system resolution which for our system was measured at 10^{-7} rad for a quartz reference sample. The amount of depolarized light increases with the PSi sample thickness, so the system resolution needs to be tested for PSi samples with different thicknesses. The resolution of the measurement system was therefore obtained from the standard deviation of the measured birefringence values of the fabricated PSi samples (10, 30 and 60 µm thick) when they were immersed in water. We observed that the resolution decreases dramatically when the thickness of the samples increases: going from $1x10^{-5}$ to $5x10^{-5}$ to $5x10^{-4}$ for 10, 30 and 60 µm, respectively.

Table 2.1 Sensitivity, resolution and LoD of the three types of PSi samples measured in aqueous environment.

PSi sample thickness (µm)	Birefringence Δn	Sensitivity (rad/RIU)	Resolution (rad)	DL (RIU)
10	0.06607	1.6	$1x10^{-5}$	$6.25x10^{-6}$
30	0.04401	4	$5x10^{-5}$	$1.25x10^{-5}$
60	0.03712	6	$5x10^{-4}$	$8.33x10^{-5}$

Combining the values of the sensitivity obtained in the previous section and the resolution values obtained above, the limits of detection that can be reached with each membrane can be determined from Eq. 2.12. Table 2.1 shows the sensitivity, resolution and DL values for all the membranes measured. We can see that although the sensitivity increases with the sample thickness, at the same time the resolution decreases dramatically due to the increasing depolarization. The thinnest fabricated membrane (10 µm) is therefore potentially the most suitable for biosensing purposes due to its lower detection limit.

Thermo-optic coefficient measurement

The refractive index of the materials used to develop photonic or optical sensors, such as semiconductors or glasses is temperature dependent. Due to that, the optical properties of the transducer not only change when the refractive index of the surrounding media does, but also as the temperature of the same media does.

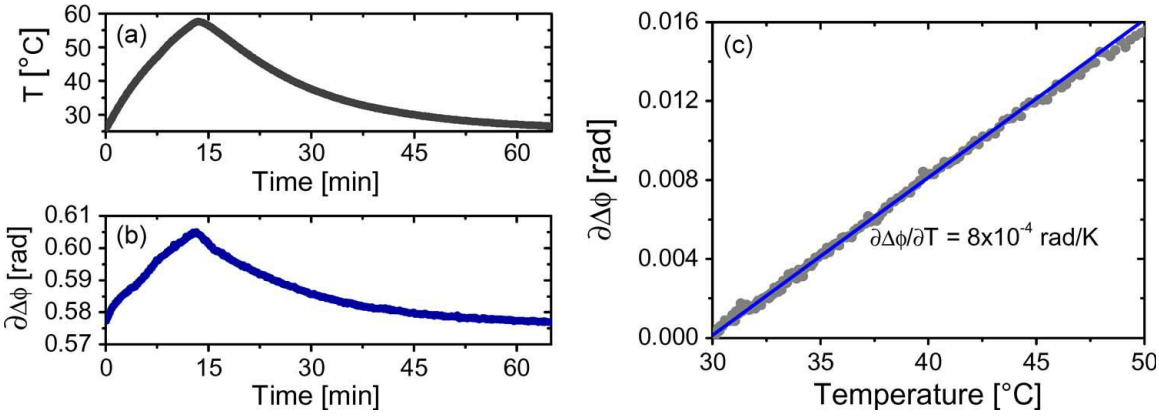

Figure 2.15 (a) Membrane temperature variation as a function of time. (b) Phase retardation as a function of time. (c) Phase retardation change as a function of the membrane temperature.

In order to quantify this change for biosensing the thermal stability of a PSi membrane in the same aqueous environment was determined. To do so, the sample holder was

placed in a closed chamber where the temperature could be increased from ambient to 50 °C and a platinum temperature sensor placed within it in order to monitor its temperature. As the chamber was heated both the phase retardation as well as the membrane temperature were monitored in time during a rising and falling cycle (Fig. 2.15(a) and Fig. 2.15(b)). The phase retardations was plotted against the chamber temperature (Fig. 2.15(c)) showing a liner dependence with a slope of $8x10^{-4}$ rad/°C. This value could be used to determine the resolution needed for the thermal stabilization system within an instrument based on such a sensing mechanism. Thus for a resolution in the phase retardation measurement of 10^{-5} rad, a thermal control with a temperature change of 12.5 mK will produce a change in the phase retardation equal to the system resolution. This means that an active thermal control with a setpoint temperature resolution of 1 mK will provide a thermal stability for phase variation one order of magnitude better than that of the overall system phase resolution.

2.2.3 Real-time polarimetric optical sensing using alumina membranes

Building on our previous demonstration of highly sensitive optical sensing with a mesoporous PSi membranes [16], we extended the polarimetric approach to macroporous AAO membranes within a flow-cell for real-time sensing. To do so, the birefringence of the macroporous AAO membranes was measured at different wavelengths and compared to those reported in the literature for AAO membranes with pores diameters below 40 nm [17]. Thereafter real-time volumetric sensing experiments were carried out at the same wavelengths in order to determine the sensitivity of the macroporous AAO membranes and therefore the detection limit of the overall polarimetric system.

Birefringence

Before running the volumetric sensing experiments the birefringence of the macroporous AAO membranes was measured at wavelengths of 808 nm, 980 nm and 1500 nm respectively. The birefringence values were obtained by measuring the phase retardation between the main components of light as a function of the light incidence angle over the AAO membrane which was mounted on a rotation stage [16]. The measured birefringence values were 0.020, 0.034 and 0.042 at the wavelengths of 808 nm, 980 nm and 1500 nm respectively. These values are comparable to the birefringence value of 0.062 reported in [17] for a nanoporous

alumina membranes with pores sizes below 40 nm. The birefringence of the macroporous AAO membranes decreases for shorter wavelengths due to the scattering depolarization process [14]. Light scattering is greater at shorter wavelengths increasing the depolarization of light and so decreasing the birefringence.

Sensitivity

After characterizing the wavelength dependent birefringence of the AAO membranes a real-time refractive index sensing experiment was carried out in order to determine the bulk refractive index sensitivity of AAO membranes as well as the detection limit of the whole polarimetric sensing system. To do so during three minutes we flowed through an AAO membrane different solutions of NaCl in deionized water (DIW) whose mass concentrations ranged from 0.2% to 2%. After each NaCl solution injection DIW was pumped through the membrane in order to prove that phase retardation had returned to its initial value and so the sensing system was reversible.

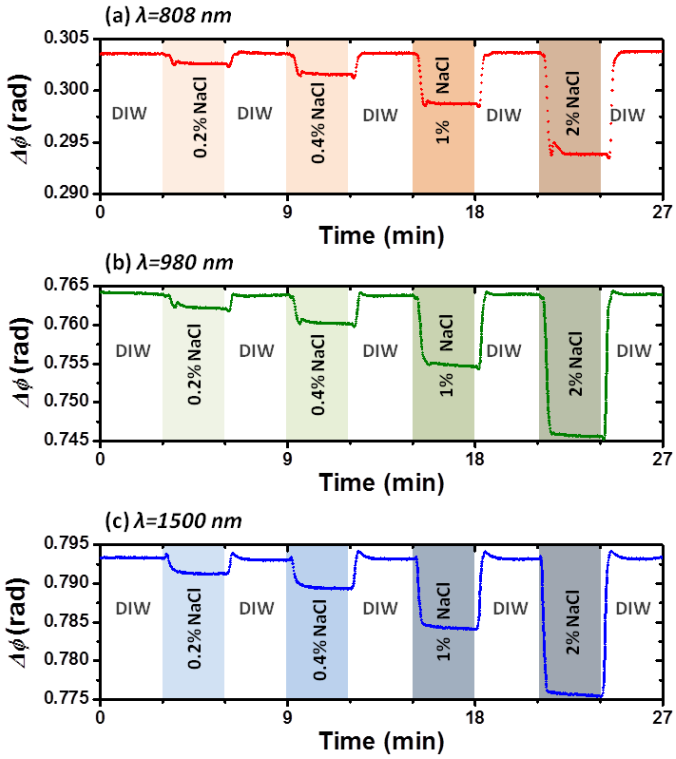

Figure 2.16 Sensorgram showing the signal response due to flowing through the macroporous AAO membrane different solutions of NaCl in deionized water when using laser diodes with wavelengths of 808 nm (a), 980 nm (b) and 1500 nm (c).

The phase retardation as a function of time is shown in Fig. 2.16 for the three wavelengths of 808 nm, 980 nm and 1500 nm. Immediately after switching, a transitory response of about one minute is produced by the new solution replacing the old one inside the pores. Furthermore, when the concentration of NaCl in the solution increases, the phase retardation decreases, as it is proportional to the index contrast between the alumina and the material filling the pores.

The phase retardation changes for the different solutions of NaCl at the three different wavelengths are plotted in Fig. 2.17 as a function of the refractive index of the NaCl solutions used.

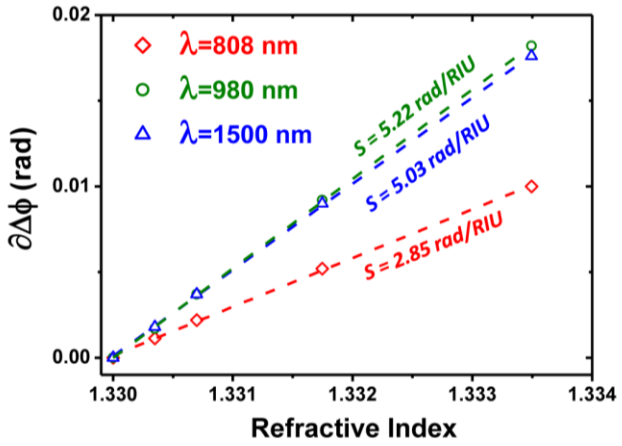

Figure 2.17 Phase retardation change as a function of the refractive index of the NaCl solutions flowing through the macroporous AAO membrane.

The bulk refractive index sensitivity S of the macroporous AAO membrane was obtained from the slope of the curves $\partial\Delta\phi$ versus refractive index. Linear fits to the curves provide values of 2.85, 5.22 and 5.03 rad/RIU at the wavelengths of 808 nm, 980 nm and 1500 nm respectively, with a correlation coefficient of $R^2=0.999$. A higher phase retardation and therefore greater sensitivity are obtained at a shorter wavelength and a higher birefringence which is itself wavelength dependent (Eq. 2.11). The highest sensitivity arises therefore not at the highest wavelength but at 980 nm.

Detection limit

The resolution of the measurement system is considered to be equal to the standard deviation of the measured phase retardation i.e. $2.3\text{x}10^{-5}$, $2.7\text{x}10^{-5}$ and $3\text{x}10^{-5}$ rad at

the wavelengths of 808 nm, 980 nm and 1500 nm respectively. The detection limits were calculated as $8.1x10^{-6}$, $5.2x10^{-6}$ and $6x10^{-6}$ refractive index units at the same wavelengths. The lowest detection limit occurs at 980 nm which enables a future low-cost multiplexed device by using Silicon CCD detectors whose prices are considerably cheaper than those of the CCD detectors in the 1500 nm range.

2.2.4 Real-time polarimetric biosensing using alumina membranes

After characterizing the bulk refractive index sensitivity and the detection limit of the alumina membranes, the immunoassay represented in Fig. 2.18 (a) was carried out at the wavelength that gave a lower detection limit (980 nm). First a baseline for the sensing system was obtained by flowing PBS solution during 10 minutes through a spotted and functionalized membrane within a flow cell. On achieving a stable baseline a 1 µg/mL concentration of primary antibody was flown through the membrane to bind specifically to the immobilized β-lactoglobulin protein. A secondary antibody (biotinilated anti-rabbit IgG) and a signal enhancer (strepavidin coated CdSe quantum dots) were used to increase the response produced by the binding between the first antibody and the b-lactoglobulin. Fig. 2.18 (b) shows the real-time response produced by the binding between the primary and secondary antibodies as well as the signal enhancement produced by the quantum dots.

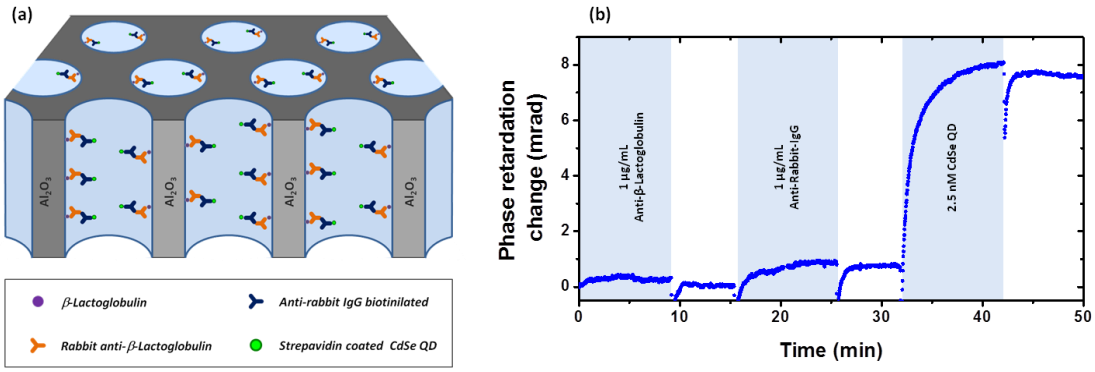

Figure 2.18 (a) A schematic representation of the immunoassay carried out in a macroporous alumina membrane. β–lactoglobulin protein was used as the immobilized antigen for the detection of rabbit anti-β-lactoglobulin. Secondary antibody biotinilated anti-rabbit-IgG and strepavidin coated CdSe quantum dots were used to increase the signal produced by the primary antibody. (b) A sensorgram showing the signal response due to the binding of the first and secondary antibodies as well as the enhancement produced by the strepavidin coated CdSe quantum dots.

Two control assays were carried out in order to demonstrate that the signal responses shown in Fig. 2.18 (b) are due to specific antigen-antibody interactions having taken place. The results of a first control assay run on an unspotted membrane shows the absence of a binding response when the β-lactoglobulin protein is not immobilized on the functionalized pores surface (Fig. 2.19 (a)). A second experiment run on a β-lactoglobulin spotted membrane shows the absence of a binding response when the first antibody (rabbit anti-β-lactoglobulin) is not present (Fig. 2.19 (b)), demonstrating that the response enhancement produced by the secondary antibody (anti-rabbit IgG biotinilated) as well as the enhancement produced by the strepavidin coated quantum dots are due to the presence of the first antibody.

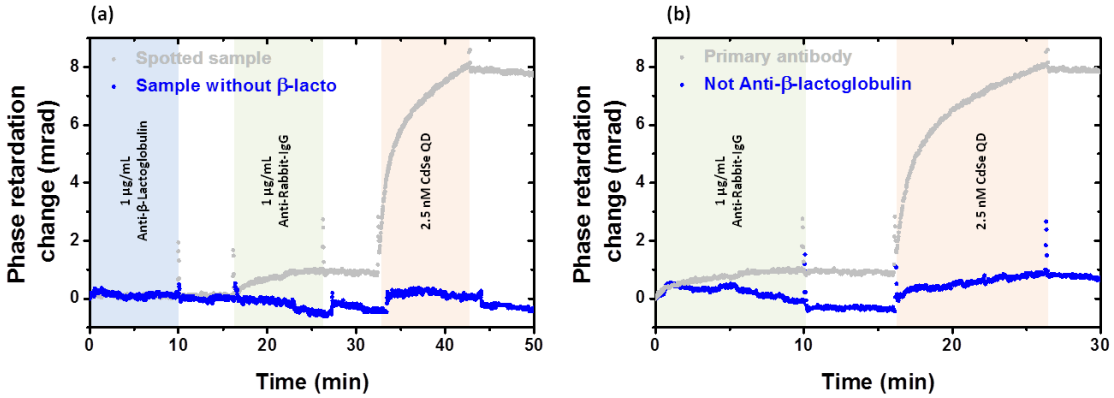

Figure 2.19 (a) Sensorgram showing a comparison between the responses of a membrane with β-lactoglobulin immobilized on its surface (gray line) and a membrane containing no β-lactoglobulin immobilized (blue line). (b) Sensorgram showing a comparison between the responses produced by the secondary antibody and the quantum dots on a membrane with the anti-β-lactoglobulin (gray line) and a membrane without the anti-β-lactoglobulin (blue line).

In summary, we have presented a biosensing device based on a free standing macroporous alumina membrane with flow-through properties that allows analytes to be targeted delivered for fast sensing response time and therefore real-time measurements for small sample volumes as it is. The interrogation mechanism of the system is based on a polarimetric readout setup for the measurement of the optical anisotropy of a macroporous alumina membrane, whose birefringence is highly sensitive to the refractive index of the material that fills its pores. Biosensing experiments carried out using β-lactoglobulin as an immobilized antigen provided a specific binding response between the rabbit anti-β-lactoglobulin and the antigen as

well as a response from the recognition between the secondary antibody anti-rabbit IgG and the primary antibody rabbit anti-β-lactoglobulin.

2.3 Conclusions

This thesis reports on the development of an optical biosensor that combines a polarimetric readout mechanism with an anisotropic free standing porous membrane. The treatment covers the complete development process, from the theoretical study of different porous membranes to the development of a high resolution polarimetric readout system as well as the characterization of a biosensor performance when an allergen protein is immobilized on the pore surfaces of an alumina membrane.

First, the use of porous silicon prepared from p-type (110) surface oriented silicon is investigated as a material for optical biosensing. Porous silicon prepared from this type of substrate presents its pores growing preferentially along the [100] and the [010] crystallographic directions which results in a difference in refractive index between the [001] and the [110] directions. This birefringence as well as its sensitivity to refractive index changes, hereafter sensitivity, were modeled theoretically using the Bruggeman model with both values presenting a maximum for a porosity of 0.55. The impact that the oxidation of the pore walls has on birefringence and sensitivity was also studied theoretically with results showing that silicon oxidation decreases the birefringence and sensitivity values and displaces the maximum to lower porosity values. Transmittance measurements were then made to obtain the birefringence values for different porous silicon samples when their pores were filled with air, ethanol and isopropanol, demonstrating a sensitivity of 1247 nm/RIU at 1500 nm. This experimental value was found to be in good agreement with the theoretical value when the effect of silicon oxidation was taken into account. Remaining (?) differences found between the theoretical transmittance spectra and the measured ones was found to be produced by a depolarization process. A statistical model was developed for determining the contributions from the depolarization sources such as the spectrometer bandwidth, the surface thickness variation and the scattering to the whole depolarization process. The main contribution to the depolarization process was found to be produced by light scattering. With the developed model it was possible to obtain the standard deviation of the birefringence measured values which is related to the measurement resolution.

The use of porous silicon membranes with 50 nm pore diameters prepared from n-type (100) surface oriented silicon was also studied. Samples prepared from this type of substrate presents their pores preferentially grown along the <100> direction with branches in the <113> directions, perpendicular to its planar surface. A high resolution phase retardation measurement system was set up for charactering the birefringence of several of these porous silicon samples, with thicknesses from 10 μm to 60 μm, at a wavelength of 1500 nm. The characterization of the porous silicon samples showed that their birefringence decreases with increasing sample thickness mainly due to the increasing amount of pores that grow in the <113> and therefore increasing depolarization from light scattering. Sensing experiments with the membranes using different solutions of water and ethanol showed that the thinner membranes (10 μm thick) present the lowest detection limit, equal to 6.25×10^{-6} RIU, due to a better resolution of measured birefringence values from less depolarization for thinner membranes. In taking account of the temperature influence on the birefringence, the thermooptic coefficient of a 10 μm thick membrane was measured in aqueous environment at 8×10^{-4} rad/°C.

As an alternative to porous silicon membranes, free standing macroporous alumina with pore diameters of 200 nm were studied as optical sensors. In comparison with the porous silicon membranes the macroporous alumina membranes have the advantage of flow-through properties due to their wider pores. With the proximity of the analytes to the pore surfaces a faster sensing response can be achieved. Initial measurements of their birefringence at a wavelength of 1500 nm show a value equal to 0.042, comparable with the value 0.062 reported in the literature for samples with pore diameters below 40 nm. Using laser diodes with wavelengths of 980 nm and 808 nm for measuring the birefringence of the same sample we observed that birefringence decreases for shorter wavelengths (0.034 at 980 nm and 0.020 at 808 nm). This fact can be attributed to the depolarization caused by the scattering of light that increases for shorter wavelength for a given pore diameter. Real-time refractive index sensing experiments were carried at the three mentioned wavelengths showing detection limits in the range of 10^{-6} RIU, with the lowest detection limit obtained at 980 nm being equal to 5.2×10^{-6} RIU.

Finally by functionalizing the alumina pore surfaces by an epoxysilane the allergen protein β-lactoglobulin was immobilized. Using a laser diode with a wavelength of 980 nm the specific binding response produced between the rabbit anti-β-

lactoglobulin and the antigen as well as a response from the recognition between the secondary antibody anti-rabbit IgG and the primary antibody rabbit anti-β-lactoglobulin was measured in real-time, demonstrating the biosensing capabilities of the free-standing membranes for obtaining fast sensing response time using small sample volumes.

For future work, a new functionalization method using a functional copolymer that reduces the non specific interactions will be tested. Furthermore, serum samples will be introduced into the functionalized porous alumina membrane to prove the application of this device for food allergy determination.

2.4 References

[1] Z. Gaburro, P. Bettotti, M. Saiani, L. Pavesi, L. Pancheri, C. J. Oton, and N. Capuj, "Role of microstructure in porous silicon gas sensors forNO2" Appl. Phys. Lett., Vol. 85(4), pp. 555-557 (2004).

[2] M. Ghulinyan, C. J. Oton, G. Bonetti, Z. Gaburro, and L. Pavesi, "Free-standing porous silicon single and multiple optical cavities," J. Appl. Phys. Vol. 93(12), pp. 9724-9729 (2003).

[3] K. A. Kilian, T. Böcking, and J. J. Gooding, "The importance of surface chemistry in mesoporous materials: lessons from porous silicon biosensors," Chem. Commun. (Camb.) Vol. 6: pp. 630-640 (2009).

[4] R. Liu, T. A. Schmedake, Y. Y. Li, M. J. Sailor, and Y. Fainman, "Novel porous silicon vapor sensor based on polarization interferometry" Sens. Actuators B, Chem., Vol. 87(1), pp. 58–62 (2002).

[5] C. F. Wong, "Birefringence measurement using a photoelastic modulator" Appl. Opt., Vol. 18(23), pp. 3996-3999 (1979).

[6] R. L. Smith and S. D. Collins, "Porous silicon formation mechanisms" J. Appl. Phys. Vol. 71(8), pp. 1-22 (1992).

[8] N. Künzner, D. Kovalev, J. Diener, E. Gross, V. Y. Timoshenko, G. Polisski, F. Koch, and M. Fujii, "Giant birefringence in anisotropically nanostructured silicon" Opt. Lett. Vol. 26(16), pp. 1265-1267 (2001).

[8] N. Künzner, J. Diener, E. Gross, D. Kovalev, V. Y. Timoshenko, and M. Fujii, "Form birefringence of anisotropically nanostructured silicon" Phys. Rev. B Vol. 71(19), pp. 195304 (2005).

[9] V. Y. Timoshenko, L. A. Osminkina, A. I. Efimova, L. A. Golovan, P. K. Kashkarov, D. Kovalev, N. Künzner, E. Gross, J. Diener, and F. Koch, "Anisotropy of optical absorption in birefringent porous silicon" Phys. Rev. B Vol. 67(11), pp. 113405 (2003).

[10] T. C. Choy, "Effective Medium Theory, Principles and Applications" Oxford University Press, (1999).

[11] K. Nishida, M. Fujii, S. Hayashi, and J. Diener, "Temperature dependence of optical anisotropy of birefringent porous silicon" Appl. Phys. Lett. Vol. 96(24), 243102 (2010).

[12] V. Kochergin, M. Christophersen, H. Föll, "Effective medium approach for calculations of optical anisotropy in porous materials" Appl. Phys. B Vol. 79, pp. 731-739 (2004).

[13] S. M. Nee, "Depolarization and retardation of a birefringent slab," J. Opt. Soc. Am. A Vol. 17(11), pp. 2067-2073 (2000).

[14] K. H. Jun and K. S. Lim, "Simulation of the depolarization effect in porous silicon," Appl. Opt. Vol 42(7), pp. 1211-1215 (2003).

[15] J. Álvarez, P. Bettotti, I. Suárez, N. Kumar, D. Hill, V. Chirvony, L. Pavesi, and J. Martínez-Pastor, "Birefringent porous silicon membranes for optical sensing" Opt. Exp., Vol. 19(27), pp. 26106-26116 (2011).

[16] J. Álvarez, N. Kumar, P. Bettotti, D. Hill, J. Martínez-Pastor, "Phase-Sensitive Detection for Optical Sensing With Porous Silicon" IEEE Photon. J., Vol. 4(3), pp. 986-995 (2012).

[17] A. Lutich, M. Danailov, S. Volchek, V. Yakovtseva, V. Sokol, and S. Gaponenko, "Birefringence of nanoporous alumina: Dependence on structure parameters" Appl. Phys. B, Vol. 84, pp. 327-331 (2006).

2.5 Resumen en Español

Los biosensores ópticos son dispositivos utilizados para la detección de sustancias biológicas. La mayor parte de estos dispositivos están basados en medir el cambio en el índice de refracción producido por la presencia de estas sustancias en su superficie. Para el desarrollo de este tipo de biosensores los materiales nanoesctruturados como el silicio poroso o la alúmina porosa han ganado especial atención debido principalmente a su gran superficie en comparación con los sensores planares. Una mayor superficie permite la captura de una cantidad mayor de sustancias lo que se traduce en mejores límites de detección. Además, para la realización de dispositivos "Point of Care" a menudo no sólo se requiere de biosensores que sean capaces de producir resultados rápidos sino también que produzcan estos resultados utilizando volúmenes pequeños de una muestra.

El tema principal de esta tesis es el desarrollo y evaluación de un biosensor óptico basado en una membrana porosa para aplicaciones que requieran volúmenes de muestra pequeños y tiempos de respuesta rápidos.

En primer lugar se ha estudiado el uso de silicio poroso fabricado a partir de substratos de silicio dopado tipo p con orientación (110). El silicio poroso fabricado a partir de éste tipo de substratos presenta sus poros orientados en las direcciones cristalográficas [100] y [010], lo que se traduce en diferentes índices de refracción efectivos en las direcciones [001] y [1$\bar{1}$0]. La birrefringencia se define como la diferencia entre el valor de los índices de refracción efectivos en las direcciones citadas previamente ($\Delta n = n_{[001]} - n_{[1\bar{1}0]}$). Los valores de birrefringencia pueden ser obtenidos utilizando el modelo de Bruggeman. Pare ellos los poros se modelan como elipsoides de revolución con sus ejes alineados en las direcciones [001] y [1$\bar{1}$0] (Fig. 2.6).

Utilizando este modelo se obtuvieron los valores teóricos de birrefringencia en función de la porosidad de la muestra para longitudes de onda de 600 a 1600 nm. Estos valores están representados en la Fig. 2.7. A continuación se calculó el cambio en la birrefringencia debido a la presencia de sustancias con distintos índices de refracción llenando los poros de la muestra. Se pudo observar que tanto la birrefringencia como su variación debida a la presencia de diferentes sustancia dentro

de los poros (sensibilidad) presentan un máximo para una porosidad de 0.55, por lo que lo que está será la porosidad óptima para obtener valores de alta sensibilidad.

Para obtener la birrefringencia de las muestras fabricadas a partir de substratos tipo p con orientación (110) se analizó el estado de polarización de una fuente de luz blanca con polarización lineal transmitida a través de las muestras.

La Fig. 2.9 a muestra los valores medidos de $T_{\perp}(\lambda)/T_{\parallel}(\lambda)$ para una muestra de 30 µm de espesor cuando sus poros están llenos de aire, y cuando la muestra está inmersa en etanol e isopropanol. A partir de los polos y ceros de los espectros mostrados en la Fig. 3.a se pueden obtener los valores de la birrefringencia cuando las diferentes sustancias llenas los poros. Estos valores están mostrados en la Fig. 2.9 b. El cambio en los valores de birrefringencia cuando las muestras están inmersas en etanol e isopropanol tiene valores de $1.8x10^{-3}$, $1.1x10^{-3}$ y $0.98x10^{-3}$ a las longitudes de onda de 810, 1300 y 1500 nm respectivamente que son similares a los valores predichos teóricamente de $1.3x10^{-3}$, $1.2x10^{-3}$ y $1.2x10^{-3}$ para las mismas longitudes de onda.

Aunque los valores máximos y mínimos de los espectros mostrados en la Fig. 2.9.a deberían ser cercanos a cero e infinito, se observa que en realidad estos valores están alrededor de 10^{2} y 10^{-2}. Esta diferencia entre los valores esperados y los obtenidos se debe a la depolarización, siendo el grado de aleatoriedad en la polarización de la luz recogida por el detector durante el proceso de medida. En el proceso de medida de la birrefringencia de las muestras de silicio poroso las tres fuentes principales que producen esta depolarización son el ancho de banda del espectrómetro utilizado en las medidas, la variación en el espesor de la muestra dentro del spot de medida y el scattering de la luz producido por los poros de la muestra. Para obtener cuantitativamente la contribución de éstos tres fuentes al proceso de depolarización se desarrolló un modelo que permite obtener la cuantificación de estas fuentes por medio de un ajuste entre los valores de los espectros medidos y los simulados teóricamente. En la Fig. 2.10.a y Fig. 2.10.b se muestran los espectros medidos y simulados utilizando el modelo desarrollado para dos muestras de 30 y 64 µm respectivamente. En ambos casos la principal fuente de depolarización es el scattering de la luz producido por los poros. Además, como era de esperar este valor crece con el grosor de la muestra. Una consecuencia del proceso de depolarización es el ensanchamiento en la función de densidad de probabilidad de los valores de birrefringencia obtenidos a partir de los espectros de transmisión. Esto implica un

empeoramiento en la resolución del sistema de medida como consecuencia del proceso de depolarización.

El uso de membranas de silicio poroso con diámetros de poro de 50 nm fabricadas a partir de sustratos de silicio dopados tipo n con orientación (100) también fue estudiado experimentalmente utilizando un sistema para obtener la birrefringencia de estas muestras a partir de medir el retardo de fase entre las componentes de la luz polarizadas en la dirección horizontal y vertical. El sistema de medida está basado en el uso de una fuente monocromática y un modulador fotoelástico para modular la polarización de la fuente monocromática. El uso de un amplificador lock-in para demodular la señal detectada se traduce en medidas de mayor resolución.

Las muestras fabricadas a partir de substratos tipo n con orientación (100) y resistividad igual a 0.01 Ω·cm presentan poros de 50 nm de tamaño que permiten la infiltración de biomoléculas en su interior. Estas muestras presentan sus poros en la dirección <100> con ramificaciones en las direcciones <113>.

Aunque el modelo de Bruggeman ha sido utilizado en la literatura para modelar muestras de alúmina porosa, su utilización para muestras de silicio poroso muestra discrepancias de alrededor de un orden de magnitud entre los valores calculados y los valores medidos experimentalmente. Esta discrepancia se debe fundamentalmente a no tener en cuenta los poros que crecen en las direcciones <113>. Para tener en cuenta estos poros se realizó una modificación en el modelo de Bruggeman introduciendo un factor r definido como la cantidad de poros en las direcciones <113> normalizado por el número total de poros.

Utilizando este nuevo modelo se calculó la birrefringencia de muestras fabricadas a partir de sustratos tipo n con orientación (100) en función de la porosidad de la muestra para distintos valores del parámetro r.

Utilizando el sistema de medida de retardo de fase con un laser de 1500 nm y montando las muestras en una plataforma de rotación que permite cambiar el ángulo de incidencia de la luz sobre las mismas, se midió el retardo de fase de muestras con grosores de 10, 30 y 60 µm cuando los poros de estás estaban vacios y tras sumergirlas en etanol y agua. Los valores del retardo de fase ($\Delta\phi$) medidos están representados y en la Fig. 2.13 para una muestra de 30 µm de grosor.

A pesar de que el retardo de fase es directamente proporcional al grosor de la muestra, se ha observado que los valores máximos de $\Delta\phi$ para la muestra de 30 µm

no son tres veces los valores de la muestra de 10 µm como cabría esperar. Esto se debe fundamentalmente a que cuando el grosor de la muestra aumenta su birrefringencia disminuye debido a que el número de poros que crece en las direcciones <113> aumenta y por lo tanto la cantidad de luz depolarizada aumenta, provocando una disminución en los valores de birrefringencia medidos.

Fijando el ángulo de rotación de la muestra a 45º se midió la sensibilidad de las distintas muestras fabricadas así como la resolución de los valores medidos, igual a la desviación estándar de estos valores. Se observó que la resolución de los valores de retardo de fase medidos empeora con el grosor de la muestra, hecho atribuido al proceso de depolarización. Relacionando la sensibilidad de las diferentes muestras con la resolución de los valores medidos se puede obtener el límite de detección del sistema de medida. Los valores de birrefringencia, sensibilidad, resolución y límite de detección de las diferentes muestras caracterizadas están mostrados en la Tabla 2.1.

La principal conclusión que se puede extraer es que aunque la sensibilidad crece con el grosor de las muestras, la resolución del sistema de medida empeora debido al proceso de depolarización, de modo que el valor más bajo del límite de detección se obtiene para la muestra de 10 µm de grosor cuyo valor es igual a 6.25×10^{-6} RIU.

Por último, dentro de la caracterización de las muestras fabricadas a partir de sustratos (100) se estudió la dependencia de los valores medidos de retardo de fase ($\Delta\phi$) con la temperatura. Para ello se utilizó la muestra de 10 µm de grosor sumergida en agua y se obtuvo un coeficiente termo-óptico igual a 8×10^{-4} rad/°C.

Como alternativa a las membranas de silicio poroso, también se ha estudiado la utilización de membranas de alúmina porosa 200 nm de tamaño de poro como sensores ópticos. Comparando estas membranas de alúmina porosa con las membranas previamente estudiadas de silicio poroso, estas membranas no sólo permiten que los analitos penetren en los poros sino que además permiten que fluyan a través de los poros, por lo que su distribución a los bioreceptores presentes en las paredes de los poros es mucho más rápida.

Inicialmente la birrefringencia de este tipo de membranas fue medida a 1500 nm obteniéndose un valor de 0.042. Este valor es comparable con el valor presentado en la literatura igual a 0.062 para membranas de alúmina con poros de 40 nm. Los valores de birrefringencia de estas membranas también se midieron a otras dos longitudes de onda inferiores, 980 nm y 808 nm, obteniendo valores de 0.034 y 0.020 respectivamente. Se puede observar que en este caso la birrefringencia disminuye para longitudes de onda más cortas debido a que la depolarización producida por el scattering de la luz se incrementa para estas longitudes de onda más cortas.

Tras medir la birrefringencia a varias longitudes de onda se procedió a realizar un experimento para obtener la sensibilidad de las membranas. Para ellos se hizo fluir a través de los poros diferentes soluciones de NaCl en agua desionizada con concentraciones desde 0.2% hasta 2% en peso. Los resultados de este experimento medidos a las longitudes de onda de 808 nm, 980 nm y 1500 nm están mostrados en la Fig. 2.16.

Los valores del cambio en el retardo de fase ($\partial\Delta\phi$) en función del índice de refracción de las diferentes soluciones NaCl utilizadas está representado en la Fig. 2.17 para las tres longitudes de onda de 808 nm, 980 nm y 1500 nm. La pendiente de las rectas a las que los valores son ajustados dan los valores de sensibilidad a las diferentes longitudes de onda, que son iguales a 2.85, 5.22 y 5.03 rad/RIU a las longitudes de onda de 808 nm, 980 nm y 1500 nm respectivamente.

A partir de las sensibilidades obtenidas a las diferentes longitudes de onda y de la resolución del sistema de medida cuyo valor es aproximadamente $\sigma \approx 2x10^{-5}$ rad se pueden obtener los límites de detección. Estos tienen valores iguales a $8.1x10^{-6}$, $5.2x10^{-6}$ y $6x10^{-6}$ RIU para las longitudes de onda de 808 nm, 980 nm y 1500 nm respectivamente. El mejor límite de detección se obtiene a una longitud de onda de 980 nm, lo que posibilitará el desarrollo de dispositivos multiplexados para la detección en paralelo de múltiples sustancias mediante el uso de detectores CCD de silicio cuyo precio es mucho menores que los detectores CCD utilizados en el rango de 1500 nm.

Por último, tras funcionalizar la superficie de los poros de alúmina utilizando un epoxisilano se depositó sobre los poros funcionalizados la proteína β–lactoglobulina. Esta proteína actúa como bioreceptor de modo que se pueden medir la respuesta específica producida por su anticuerpo anti-β-lactoglobulina cuando esta se une a ella. Además de esta interacción, en el bioensayo realizado de midió la interacción de este anticuerpo primario con su anticuerpo secundario "anti-rabbit-IgG" y el de este con un punto cuántico de alto índice de refracción conjugado con strepavidina. Este esquema de bioensayo está mostrado en la Fig. 2.18.a. El resultado de la variación en el retardo de fase de la muestra de alúmina porosa producida por el bioensayo representado en la Fig. 2.18.a está representado en la Fig. 2.18.b. Tras fluir a través de la membrana PBS durante 10 minutos y haberse obtenido una señal estable se introdujo en la celda de flujo el anticuerpo primario con una concentración de 1 µg/mL durante 10 minutos. Una vez que se inyectó el anticuerpo primario y tras lavar la membrana durante 6 minutos con PBS se introdujo el anticuerpo secundario con concentración de 1 µg/mL durante 10 minutos. Por último se probó el uso de puntos cuánticos de CdSe amplificadores de señal debido a que su índice de

refracción es mucho mayor al de las proteínas. Según se observa en la Fig. 2.18.b la señal producida por los puntos cuánticos es unas 7 veces igual a la señal producida por el anticuerpo secundario, de modo que queda demostrado su utilizad como amplificadores de señal.

Con el fin de demostrar que la señal medida y representada en la Fig. 2.18.b se debe a la interacción especifica entre la proteína β-lactoglobulina utilizada como receptor y su anticuerpo primario se repitió el bioensayo mostrado en la Fig. 2.18.a en una muestra donde el bioreceptor no está presente. El resultado de este bioensayo está representado en la Fig. 2.19.a. Se puede observar que cuando el bioreceptor no está presente no se obtiene ninguna señal, lo que indica que la señal obtenida en el experimento anterior se debe únicamente a la interacción entre la proteína β-lactoglobulina y su anticuerpo primario.

Un segundo experimento de control se llevó a cabo sobre una membrana donde se había inmovilizado la proteína β-lactoglobulin pero donde no se inmovilizó el anticuerpo primario. La respuesta producida por el anticuerpo secundario y por los puntos cuánticos se muestra en la Fig. 2.19.b. De nuevo se obtiene que ante la ausencia del anticuerpo primario el anticuerpo secundario no tiene donde anclarse por lo cual no obtiene señal.

Mediante el estudio teórico y los experimentos llevados a cabo se ha demostrado la posibilidad de desarrollar biosensores ópticos basados en medir la birrefringencia de membranas de material poroso como silicio o alúmina. Además, mediante el uso de membranas de alúmina con tamaños de poro de 200 nm se puede no sólo infiltrar las biomoléculas en los poros sino también hacerlas fluir a través de ellos, por lo que el tiempo del bioensayo es mucho menor además de tener que utilizar un volumen de muestra menor ya que cuando el analito se mueve cerca de su bioreceptor la probabilidad de ser capturado aumenta considerablemente.

Anexo de Publicaciones

(Paper Reprints)

1.

Birefringent porous silicon membranes for optical sensing

J. Álvarez, P. Bettotti, I. Suárez, N. Kumar, D. Hill, V. Chirvony, L. Pavesi, J. Martínez-Pastor, Opt. Express, Vol. 19 (27), pp. 26106-26116 (2011)

Birefringent porous silicon membranes for optical sensing

Jesús Álvarez,[1,*] Paolo Bettotti,[2] Isaac Suárez,[1] Neeraj Kumar,[2] Daniel Hill,[1] Vladimir Chirvony,[1] Lorenzo Pavesi,[2] and Juan Martínez-Pastor[1]

[1]*UMDO, Materials Science Institute, University of Valencia, P.O. Box 22085, 46071 Valencia, Spain*
[2]*Nanoscience Laboratory, Department of Physics, University of Trento, via Sommarive 14,38050 Povo-Trento, Italy*
[*]*jesus.alvarez@uv.es*

Abstract: In this work anisotropic porous silicon is investigated as a material for optical sensing. Birefringence and sensitivity of the anisotropic porous silicon membranes are thoroughly studied in the framework of Bruggeman model which is extended to incorporate the influence of environment effects, such as silicon oxidation. The membranes were also characterized optically demonstrating sensitivity as high as 1245 nm/RIU at 1500 nm. This experimental value only agrees with the theory when it takes into consideration the effect of silicon oxidation. Furthermore we demonstrate that oxidized porous silicon membranes have optical parameters with long term stability. Finally, we developed a new model to determine the contribution of the main depolarization sources to the overall depolarization process, and how it influences the measured spectra and the resolution of birefringence measurements.

OCIS codes: (260.1440) Birefringence; (290.5855) Scattering, polarization; (280.4788) Optical sensing and sensors.

References and links

1. A. Jane, R. Dronov, A. Hodges, and N. H. Voelcker, "Porous silicon biosensors on the advance," Trends Biotechnol. **27**(4), 230–239 (2009).
2. X. D. Hoa, A. G. Kirk, and M. Tabrizian, "Towards integrated and sensitive surface plasmon resonance biosensors: a review of recent progress," Biosens. Bioelectron. **23**(2), 151–160 (2007).
3. S. Patskovsky, M. Meunier, P. N. Prasad, and A. V. Kabashin, "Self-noise-filtering phase-sensitive surface plasmon resonance biosensing," Opt. Express **18**(14), 14353–14358 (2010).
4. F. Prieto, L. Lechuga, A. Calle, A. Llobera, and C. Dominguez, "Optimized silicon antiresonant reflecting optical waveguides for sensing applications," J. Lightwave Technol. **19**(1), 75–83 (2001).
5. X. Wei and S. M. Weiss, "Guided mode biosensor based on grating coupled porous silicon waveguide," Opt. Express **19**(12), 11330–11339 (2011).
6. K. De Vos, I. Bartolozzi, E. Schacht, P. Bienstman, and R. Baets, "Silicon-on-Insulator microring resonator for sensitive and label-free biosensing," Opt. Express **15**(12), 7610–7615 (2007).
7. T. Claes, J. Molera, K. De Vos, E. Schacht, R. Baets, and P. Bienstman, "Label-Free Biosensing With a Slot-Waveguide-Based Ring Resonator in Silicon on Insulator," IEEE Photon. J. **1**(3), 197–204 (2009).
8. N. Skivesen, A. Têtu, M. Kristensen, J. Kjems, L. H. Frandsen, and P. I. Borel, "Photonic-crystal waveguide biosensor," Opt. Express **15**(6), 3169–3176 (2007).
9. T. Xu, N. Zhu, M. Y. Xu, L. Wosinski, J. S. Aitchison, and H. E. Ruda, "Pillar-array based optical sensor," Opt. Express **18**(6), 5420–5425 (2010).
10. C. Kang, C. T. Phare, Y. A. Vlasov, S. Assefa, and S. M. Weiss, "Photonic crystal slab sensor with enhanced surface area," Opt. Express **18**(26), 27930–27937 (2010).
11. O. Bisi, S. Ossicini, and L. Pavesi, "Porous silicon: a quantum sponge structure for silicon based optoelectronics," Surf. Sci. Rep. **38**(1–3), 1–126 (2000).
12. V. S. Lin, K. Motesharei, K. P. Dancil, M. J. Sailor, and M. R. A. Ghadiri, "A porous silicon-based optical interferometric biosensor," Science **278**(5339), 840–843 (1997).
13. V. Mulloni and L. Pavesi, "Porous silicon microcavities as optical chemical sensors," Appl. Phys. Lett. **76**(18), 2523–2525 (2000).
14. M. S. Salem, M. J. Sailor, K. Fukami, T. Sakka, and Y. H. Ogata, "Sensitivity of porous silicon rugate filters for chemical vapor detection," J. Appl. Phys. **103**(8), 083516 (2008).

#150731 - $15.00 USD Received 11 Jul 2011; revised 7 Oct 2011; accepted 31 Oct 2011; published 7 Dec 2011

15. T. Jalkanen, V. Torres-Costa, J. Salonen, M. Björkqvist, E. Mäkilä, J. M. Martínez-Duart, and V. P. Lehto, "Optical gas sensing properties of thermally hydrocarbonized porous silicon Bragg reflectors," Opt. Express **17**(7), 5446–5456 (2009).
16. E. Gross, D. Kovalev, N. Künzner, V. Y. Timoshenko, J. Diener, and F. Koch, "Highly sensitive recognition element based on birefringent porous silicon layers," J. Appl. Phys. **90**(7), 3529–3532 (2001).
17. M. Kompan, J. Salonen, and I. Shabanov, "Anomalous birefringence of light in free-standing samples of porous silicon," J. Exp. Theor. Phys. **90**(2), 324–329 (2000).
18. B-H. O, R. Liu; Y. Y. Li, M. Sailor, and Y. Fainman, "Vapor sensor realized in an ultracompact polarization interferometer built of a freestanding porous-silicon form birefringent film," IEEE Photo. Technol. Lett. **15**(6), 834–836 (2003).
19. R. L. Smith and S. D. Collins, "Porous silicon formation mechanisms," J. Appl. Phys. **71**(8), R1– R22 (1992).
20. N. Künzner, D. Kovalev, J. Diener, E. Gross, V. Y. Timoshenko, G. Polisski, F. Koch, and M. Fujii, "Giant birefringence in anisotropically nanostructured silicon," Opt. Lett. **26**(16), 1265–1267 (2001).
21. N. Künzner, J. Diener, E. Gross, D. Kovalev, V. Y. Timoshenko, and M. Fujii, "Form birefringence of anisotropically nanostructured silicon," Phys. Rev. B **71**(19), 195304 (2005).
22. V. Y. Timoshenko, L. A. Osminkina, A. I. Efimova, L. A. Golovan, P. K. Kashkarov, D. Kovalev, N. Künzner, E. Gross, J. Diener, and F. Koch, "Anisotropy of optical absorption in birefringent porous silicon," Phys. Rev. B **67**(11), 113405 (2003).
23. J. E. Sipe and R. W. Boyd, "Nonlinear susceptibility of composite optical materials in the Maxwell Garnett model," Phys. Rev. A **46**(3), 1614–1629 (1992).
24. H. Looyenga, "Dielectric constants of heterogeneous mixtures," Physica **31**(3), 401–406 (1965).
25. T. C. Choy, "Effective Medium Theory, Principles and Applications," Oxford University Press, (1999).
26. K. Nishida, M. Fujii, S. Hayashi, and J. Diener, "Temperature dependence of optical anisotropy of birefringent porous silicon," Appl. Phys. Lett. **96**(24), 243102 (2010).
27. V. Kochergin, M. Christophersen, H. Föll, "Effective medium approach for calculations of optical anisotropy in porous materials," Appl. Phys. B **79**, 731–739 (2004).
28. K. A. Kilian, T. Böcking, and J. J. Gooding, "The importance of surface chemistry in mesoporous materials: lessons from porous silicon biosensors," Chem. Commun. (Camb.) (6): 630–640 (2009).
29. I. Suárez, V. Chirvony, D. Hill, and J. Martínez-Pastor, "Simulation of surface-modified porous silicon photonic crystals for biosensing applications," Phot. Nano. Fund. Appl., doi:10.1016, (2011)
30. M. Ghulinyan, C. J. Oton, G. Bonetti, Z. Gaburro, and L. Pavesi, "Free-standing porous silicon single and multiple optical cavities," J. Appl. Phys. **93**(12), 9724–9729 (2003).
31. A. E. Pap, K. Kordás, T. F. George, and S. Leppävuori, "Thermal Oxidation of Porous Silicon: Study on Reaction Kinetics," J. Phys. Chem. B **108**(34), 12744–12747 (2004).
32. S. M. Nee, "Depolarization and retardation of a birefringent slab," J. Opt. Soc. Am. A **17**(11), 2067–2073 (2000).
33. K. H. Jun and K. S. Lim, "Simulation of the depolarization effect in porous silicon," Appl. Opt. **42**(7), 1211–1215 (2003).

1. Introduction

During the last decade the development of optical sensors has been pursued by many research groups due to the need for simple, low cost, fast and accurate substance identification in applications such as clinical diagnosis, food safety, environmental monitoring and homeland security [1]. To this end, various materials and detection mechanisms such as Surface Plasmon Resonance (SPR) [2,3], photonic waveguides [4,5], microring resonators [6,7], and photonic crystals [8–10] have been designed and implemented as optical sensors.

Porous Silicon (PSi) has unique properties for sensing application due to its morphological structure that presents a large surface area/volume ratio, adjustable porosity, pore sizes and layer thickness [11]. Moreover its low cost fabrication process and its compatibility with microfabrication technologies make possible to use it for the fabrication of highly integrated sensors. In consequence, several interferometric schemes using (100) PSi have been proposed for optical sensors [12–15]. PSi made from (110) Si wafers however, presents very high birefringence values, which is very sensitive to the presence of different substances within its pores [16–18]. The use of this anisotropic PSi together with optical polarimetric schemes for measurement of birefringence therefore makes it an ideal candidate for commercially viable highly sensitive optical sensors.

In this work PSi membranes produced from (110) surface oriented silicon are evaluated as a material for sensing applications. Firstly, in section 2 a theoretical study of the birefringence and sensitivity of the membranes is presented. For this purpose, we extend the binary

#150731 - $15.00 USD Received 11 Jul 2011; revised 7 Oct 2011; accepted 31 Oct 2011; published 7 Dec 2011

Bruggeman model used in literature by including an important external effect in PSi such as the oxidation of the pore surface walls. Then, the changes in the birefringence from filling the pores by different substances are calculated theoretically. Section 3 describes the fabrication process for anisotropic PSi membranes with different pore sizes and thicknesses, with and without a post thermal oxidation process. Section 4 reports the optical characterization of the samples when the pores are filled by different liquids. Birefringence measurements are only found to be in good agreement with those predicted by the model when the effect of silicon oxidation is considered. It is remarkable to say that these measurements show long time stability, with the thermal oxidation having reduced drift. Within these birefringence sensitivities of the membranes are found to be as high as 1250nm/RIU at 1500 nm. Finally, in Section 5 depolarization is identified as the cause of the discrepancies between measured and theoretical spectra. These discrepancies have already been found in previous work; however, to the best of our knowledge, it is the first time when they are studied. The three main factors contributing to the depolarization were found to be: spectrometer bandwidth, thickness variations of PSi and scattering. Using a novel developed statistical model the contribution of each factor to the total depolarization is identified by fitting the measured spectra to the theoretical one. This model also allows obtaining the standard deviation of the measured birefringence.

2. Theoretical

Bulk silicon is an isotropic material due to its diamond cubic crystal structure, however PSi prepared from (110) Si surface oriented substrates presents a high anisotropy due to pores grow preferentially along the $[100]$ and $[010]$ crystallographic directions [19], as seen in Fig. 1. The orientation of the pores along those directions results in a difference in the refractive indices along the $[001]$ and the $[1\bar{1}0]$ directions [20].

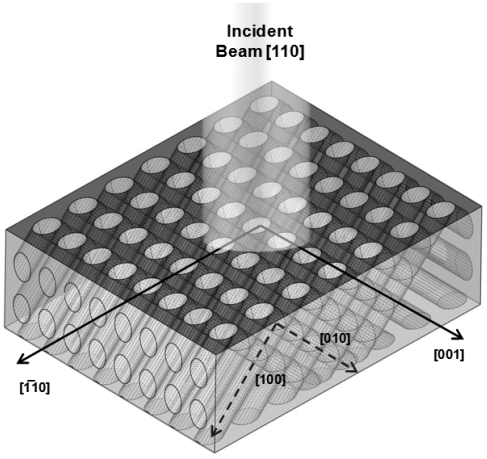

Fig. 1. Scheme of an anisotropic PSi layer produced from a (110) surface oriented Si wafer.

In accounting for the anisotropic microstructure of this type of PSi, the pores are modeled as ellipsoids of revolution with their axes of symmetry aligned along the $[001]$ direction and the $[1\bar{1}0]$ direction lying on the (110) surface plane. The depolarization factors, $L_{[001]}$ and $L_{[1\bar{1}0]}$, describe the screening efficiency of external electromagnetic fields inside the ellipsoids, characterizing the optical properties of the PSi layer. Their values are given by Eq. (1) and Eq. (2) [21,22]:

#150731 - $15.00 USD Received 11 Jul 2011; revised 7 Oct 2011; accepted 31 Oct 2011; published 7 Dec 2011

$$L_{[1\bar{1}0]} = \frac{1}{1-\xi^2}\left(1-\xi\cdot\frac{\arcsin\left(\sqrt{1-\xi^2}\right)}{\sqrt{1-\xi^2}}\right) \quad (1)$$

$$L_{[001]} = \frac{1-L_{[1\bar{1}0]}}{2} \quad (2)$$

where $\xi = a/b$, being a and b the major and minor ellipse axes respectively. As the directions [100] and [010] form an angle of 50.77° with respect to the normal plane (110) [19], the ratio ξ has a value of 0.7746. Substituting this value into Eq. (1) and (2) depolarization factors of $L_{[001]}$ equal to 0.2938 and $L_{[1\bar{1}0]}$ equal to 0.4035 are obtained.

Among the various methods that can be used to estimate the birefringence of an anisotropic PSi layer, such as the Maxwell-Garnett theory [23], the Looyenga method [24] or the Bruggeman model [25], for this work the Bruggeman model was chosen since for samples with porosities below 0.8 it provides more accurate predictions than the other methods [26,27]. The only assumption made by this model is the static electric field condition, which is satisfied when wavelength of light is much longer than the transverse pore size. As is described in section 3, fabricated samples have porosities below 0.8 and pore diameters smaller than 100 nm, fulfilling the static electric field condition. The Bruggeman model is described by Eq. (3):

$$\sum_i f_i \frac{n_i^2(\lambda)-n_{[001],[110]}^2}{n_{[001],[110]}^2+L_{[001],[110]}\cdot(n_i^2(\lambda)-n_{[001],[110]}^2)} = 0 \quad (3)$$

where f_i is the volume fraction of the different materials that form the PSi membrane, $n_i(\lambda)$ their refractive indices, and $L_{[001]}$ and $L_{[1\bar{1}0]}$ the previously described depolarization factors. The unknown $n_{[001]}$ and $n_{[1\bar{1}0]}$ are the refractive indices along the main axes and are related to the birefringence by means of $\Delta n = n_{[001]} - n_{[1\bar{1}0]}$. Equation (3) can be solved using numerical methods.

2.1 PSi birefringence and sensitivity

The main objective in using PSi for polarimetry based sensing is to maximize the birefringence change coming from the presence of different substances filling the pores. For this purpose Eq. (3) was solved for wavelengths from 600 nm to 1600 nm and porosities ranged from 0 to 1. It was considered a binary PSi layer composed by silicon and empty pores ($n_{Pore} \approx 1$). The results of the calculated birefringence are displayed in Fig. 2 (a).

#150731 - $15.00 USD Received 11 Jul 2011; revised 7 Oct 2011; accepted 31 Oct 2011; published 7 Dec 2011

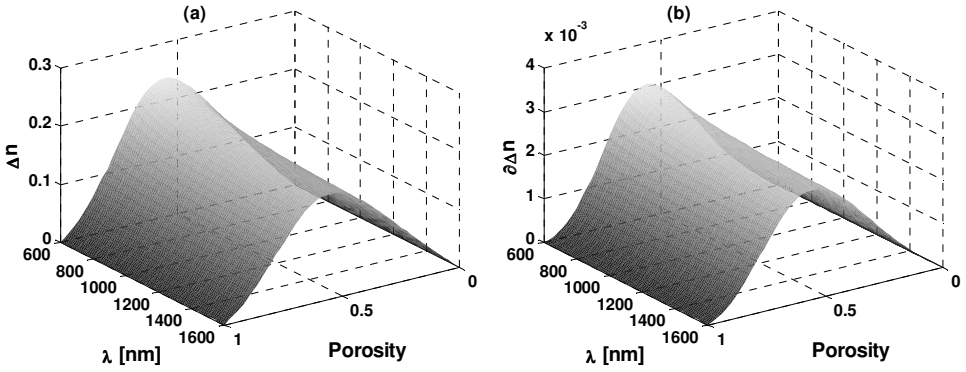

Fig. 2. (a) Birefringence computed using the Bruggeman model for a binary PSi layer (silicon and pores filled with air) as a function of wavelength and porosity. (b) Birefringence change due to presence of different substances inside the pores (ethanol and isopropanol) as a function of wavelength and porosity.

Two clear observations can be made. First, it can be noted that birefringence has a maximum for a porosity of 0.55. Secondly, it decreases with wavelength, following the behavior of silicon refractive index.

In a second step the birefringence change when pores are filled by different material is simulated. For this purpose, Eq. (3) was solved for the pores being filled with ethanol ($n_{Pore} \approx 1.36$) and isopropanol ($n_{Pore} \approx 1.377$). Birefringence changes due to refractive index changes within the pores ($\partial\Delta n = \Delta n\big|_{n_{Pore}=1.36} - \Delta n\big|_{n_{Pore}=1.377}$) are shown in Fig. 2 (b). Like in the case of filling the pores by air, the maximum birefringence change is seen for a porosity of 0.55. It can therefore be concluded that in order to have an efficient PSi membrane sensor, the refractive index contrast must be as high as possible and porosity should be as near to 0.55 as fabrication permits.

2.2 Effect of silicon oxidation

The internal pore surfaces of freshly prepared PSi are prone to oxidize under ambient conditions leaving a thin SiO_2 layer over recently etched PSi pores, see Fig. 3 (a). Furthermore, in order to stabilize the surface and avoid changes in the PSi during sensing the silicon dioxide layer is purposely increased via a thermal oxidation process [28]. Here, the effect that this silicon dioxide layer has over the birefringence is modeled by including its volume fraction in Eq. (3). Thus, a three component medium has now been formed consisting of silicon, silicon dioxide and pores. The bonding of silicon with oxygen produces a 2.27 fold increase in volume over bulk silicon, so silicon oxidation produces a reduction of pores and silicon volume fractions [29]. The new volume fractions of silicon and pores are related to the silicon dioxide volume fraction by Eq. 4 and 5 respectively:

$$f_{Si} = f_{Si_0} - f_{SiO_2} / 2.27 \tag{4}$$

$$f_{Pores} = f_{Pores_0} - 1.27 / 2.27 \cdot f_{SiO_2} \tag{5}$$

where f_{Si_0} and f_{Pores_0} denotes the volume fraction of the silicon and pores prior to oxidation. The effect that grown silicon dioxide has over the birefringence is depicted in Fig. 3 (b). As can be seen, silicon dioxide reduces the birefringence for porosities above 0.33. This reduction in birefringence is attributed to the decrease of the index contrast between the initial PSi layer, and the same layer after the oxidation process. For porosities below 0.33 the

#150731 - $15.00 USD Received 11 Jul 2011; revised 7 Oct 2011; accepted 31 Oct 2011; published 7 Dec 2011

volume fraction of silicon is so high that its oxidation causes an increase in the index contrast, and then, a small increment in the birefringence value.

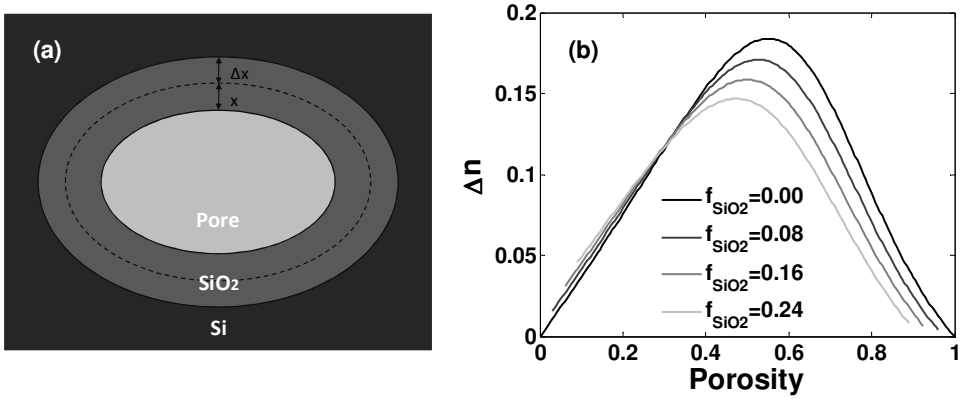

Fig. 3. (a) Pore cross-section scheme. The surface oxidation of the pores walls leads to a volume expansion (dashed line). (b) Birefringence variation as a function of the PSi layer porosity for several silicon dioxide volume fractions.

3. Fabrication

The PSi birefringent properties were characterized for a set of samples consisting of nanoporous silicon etched into p-type (110) Si with resistivity of 0.01-0.001 Ohm/cm. Pores sizes were in the range of few tens of nanometers, as shown in Fig. 4. Samples were prepared by electrochemical etching using a solution composed of HF:Ethanol = 3:7 by volume, considering an initial HF concentration of 48%. A current density of 25 mA/cm^2 was used during the etching.

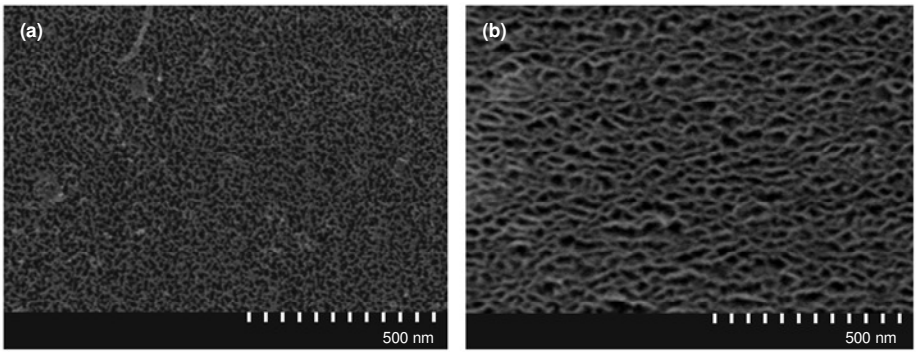

Fig. 4. Surface SEM images of two fabricated and optically characterized samples: (a) PSi sample with pore size in the order of a 10 nm, (b) PSi sample with pores size in the order of 50 nm.

For subsequent optical characterization, porous membranes were detached from the bulk silicon layer that supports them by applying a strong current burst at the end of the etching completely dissolving the bottom silicon layer that surrounds the etched area. With this procedure the membrane can be transferred to another substrate. More details can be found in [30]. Several (110) PSi membranes of various thicknesses were fabricated and transferred to a glass substrate in which a 3-4 mm circular hole was made in order to characterize the birefringence and depolarization effects as a function of optical path.

Before measuring the birefringence of the fabricated samples, a thermal oxidation at 200°C for 12 hours was carried out in order to stabilize pore surfaces during the

#150731 - $15.00 USD Received 11 Jul 2011; revised 7 Oct 2011; accepted 31 Oct 2011; published 7 Dec 2011

measurements. At this temperature, after 12 hours, the silicon dioxide grown has already saturated to a volume fraction ratio of 0.16 ($f_{SiO_2} / f_{Si} = 0.16$) [31].

4. Experimental and results

The optical anisotropy of fabricated samples was determined by analyzing the state of polarization of the light transmitted through them. The setup depicted in Fig. 5 shows how the output light from a tungsten halogen lamp is collimated and then polarized linearly at 45° with respect to the horizontal direction. The linearly polarized light passes through the anisotropic PSi sample which is oriented with its [001] and $[1\bar{1}0]$ crystallographic directions parallel to the vertical and horizontal directions, respectively. The lamp spot in the position where the PSi samples are placed had a size of 1.2 mm with a divergence of 1°. The components of light along the [001] and $[1\bar{1}0]$ directions experiment a phase shift given by:

$$\Delta\phi(\lambda) = \frac{2\pi}{\lambda} \cdot d \cdot \Delta n(\lambda) \tag{6}$$

where λ is the incident wavelength of light, d the PSi membrane thickness and $\Delta n(\lambda)$ its birefringence. The phase shift is converted into an amplitude shift through traversing a second polarizer (usually called analyzer), which is then recorded by a spectrometer. To cover the transmission spectrum in the whole region of interest, from 600 to 1600 nm, the spectrometers used were an Ocean Optics NIR512 with a bandwidth of 3.1 nm and an Ocean Optics RedTide 650 with a bandwidth of 2 nm.

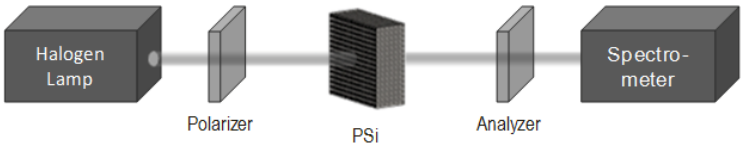

Fig. 5. Scheme of the setup used for the optical characterization of the PSi membranes.

The normalized transmittance (light recorded in the parallel or cross direction divided by the sum of the light in the parallel and cross directions) for polarizers placed in parallel or crossed is given by:

$$T_{\parallel}(\lambda) = \cos^2\left(\Delta\phi(\lambda)/2\right) \tag{7}$$

$$T_{\perp}(\lambda) = \sin^2\left(\Delta\phi(\lambda)/2\right) \tag{8}$$

where $\Delta\phi(\lambda)$ is the phase retardation given by Eq. (6).

4.1. Sensitivity

The sensitivity of the PSi membranes was determined by filling the samples with the different liquids studied in section 2 and then measuring the shift produced in the transmission spectrum. For this purpose we placed a thermally treated PSi sample in a flow cell made from optical glass. This flow cell was then filled with ethanol ($n_{Etha} \approx 1.36$) and isopropanol ($n_{Isop} \approx 1.377$). A few seconds after filling the flow cell with the liquids, the transmission spectra stabilize, indicating that the liquids had completely filled the pores. Figure 6 (a) shows the values of $T_{\perp}(\lambda)/T_{\parallel}(\lambda)$ versus wavelength for a thermally oxidized PSi sample with a thickness of 30 μm when the pores are empty (red line), when filled with isopropanol (green

#150731 - $15.00 USD Received 11 Jul 2011; revised 7 Oct 2011; accepted 31 Oct 2011; published 7 Dec 2011

line) or ethanol (blue line). From this graph, the birefringence was obtained and is depicted in Fig. 6 (b). A blue shift in the $T_{\perp}(\lambda)/T_{\parallel}(\lambda)$ can be clearly seen in Fig. 6 (a) that is associated with the birefringence change seen in Fig. 6 (b). The birefringence change between the samples filled with isopropanol and filled with ethanol was obtained from the curves fitted to experimental birefringence values depicted in Fig. 6 (b). These values are $1.8\text{x}10^{-3}$, $1.1\text{x}10^{-3}$, and $0.98\text{x}10^{-3}$ for the wavelengths of 810, 1300 and 1500 nm respectively. The values predicted in the model proposed in section 2 when a silicon oxide volume fraction of 0.16 was considered were $1.3\text{x}10^{-3}$ at 810 nm, and $1.2\text{x}10^{-3}$ at 1300 and 1500 nm. Then, the model for estimating the optical sensitivity of a PSi membrane in a polarimetric scheme is thereby validated with the effect of silicon oxidation found to be a critical parameter.

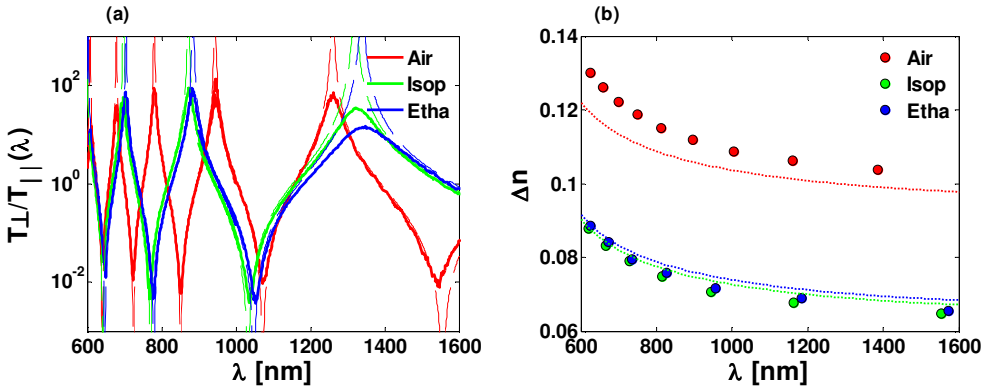

Fig. 6. (a) Transmission spectra for empty pores (red line), pores completely filled with isopropanol (green line) and ethanol (blue line). Dashed lines represent the corresponding theoretical curves. (b) Birefringence data obtained from the measured spectra (dots) and simulated curves using the Bruggeman model (dashed lines) for air (red), isopropanol (green) and ethanol (blue).

In order to compare PSi membranes with other sensing platforms, optical sensitivity was obtained in terms of nm per Refractive Index Unit (RIU). This calculation was done by dividing the measured blueshift by the refractive index change ($n_{IPA} - n_{ETHA} = 0.017$) from the spectra and data shown in Fig. 6 (a)-(b). In this way, the anisotropic PSi membranes exhibit sensitivities of 626 nm/RIU at 810 nm, 1135 nm/RIU at 1300 nm and 1247 nm/RIU at 1500 nm. In comparison, for microring resonators made in SOI, sensitivities of 293 nm/RIU for bulk refractive index measurements were reported [7], whilst for photonic crystals made from Si pillars in a SiO_2 substrate, sensitivities of 350 nm/RIU were reported [9]. Therefore, the sensitivity provided by our anisotropic PSi membranes indicates their high potential for chemical and biomolecular sensing applications.

4.2. PSi stability over time

An important issue for optical sensors is the stability of their properties with time. In order to characterize this limitation in our PSi membranes an experiment was carried out to determine the drift of the birefringence over time. Two PSi samples were used for this purpose, both of them with similar pore diameters. The first sample consisted of a porous silicon membrane without any thermal treatment. The second one was thermally oxidized in an oven at 200 °C during twelve hours. The birefringence of both samples was measured immediately after the fabrication process, and again one hundred and fifteen days later (Fig. 7). The variation of the birefringence for the first sample is equal to $1.2\text{x}10^{-2}$ RIU at 1500 nm, corresponding to a birefringence drift of $7\text{x}10^{-8}$ RIU/min. For the thermally treated sample, the birefringence

#150731 - $15.00 USD Received 11 Jul 2011; revised 7 Oct 2011; accepted 31 Oct 2011; published 7 Dec 2011

variation is approximately seven times less at $1.6\text{x}10^{-3}$ RIU at 1500 nm, corresponding to a drift of $9\text{x}10^{-9}$ RIU/min.

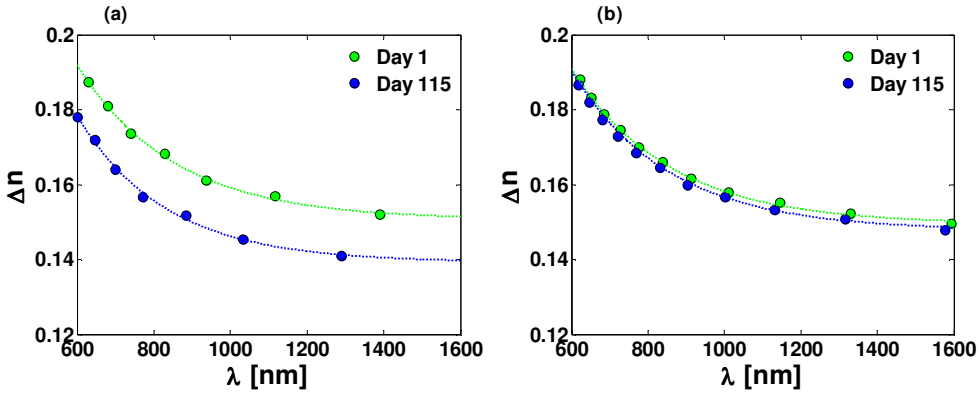

Fig. 7. Birefringence measured immediately after samples fabrication (green dots) and one hundred fifteen days later (blue dots) for a PSi sample without thermal treatment (a) and for a sample oxidized at 200° during 12 hours (b).

5. Depolarization effects in anisotropic PSi

Although poles and zeros (ideal theoretical curves shown in Fig. 6 (a) by dashed lines) are expected when $T_{\parallel}(\lambda)$ and $T_{\perp}(\lambda)$ are respectively zero in Eqs. (7-8), we observed in Fig. 6 (a) that local maxima and minima values of 10^{2} and 10^{-2} were measured, respectively. Depolarization is known to be the cause of the difference between the ideal response and that measured [32]. The depolarization represents the degree of random polarization during the measurement process. In the birefringence measurements of PSi membranes, we identify the three main sources of depolarization to be: (1) spectrometer bandwidth, (2) thickness variations in the PSi membrane across the light spot area and (3) light scattering produced by pores with a random spatial distribution:

(1) The spectrometer bandwidth affects the phase retardation in two different ways. First the quasi-monochromatic waves superimpose incoherently providing different phase retardation values for each wave. Secondly, since the PSi birefringence is wavelength dependent, light waves with different wavelengths have different birefringence.

(2) Phase retardation is a function of sample thickness and so thickness variations across the spot area will result in superimposing waves that see different thicknesses of the sample.

(3) Volume scattering in the inhomogeneous medium of PSi generates incoherent light which also contributes to the depolarization process [33].

We take into account the previously described effect by modeling the phase retardation as a stochastic process where the each of the light waves that pass through the porous silicon has a phase retardation given by:

$$\Delta\phi_s(\lambda) = \frac{2\pi}{\lambda+\Lambda}\cdot(d+\Gamma)\cdot\Delta n(\lambda+\Lambda)+\Psi \qquad (9)$$

where Λ, Γ and Ψ are random variables with a Gaussian distribution whose most probable values are zero; and their standard deviation correspond to the above described effects (1)-(3): Λ represents the variance in the wavelength due to the effect of the spectrometer bandwidth, Γ represents the irregularities in the porous silicon samples thickness and Ψ represents the contribution of the scattering to the depolarization process.

#150731 - $15.00 USD Received 11 Jul 2011; revised 7 Oct 2011; accepted 31 Oct 2011; published 7 Dec 2011

From Eq. (9) the normalized transmittance for the parallel and crossed polarizers is obtained be means of averaging an infinite (or high enough) number of light waves whose phase retardation is the random variable declared in Eq. (9). Those averaged transmittances can be thus calculated by the expressions:

$$T_{\parallel}(\lambda) = \lim_{N\to\infty}\left(\frac{1}{N}\sum_{1}^{N}\cos^2\left(\Delta\phi_s(\lambda)/2\right)\right) \tag{10}$$

$$T_{\perp}(\lambda) = \lim_{N\to\infty}\left(\frac{1}{N}\sum_{1}^{N}\sin^2\left(\Delta\phi_s(\lambda)/2\right)\right) \tag{11}$$

Using Eq. (10) and Eq. (11), the depolarization effect observed in the PSi membrane measurements were evaluated. Since the bandwidth of the spectrometer is known, and equal to 2 nm for 600-1000 nm and 3.1 nm for 1000-1600 nm, the standard deviation of the variables Γ and Ψ could be obtained by fitting calculated spectra from Eq. (10) and 11 to the measured spectrum. Figure 8 (a) displays the $T_{\perp}(\lambda)/T_{\parallel}(\lambda)$ measured spectra and the simulated one from the previously described model for a 30 μm thickness sample. The best fitting between the experimental data and the simulation was obtained for standard deviations of Γ and Ψ equal to 100 nm and 0.13 rad, respectively. Figure 8 (b) displays the measured and simulated spectra of a 64 μm thick PSi sample. In this case, the experimental data was fitted with standard deviations of Γ and Ψ of 100 nm and 0.3 rad, respectively. In other samples, the standard deviation of Γ was always found to be equal to 100 nm. However in the case of Ψ its standard deviation clearly increases with sample thickness.

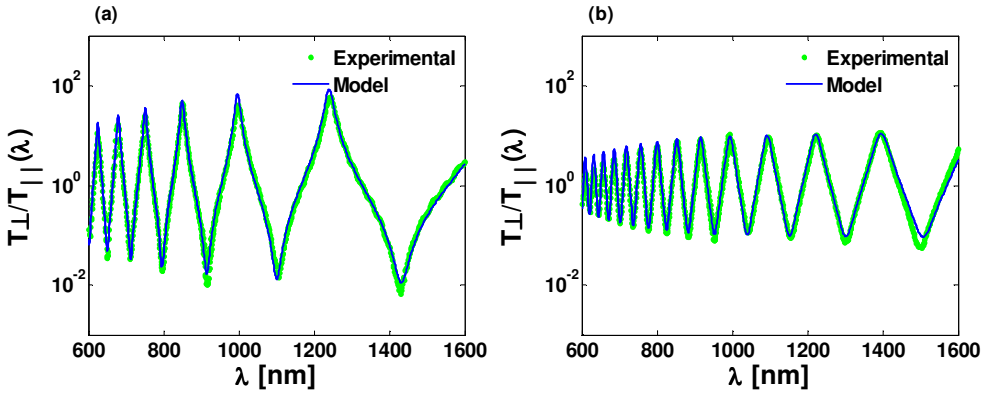

Fig. 8. (a) Measured (green line) and fitted transmittance spectra (dotted blue line) for a PSi sample with thickness of 30 μm (a) and a PSi sample with thickness of 64 μm (b).

A consequence of the depolarization process is the spreading of the phase retardation given by Eq. (9). These uncertainties in the phase retardation produced by the depolarization will be related with the resolution in the measurement of the PSi samples birefringence. Theoretically, in an ideal system where there is no depolarization, the resolution of phase retardation (or birefringence) measurements is determined solely by the instrumentation limits. In reality since depolarization characterizes the randomness of the measurement process the resolution of phase retardation measurements will be related to depolarization.

Figure 9 (a) and (b) show the probability density function of the birefringence calculated from Eq. (6) when the effect that depolarization has over the phase retardation is taken into account for the 30 μm and 64 μm samples, respectively. Comparing both graphs we can see that the main contribution to the total depolarization is the depolarization caused by the scattering. It can be concluded that for both samples the main source of the depolarization is the light scattering by the pores being more important for thicker samples, as expected. The

#150731 - $15.00 USD Received 11 Jul 2011; revised 7 Oct 2011; accepted 31 Oct 2011; published 7 Dec 2011

depolarization process affects the measurement birefringence by increasing its standard deviation, which reduces the precision of the measured value.

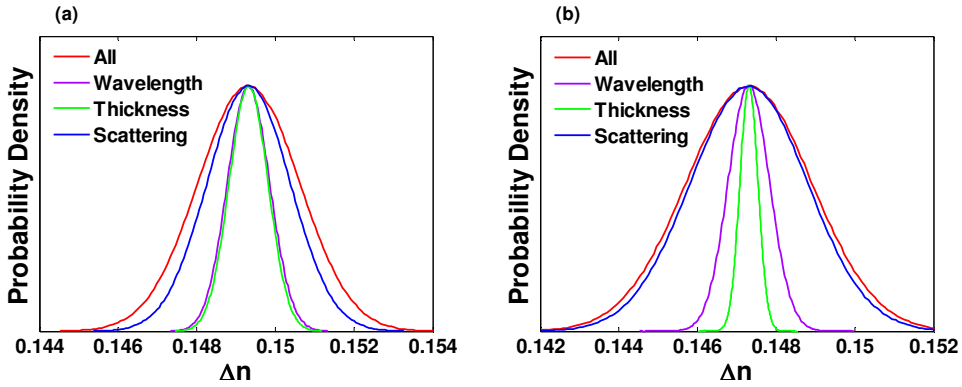

Fig. 9. (a) Birefringence probability density functions in account for the three main factors that produces the depolarization for a 30 μm thick sample (a) and a 64 μm thick sample (b).

6. Conclusion

The modeling, fabrication and characterization of PSi membranes made from (110) silicon was reported. Based on the Bruggeman model the theoretical birefringence and sensitivity was obtained as a function of the porosity and wavelength, with both values have a maximum shown for porosities of 0.55. The impact that the oxidation of pore walls has on birefringence and sensitivity was also studied theoretically. Thereafter a set of PSi samples with different pore sizes and thicknesses were fabricated and characterized. Experimentally determined values of birefringence were obtained for samples filled with air, ethanol and isopropanol, obtaining a sensitivity of 1247 nm/RIU at 1500 nm. This experimental value were found to be in good agreement with the value obtained theoretically by using the model described in section 2 when the effect of silicon oxidation is taken into account. The final part of the work identifies the effect of depolarization for difference between the theoretical spectra and those measured. A statistical model was demonstrated that takes into account the main depolarization sources such as the spectrometer bandwidth, the surface thickness variation and the scattering. With this model it was possible to obtain the standard deviations of the variables that are used to model each of the depolarization sources, as well as the standar deviation of the birefringence measured value.

Acknowledgments

This work was supported by EC through the project FP7-257401 POSITIVE.

#150731 - $15.00 USD Received 11 Jul 2011; revised 7 Oct 2011; accepted 31 Oct 2011; published 7 Dec 2011

2.

Highly-sensitive anisotropic porous silicon based optical sensors

J. Álvarez, P. Bettotti, N. Kumar, I. Suarez, D. Hill, J. Martinez-Pastor, Proc. SPIE Vol. 8212, Frontiers in Biological Detection: From Nanosensors to Systems IV, pp. 821209 (2012)

Highly-sensitive anisotropic Porous Silicon based optical sensors

Jesús Álvarez*[a], Paolo Bettotti[b], Neeraj Kumar[b], Isaac Suárez [a], Daniel Hill[a], and Juan Martínez-Pastor[a]
[a]UMDO, Materials Science Institute, University of Valencia, P.O. Box 22085, 46071 Valencia, Spain
[b]Nanoscience Laboratory, Department of Physics, University of Trento, via Sommarive 14, 38050 Povo-Trento, Italy

ABSTRACT

The modeling, fabrication and characterization of PSi fabricated from both (110) and (100) surface oriented silicon for optical sensing is thoroughly reported. First, based on the generalized Bruggeman method, the birefringence and sensitivity of the fabricated membranes were calculated as a function of the fabrication parameters such as porosity and pore sizes; and external effects, such as the pores surface oxidation. Thereafter we report on the fabrication of PSi membranes from (110) and (100) surface oriented silicon with pore sizes in the range of 50 – 80 nm, and the characterization of their birefringence using a polarimetric setup. Their sensitivities were determined by filling the pores with several liquids having different refractive index. As a result, sensitivities as high as 1407 nm/RIU were obtained for the (110) samples at a 1500 nm wavelength and 382 nm/RIU for the (100) samples at the same wavelength.

Keywords: Porous silicon, birefringence, phase retardation, optical sensor.

1. INTRODUCTION

Nowadays there is an increasing need of developing biological sensors for medical, environmental monitoring, food safety and research applications [1]. Porous Silicon (PSi) has unique properties for the development of these sensors since its huge surface/volume ratio enables the capture of greater amounts of the target molecules that planar sensors. Moreover, its porosity, thickness and pore diameters can be tuned by changing the etching conditions during the fabrication process. Up to now, several interferometric schemes using PSi have been proposed for the realization of chemical and biological sensors [2-5]. Other works [6-8] have demonstrated experimentally the possibility of using PSi made from (110) wafer for sensing applications due to the fact that this orientation presents a very high birefringence, being it possibly to detect different substances within its pores by means of the changes of this value. The use of this anisotropic PSi together with optical polarimetric schemes for measurement of phase retardation therefore makes it an ideal candidate for commercially viable highly sensitive optical sensors.

In this work, based on the theoretical approached developed previously in [9-10] the theoretical optical properties of PSi fabricated from (110) and (100) silicon substrates is studied. For this purpose the binary Bruggeman model [16] is extended by including an important external effect in PSi like silicon oxidation. Then, the measured birefringence values for samples filled with several liquids are compared with the theoretical ones obtained using this extended model. Lastly the measured birefringence and sensitivity for both type of samples (110) and (100) are evaluated and compared. Thereafter we report on the fabrication of several PSi membranes from both types of substrates. Using two different polarimetric setups the birefringence and sensitivity of the fabricated samples are determined; a bulk refractive index sensitivity of 1407 nm/RIU comparable to the 1525 nm/RIU predicted by the theory is reported.

*jesus.alvarez@uv.es; phone 0034963544875; fax 0034963543633; www.uv.es/umdo

rontiers in Biological Detection: ro anosensors to Syste s IV,
edited by Ben a in . Miller, P ilippe M. auc et, Proc. of SPIE Vol. 8212, 82120

2. THEORY

PSi prepared from (110) Si surface oriented substrates presents a high anisotropy due to pores grow preferentially along the [100] and [010] crystallographic directions [12]. The orientation of the pores along those directions results in a difference in the refractive indices along the [001] and the [1$\bar{1}$0] directions [13]. In accounting for the anisotropic microstructure of this type of PSi, the pores are modeled as ellipsoids of revolution with their axes of symmetry aligned along the [001] direction and the [1$\bar{1}$0] direction lying on the (110) surface plane. The depolarization tensor factors, L_e and L_o, describe the screening efficiency of external electromagnetic fields inside the ellipsoids, characterizing the optical properties of the PSi layer. As the directions [100] and [010] form an angle of 50.77º with respect to the normal plane (110) [14], the depolarization tensor factors are: L_e equal to 0.2938 and L_o equal to 0.4035.

For the case of PSi prepared from (100) surface oriented silicon, the pores are modeled as cylinders oriented in the [100] direction. For cylindrical pores the depolarization factor tensors have values of L_e equal to 0.5 and L_o equal to 0 [15].

Using the generalized Bruggeman model [16] the birefringence can be obtained as a function of the fabrication parameters such as porosity and refractive index of the material that fills the pores. The only assumption made by this model is the static electric field condition, which is satisfied when the wavelength of light is much longer than the pore diameter. That is the case of the presented in this work, where the pore diameters are in the range of 50-80nm. The Bruggeman model is described by:

$$\sum_i f_i \frac{n_i^2(\lambda) - n_{e,o}^2}{n_{e,o}^2 + L_{e,o} \cdot (n_i^2(\lambda) - n_{e,o}^2)} = 0 \tag{1}$$

where f_i is the volume fraction of the different materials that form the PSi membrane, $n_i(\lambda)$ the refractive indices, and L_e and L_o the previously described depolarization tensor factors. The unknown n_e and n_o are the refractive indices along the main axes of the pore and the birefringence is obtained by its difference $\Delta n = n_e - n_o$. Then, solving Equation 1 with numerical methods we obtained the theoretical birefringence values as a function of the porosity considering different pore refractive indexes. These results are depicted in Figure 1 for both (110) and (100) PSi samples.

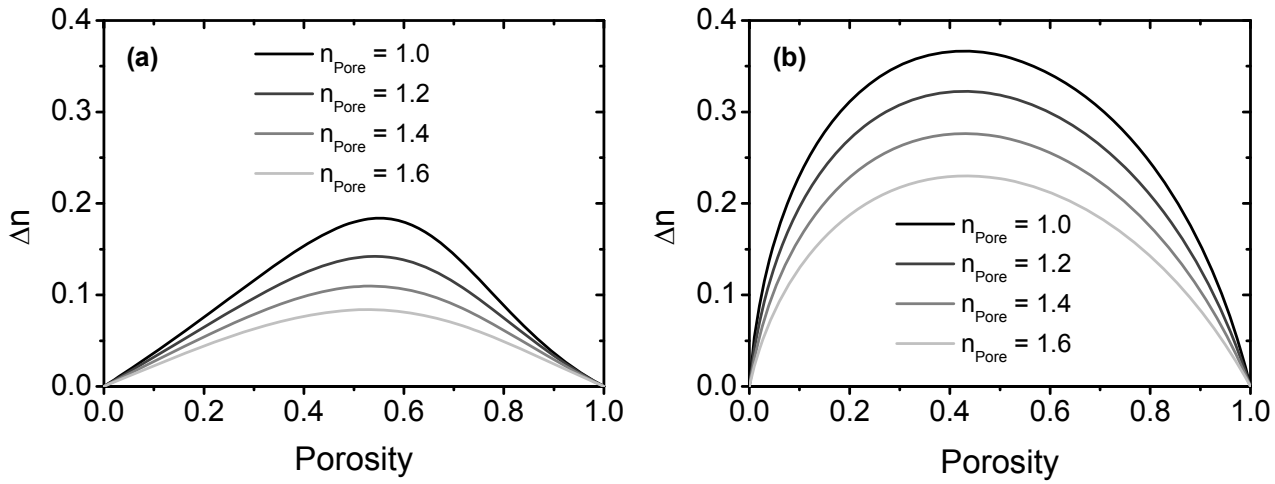

Figure 1. Birefringence as a function of the PSi layer porosity considering several refractive index of the material that fills the pores for a (110) sample (a) and (100) sample (b).

Figure 1 shows that birefringence presents a maximum value for a porosity of 0.55 in the case of the (110) PSi and 0.45 for the (100) samples. Also, for both type of samples the birefringence decreases with the refractive index contrast between the silicon and the material filling the pores. That is transducer mechanism of anisotropic porous silicon to be used an optical sensor: variations in the refractive index of material filling the pores will modify the global birefringence of the sample. From Figure 1, we can also see that the birefringence increase is optimized in the cases where when the initial birefringence achieves its maximum value, so we can conclude that for having an efficient sensing mechanism the birefringence should be as high as the fabrication process makes it possible.

2.1 Effect of silicon oxidation

The internal pore surfaces of freshly prepared PSi are prone to oxidize under ambient conditions leaving a thin SiO_2 layer over recently etched PSi pores. This oxidation process continues over time changing the optical properties of the PSi, so a method to stabilize the pores surface is needed in order to avoid this change in the optical properties. One of the simplest solutions for the surface stabilization is to purposely increase this silicon dioxide layer via a thermal oxidation process [17]. The silicon dioxide need to be taken into account to give accurate prediction of the theoretical birefringence and sensitivity values. This can be done by including the volume of the silicon dioxide layer in Equation 1. Thus, a three component medium has now been formed consisting of silicon, silicon dioxide and pores. The bonding of silicon with oxygen produces a 2.27 fold increase in volume over bulk silicon, so silicon oxidation produces a reduction of pores and silicon volume fractions [18]. The new volume fractions of silicon and pores are related to the silicon dioxide volume fraction by Equations. 2 and 3 respectively:

$$f_{Si} = f_{Si_0} - f_{SiO_2} / 2.27\,; \qquad f_{Pores} = f_{Pores_0} - 1.27 / 2.27 \cdot f_{SiO_2} \qquad (2), (3)$$

where f_{Si_0} and f_{Pores_0} denotes the volume fraction of the silicon and pores prior to oxidation. The effect that grown silicon dioxide has over the birefringence is depicted in Figure 2. As can be seen, silicon dioxide reduces the birefringence for both types of samples. This reduction in birefringence is attributed to the decrease of the index contrast between the initial PSi layer, and the same layer after the oxidation process.

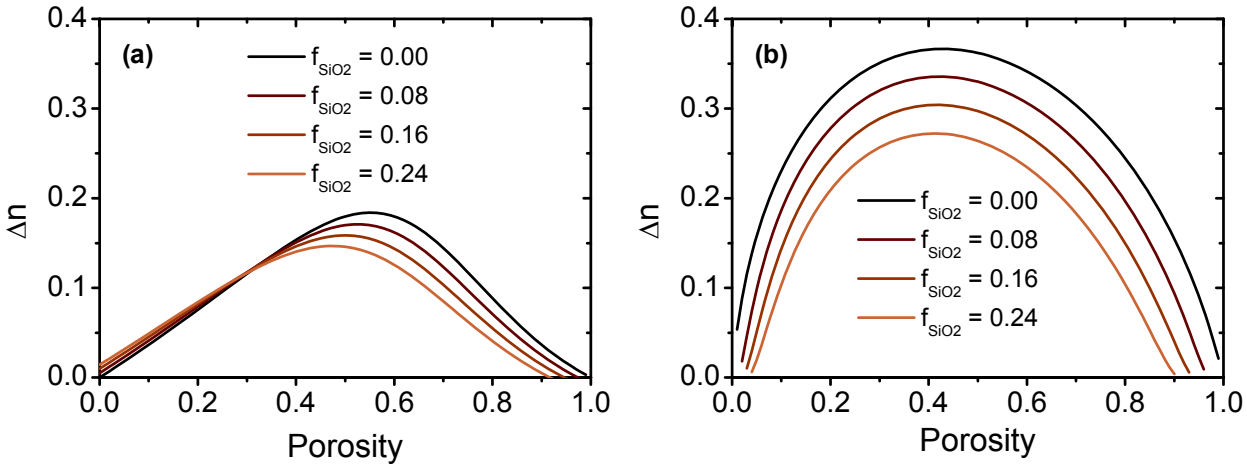

Figure 2. Birefringence as a function of the PSi layer porosity for several silicon dioxide volume fractions for a (110) sample (a) and (100) sample (b).

3. FABRICATION

The set of the fabricated samples from (110) surface oriented silicon consisted of mesoporous silicon etched into n-type Si with resistivity of 0.01-0.001 Ohm/cm. Pores sizes were around 50 nanometers, as shown in Figure 3 (a). Samples were prepared by electrochemical etching using a solution composed of HF:Ethanol=3:7 by volume, considering an initial HF concentration of 48%. A current density of 25 mA/cm^2 was used during the etching.

The other set of samples, prepared from (100) surface oriented silicon, consisted of mesoporous silicon etched into p-type Si with resistivity of 0.01-0.001 Ohm/cm. In this case the pore sizes were around 80 nanometers, as shown in Figure 3 (b).

For subsequent optical characterization, porous membranes were detached from the bulk silicon layer that supports them by applying a strong current burst at the end of the etching completely dissolving the bottom silicon layer that surrounds the etched area. With this procedure the membrane can be transferred to another substrate. More details can be found in [19].

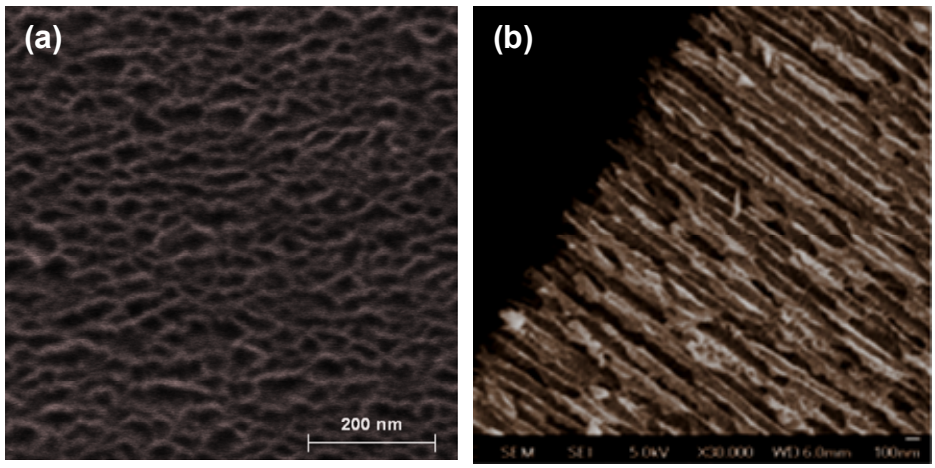

Figure 3. (a) Surface SEM image of the fabricated sample from (110) surface oriented silicon. Pore diameter is around 50 nm. (b) Cross section SEM image of the fabricated sample from (100) surface oriented silicon. Pore diameters are around 80 nm.

4. EXPERIMENTAL AND RESULTS

The optical anisotropy of the samples was determined by analyzing the state of polarization of the light transmitted through them. Since the two types of samples have different properties, as it will be show in the next subsections, two different polarimetric setups were employed to determine the birefringence and sensitivity.

4.1 PSi made from (110) substrate

For this type of samples, the birefringence was determined by using a tungsten halogen lamp and two spectrometers to record the phase retardation as a function of the wavelength in the range from 600 nm to 1600 nm. The phase retardation is related to the samples birefringence by means of:

$$\Delta\phi(\lambda) = \frac{2\pi}{\lambda} \cdot d \cdot \Delta n(\lambda) \tag{4}$$

where λ is the incident wavelength of light, d the PSi membrane thickness and $\Delta n(\lambda)$ its birefringence.

The output light from a tungsten halogen lamp is collimated and then polarized linearly at 45º with respect to the horizontal direction. The linearly polarized light passes through the anisotropic PSi sample which is oriented with its $[001]$ and $[1\bar{1}0]$ crystallographic directions parallel to the vertical and horizontal directions, respectively. The phase shift is converted into an amplitude shift through traversing a second polarizer (usually called analyzer), which is then recorded by the spectrometers. The analyzer is placed parallel and crossed with respect to the first polarizer, so the ratio of the transmitted linearly polarizer light components, *R(λ)*, is obtained by dividing the spectrum measured when the polarizers are crossed by the one obtained when the polarizers are placed in parallel. The relation between the phase retardation and *R(λ)* is given by:

$$R(\lambda) = \frac{T_{\perp}(\lambda)}{T_{\parallel}(\lambda)} = \frac{\sin^2\left(\Delta\phi(\lambda)/2\right)}{\cos^2\left(\Delta\phi(\lambda)/2\right)} \tag{5}$$

So, using the previously described method, *R(λ)* were obtained for a 42 μm sample thick when its pores were filled with air, and then with different liquids such as water ($n_{Water} \approx 1.33$), ethanol ($n_{Ethanol} \approx 1.36$) and isopropanol ($n_{Isop} \approx 1.377$). Figure 4 (a) shows the values of *R(λ)* recorded in the range of 600 nm – 1600 nm for the previously cited cases. A blue-shift can clearly be seen from the sample filled when the pores are filled with liquids. From the position of the zeros and poles of *R(λ)*, the birefringence values for the four cases were obtained as a function of the wavelength by using Equations (5) and (6) to relate the position of the poles and zeros with the phase retardation, and consequently with the

birefringence. Figure 4 (b) depicts the obtained values of the birefringence under the four different conditions of the sample, voids pores (gray dots), pores filled with water (blue dots), ethanol (green line) and isopropanol (orange line).

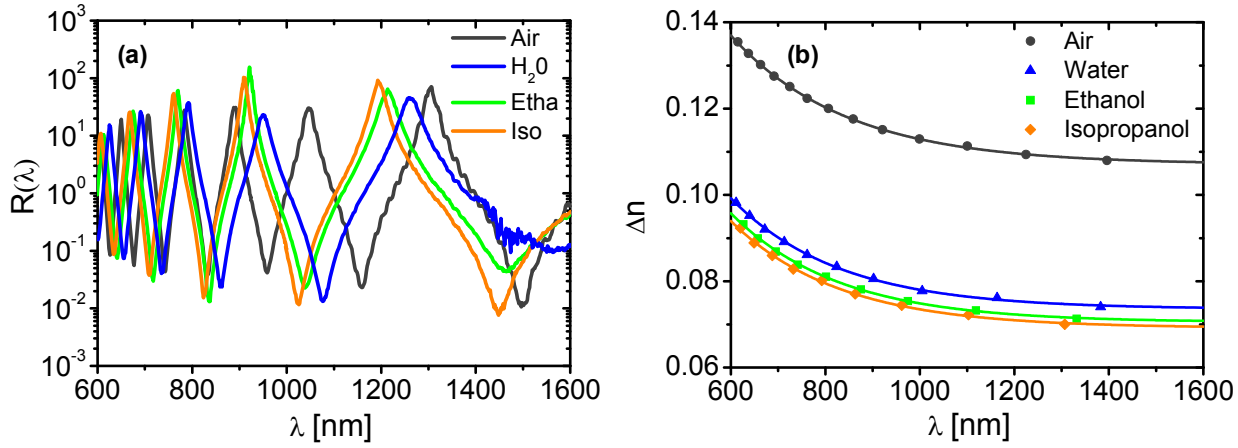

Figure 4. (a) Measured R(λ) from a 42 μm thick (110) PSi sample for: empty pores (gray line), pores filled with water (blue line), ethanol (green line) and isopropanol (orange line). (b) Birefringence values obtained from the position of the poles and ceros of R(λ) for empty pores (gray), pores filled with water (blue), ethanol (green) and isopropanol (orange).

As it was expected from the results shows in Section 2, a decrease in the birefringence is clearly seen when the refractive index of the liquids that fills the pores increases. Also we can see that for larger wavelengths both the birefringence and its change are smaller than the ones obtained at shorter wavelength, due to the fact that silicon refractive index decreases with the wavelength. At a wavelength of 808 nm we measured birefringence values of 0.120, 0.084, 0.081, 0.079 for pores filled with air, water, ethanol and isopropanol respectively. The sensitivity in terms of phase retardation is 35.47 rad/RIU corresponding to a blue-shift of 755 nm/RIU. At a wavelength of 1500 nm the birefringence values are slightly smaller than the ones at 808 nm, 0.108, 0.074, 0.071 and 0.070. The sensitivity in terms of phase retardation is 17.89 corresponding to a blue-shift of 1407 nm/RIU.

4.2 PSi made from (100) substrate

In this type of samples the phase retardation at normal incidence is almost zero, In so another experimental setup for obtaining the birefringence of the samples, different from the one used in the (110) PSi, has to be used. In this case the phase retardation was measured as a function of the incidence angle of a monochromatic light source. Thus, the output light from a laser is linearly polarized at 45º with respect to the horizontal direction. Then, the linearly polarized light passes through the PSi sample which is mounted on a rotation stage that allows changing the incidence angle of the light at the sample. When the linearly polarized light passes through the sample its main components experience a phase shift that is converted into an amplitude shift by placing a second polarizer (analyzer). Finally, the light intensity is measured by means of a photodiode. Again, similarly to the case of the (110) sample, the phase retardation is obtained by measuring the ratio between the intensity of the light when the polarizer are placed crossed and parallel. The phase retardation is related to the sample birefringence and the incidence angle by:

$$\Delta\phi(\alpha)=\frac{2\pi}{\lambda}\cdot\left(d_e(\alpha)\cdot\eta_e(\alpha)-d_o(\alpha)\cdot\eta_o(\alpha)\right) \tag{6}$$

where λ is the incident wavelength of light, and d_e, d_o, η_e, η_o are given by the following equations:

$$d_{e,o}(\lambda,\alpha)=\frac{d}{\sqrt{1-\dfrac{\sin^2\alpha}{n_{e,o}^2(\alpha)}}};\quad \eta_e(\alpha)=\frac{1}{\sqrt{\dfrac{\sin^2\alpha}{n_e^2}+\dfrac{\cos^2\alpha}{n_o^2}}};\quad \eta_o(\alpha)=n_o; \tag{7),(8),(9)}$$

where d the PSi membrane thickness, α the rotation angle of the sample and n_e, n_o the ordinary and extraordinary refractive index.

Using the previously described setup the phase retardation was measured as a function of the light incidence angle on the sample first using a 808 nm laser and then using a 1500 nm laser. Figure 5 (a) shows the measured phase retardation at a wavelength first cited wavelength and Figure 5 (b) depicts the results using a 1500 nm laser. In both cases the phase retardation were measured when the pores were filled with air (gray lines), and after immersing the sample in the same liquids that the (110) PSi sample was, that is water (blue lines), ethanol (green lines) and isopropanol (orange lines). The birefringence were obtained by fitting the measured data with the theoretical ones given by Equation 6 having values of 0.044, 0.0201, 0.019,0.018 at 808 nm and 0.041, 0.020, 0.019, 0.017, at 1500 nm for the sample being filled with air, water, ethanol and isopropanol respectively. The sensitivity in terms of phase retardation at 808 nm for an incidence angle of light of 45º is 9.62 rad/RIU corresponding to a blue-shift of 204 nm/RIU. At a wavelength of 1500 nm the sensitivity value is 4.86 rad/RIU corresponding to a blue-shift of 382 nm/RIU.

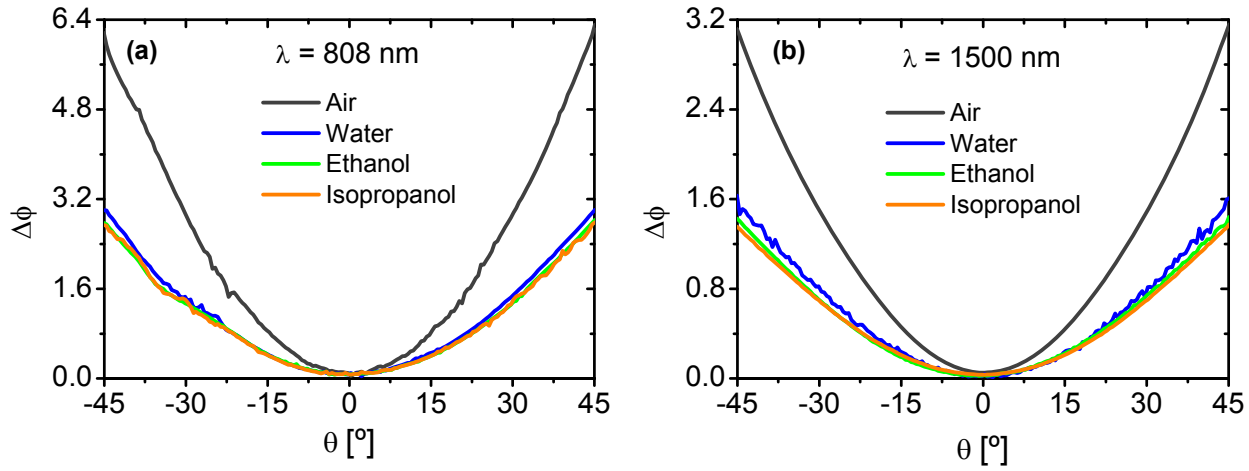

Figure 5. (a) Phase retardation as a function of the light incidence angle for pores filled with air (gray line), water (blue line), ethanol (green line) and isopropanol (orange line) at the wavelengths of 808 nm (a) and 1500 nm (b).

4.3 Comparison

Lastly, we compared the birefringence and sensitivity of the both type of samples at the wavelengths of 808 nm and 1500 nm. Beginning with the values of birefringence, we obtained that the theoretical values of the birefringence were higher in the (100) sample. On the contrary, the experimental results show the opposite behavior: higher birefringence for the (110) samples. These results comes from the ideal modeling of the (100) structure and its difference with the real structure of the fabricated samples where branches of the pores are observed which contributed to homogenize the sample and so to reduce the birefringence. The changes in the phase retardation as a result of filling both types of samples with liquids having different refractive index are shown in Figure 6. We can observe that the higher birefringence change (and so higher sensitivity) were obtained with the (110) samples due to its highest birefringence. On the other hand, since the phase retardation is proportional to the inverse of the wavelength we see that always the phase retardation change is always higher at shorter wavelengths. So we can conclude that to achieve the highest sensitivities using porous silicon as an optical sensor shorter wavelengths are better if one measures the phase retardation shift; on the contrary if the measure the blue-shift in the spectra, longer wavelengths give better sensitivities.

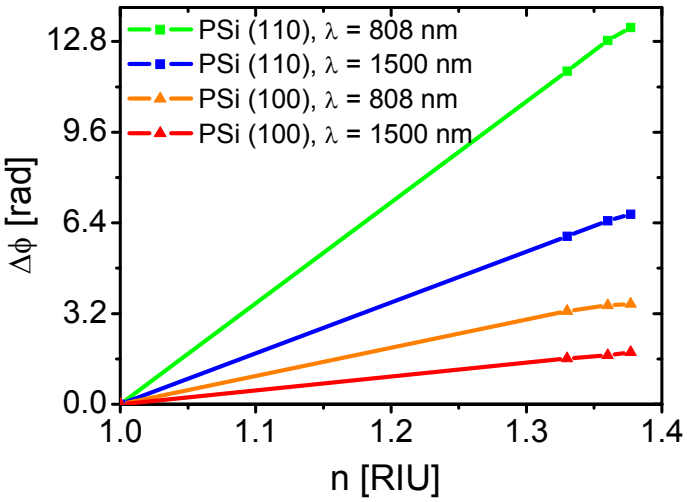

Figure 6. Phase retardation shift as a function of the material that fills the pores for the following cases: PSi sample fabricated from (110) surface oriented silicon at the wavelengths of 1500 nm (green line) and at 808 nm (blue line); PSi sample fabricated from (100) surface oriented silicon at the wavelengths of 1500 nm (orange line) and at 808 nm (red line).

5. CONCLUSION

The modeling, fabrication and characterization of PSi membranes from both (110) and (100) silicon was reported. Based on the Bruggeman model the theoretical birefringence and sensitivity was obtained as a function of the porosity and wavelength, with both values have a maximum shown for porosities around 0.5. The impact that the oxidation of pore walls has on birefringence and sensitivity was also studied theoretically. Thereafter a set of PSi samples from different oriented substrates fabricated and characterized. Porous silicon made from (110) shown to be higher values of birefringence than the ones obtained from a (100) surface oriented silicon. Due to the highest birefringence, also the better sensitivity is found in the (110) samples, measuring a value as high as 1407 nm/RIU at a wavelength of 1500 nm.

REFERENCES

[1] A. Jane, R. Dronov, A. Hodges, and N.H. Voelcker, "Porous silicon biosensors on the advance," Trends Biotechnol., **27**(4), 230-239 (2009).

[2] V.S. Lin, K. Motesharei, K.P. Dancil, M.J. Sailor, and M.R.A. Ghadiri, "Porous Silicon-Based Optical Interferometric," Biosens. Sci., 278(5339), 840-843 (1997).

[3] V.Mulloni, and L. Pavesi, "Porous silicon microcavities as optical chemical sensors," Appl. Phys. Lett., 76(18), 2523-2525 (2000).

[4] M.S. Salem, M.J. Sailor, K. Fukami, T. Sakka, and Y.H. Ogata, "Sensitivity of porous silicon rugate filters for chemical vapor detection," J. Appl. Phys., 103(8), 083516 (2008).

[5] T. Jalkanen, V. Torres-Costa, J. Salonen, M. Björkqvist, E. Mäkilä, J. Martínez-Duart, and V. Lehto, "Optical gas sensing properties of thermally hydrocarbonized porous silicon Bragg reflectors," Opt. Express, 17(7), 5446-5456 (2009).

[6] E. Gross, D. Kovalev, N. Künzner, V.Y. Timoshenko, J. Diener, and F. Koch, "Highly sensitive recognition element based on birefringent porous silicon layers," J. Appl. Phys., 90(7), 3529-3532 (2001).

[7] O.B. Hoan R. Liu, Y.Y. Li, M. Sailor, and Y. Fainman, "Vapor sensor realized in an ultracompact polarization interferometer built of a freestanding porous-silicon form birefringent film," IEEE. Photonic. Tech. L., 15(6), 834-836 (2003).

[8] J. Álvarez, P. Bettotti, I. Suárez, N. Kumar, D. Hill, V. Chirvony, L. Pavesi, and J. Martínez-Pastor, "Birefringent porous silicon membranes for optical sensing," Opt. Express 19, 26106-26116 (2011).
[9] M. Kompan, J. Salonen, and I. Shabanov, "Anomalous birefringence of light in free-standing samples of porous silicon," J. Exp. Theor. Phys., 90, 324-329 (2000).
[10] V. Kochergin M. Christophersen, H. Foll, "Effective medium approach for calculations of optical anisotropy in porous materials" Appl. Phys. B, 79, 731-739 (2004).
[11] O. Bisi, S. Ossicini, and L. Pavesi, "Porous silicon: a quantum sponge structure for silicon based optoelectronics," Surf. Sci. Rep., 38(1-3), 1-126 (2000).
[12] N. Künzner, J. Diener, E. Gross, D. Kovalev, V.Y. Timoshenko, and M. Fujii, "Form birefringence of anisotropically nanostructured silicon," Phys. Rev. B, 71(19), 195304 (2005).
[13] V.Y. Timoshenko, L.A. Osminkina, A.I. Efimova, L.A. Golovan, P.K. Kashkarov, D. Kovalev, N. Künzner, E. Gross, J. Diener, and F. Koch, "Anisotropy of optical absorption in birefringent porous silicon," Phys. Rev. B, 67(11), 113405 (2003).
[14] R.L. Smith, and S.D. Collins, "Porous silicon formation mechanisms," J. Appl. Phys., 71(8), 1-22 (1992).
[15] Lutich, A.A., Danailov, M.B., Volchek, S., Yakovtseva, V.A., Sokol, V.A., Gaponenko, S.V., "Birefringence of nanoporous alumina: dependence on structure parameters", Applied Physics B: Lasers and Optics, 84,1, 327-331, (2006)
[16] T.C. Choy, "Effective Medium Theory, Principles and Applications," Oxford University Press, (1999).
[17] K.A. Kilian, T. Bocking, and J.J. Gooding, "The importance of surface chemistry in mesoporous materials: lessons from porous silicon biosensors," Chem. Commun., 630-640 (2009).
[18] I. Suárez, V. Chirvony, D. Hill, and J. Martínez-Pastor, "Simulation of surface-modified porous silicon photonic crystals for biosensing applications," Phot. Nano. Fund. Appl., doi:10.1016, (2011)
[19] M. Ghulinyan, C.J. Oton, G. Bonetti, Z. Gaburro, and L. Pavesi, "Free-standing porous silicon single and multiple optical cavities," J. Appl. Phys., 93(12), 972 (2003).

3.

Phase-Sensitive Detection for Optical Sensing With Porous Silicon

J. Álvarez, N. Kumar, P. Bettotti, D. Hill, J. Martinez-Pastor, IEEE Photonics Journal, Vol. 4(3), pp. 986 (2012)

Phase-Sensitive Detection for Optical Sensing With Porous Silicon

J. Álvarez,[1] N. Kumar,[2] P. Bettotti,[2] D. Hill,[1] *Member, IEEE*, and J. Martínez-Pastor[1]

[1]UMDO, Materials Science Institute, University of Valencia, 46071 Valencia, Spain
[2]Nanoscience Laboratory, Department of Physics, University of Trento, 38050 Povo-Trento, Italy

DOI: 10.1109/JPHOT.2012.2201461
1943-0655/$31.00 ©2012 IEEE

Manuscript received March 10, 2012; revised May 18, 2012; accepted May 20, 2012. Date of publication May 25, 2012; date of current version June 13, 2012. This research was supported by the EC through the project FP7-257401 POSITIVE. Corresponding author: J. Álvarez (e-mail: jesus.alvarez@uv.es).

Abstract: We report on a photonic sensor with an ultralow limit of detection (LoD) based on a phase interrogation readout scheme together with an anisotropic porous silicon (PSi) membrane. First, the fabrication of porous free-standing membranes from medium doped (100) surface oriented silicon, with pore diameters suitable for the infiltration of biomolecules, around 50 nm, is reported. Then, the phase interrogation scheme for characterizing the PSi membranes is presented whose results show that while volumetric sensitivity increases with the membrane thickness, the resolution in the birefringence measurements decrease dramatically due to depolarization effects. The best LoD was found to be equal to 6.25×10^{-6} RIU, from the thinnest 10-μm-thick membrane. Finally, the thermooptic coefficient of the 10 μm membrane was measured in an aqueous environment and shown to be equal to 8×10^{-4} rad/°C.

Index Terms: Sensors, fabrication and characterization, subwavelength structures, scattering, metrology.

1. Introduction

Today there is an ever increasing need to develop sensitive optical and photonic biosensors capable of quantitative multiparameter measurements for medical analyzes, food quality control, drug development, environmental monitoring and research applications [1], [2]. Many are capable of being incorporated into lab-on-a-chip devices for the added advantages of performing measurements at the point-of-care and at an affordable cost [3]. A key component of these biosensors is the transducer, which is responsible for the transformation of variations in physical environmental parameters (e.g., refractive index) into a measurable signal (e.g., optical power). Porous silicon (PSi) as a transducer has unique properties. Its huge internal surface/volume ratio (on the order of 100 m^2/cm^3) when functionalized by a suitable surface chemistry [4] permits a greater number of target molecules to be captured per chip area compared to planar sensors, allowing a higher integration of assays [5]. In doing so, the surface can be left either hydrophobic or hydrophilic to allow a large range of biomolecules to immobilize within the pores. Furthermore, its porosity, thickness and pore diameters can be tuned according to the biorecognition application by changing the etching conditions during the fabrication process [4].

To date, a large volume of work has been done in the pursuit of realizing optical sensors based on PSi [6], [7]. The simplest such device consists of a PSi layer etched into p-type silicon. The presence of a different substance in the PSi layer modifies its effective refractive index, producing a

shift in the fringe spectrum [8]. More complex designs such as multilayer structures have also been studied for biosensing purposes [9]. In this case, a defect layer is buried in a multilayer structure composed of successive layers of high and low refractive index PSi. A narrow resonance is observed in the transmission spectra whose position is highly sensitive to the presence of molecules inside the defect region [10], [11]. The main limitation of these approaches lies in the difficulty for the target molecules to infiltrate the cavity region due to differences between the porosity or pore sizes of the multilayer structure. Photonic waveguides made from PSi have been also proposed as sensors [12] where light is confined and propagated in a medium porosity layer on top of a high porosity layer. The sensing mechanism is based on the variation of waveguide-mode excitation angle when the analyte enters into the waveguide. More recently, another design based on the Bloch surface waves present at the truncated end of a 1-D photonic has been presented for sensing applications [13]. Finally, other designs have been proposed that utilize the anisotropy of PSi and the sensitivity of the associated birefringence to refractive index changes within the pores. The first uses PSi made from (110) surface oriented silicon as this presents high birefringence [14], [15], others are based on PSi prepared from (100) surface oriented silicon as this too presents high anisotropy when the incident light direction is tilted with respect to pore grown direction due to the difference in the effective index between the ordinary, no, and extraordinary, ne, directions. To date this dependence has only been exploited for vapor sensing through nanoporous silicon membranes [16], [17].

In our previous work [18] we studied the sensing properties of PSi membranes in the wavelength range from 600 nm to 1600 nm. The long term stability of the fabricated membranes was demonstrated when the PSi was thermally oxidized. Furthermore, a new model was developed in order to determine the depolarization sources and its contribution to the overall depolarization process.

In the present paper, we report on an ultralow limit of detection (LoD) sensing mechanism based on a phase interrogation scheme for characterizing the optical anisotropy of mesoporous silicon membranes. First, we report how PSi membranes with thickness of 10, 30 and 60 μm were fabricated from n-type (100) surface oriented silicon allowing a pore size desirable for biomolecules infiltration, around 50 nm. The readout scheme for the birefringence measurements is then presented. It is based on the use of a photoelastic modulator to modulate the light polarization, which allows a resolution to be reached of down to 10^{-7} rad. We then show how with this scheme the birefringence of the fabricated membranes was obtained by means of measuring the phase retardation as a function of the light incidence angle. Thereafter sensing results from immersing the samples in several solutions of water and ethanol are reported, demonstrating that thicker membranes are more sensitive. The resolutions that can be reached with the different membranes when measured are then shown where it can be clearly seen that when the sample thickness increases the depolarization does also, which deteriorates the resolution in the phase retardation measurement. Combining the sensitivity and the resolution results, we show that the thinnest membrane (10 μm) presents the lowest LoD, being equal to 6.25×10^{-6} RIU (Refractive Index Unit). The last section of this work shows the characterization of the thermal stability of the 10 μm thin membrane in aqueous environment, showing a thermooptic coefficient of 8×10^{-4} rad/RIU.

2. Fabrication

PSi is typically prepared by electrochemical etching of silicon using HF dissolved in water or ethanol. Parameters such as pore size, porosity and layer thickness can be adjusted by correctly choosing the resistivity of the silicon wafer, the HF concentration and the etch time [19]. In the present work, the fabrication of the macroporous silicon membranes was carried out using an n-type (100) surface oriented silicon wafer with a resistivity of 0.01 $\Omega \cdot$cm. Membranes with thicknesses of 10, 30 and 60 μm were obtained via the following two step process; the first consisted of etching the PSi layer on the silicon wafer using HF with a concentration of 17% diluted in a solution of water and ethanol; the second consisted of applying a large current in order to completely dissolve the underneath of the etched layer [20]. The current density used for producing

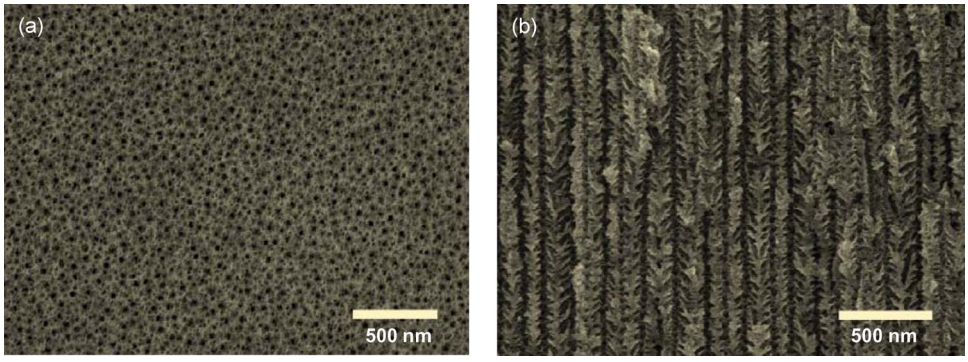

Fig. 1. (a) Surface SEM image of one of the fabricated samples made from (100) surface oriented silicon. (b) Cross section SEM image of the same sample. Pores diameter is around 50 nm.

the membranes was 25 mA/cm^2, and by applying it during 360, 600 and 1200 seconds, the 10, 30 and 60 μm thick membranes were produced respectively with etch rates of 28 nm/s for the 10 μm thick sample and 50 nm/s for the 30 and 60 μm thick samples. Scanning electron microscope (SEM) images of the fabricated samples (Fig. 1) show that the pore sizes of the samples were around 50 nm. An effective refractive index of 2.9 for the samples was measured from the fringes of the reflectance spectra in the infrared region, which corresponds to a porosity of about 0.3. After the optical characterization of several membranes with the same thickness we found that the differences in their optical properties (absorbance and birefringence) was smaller than 5%, which demonstrates the reliability of the fabrication process.

After the two step fabrication process, the free-standing membranes were mounted on borosilicate glass frames using a 1 μm thick of PMMA (Poly(methyl methacrylate)) resist as the adhesion layer between the borosilicate frame and the free-standing PSi membrane. Before the optical characterization, the PSi samples were thermally oxidized at 200 °C for 12 hours. This oxidation process has two purposes; first a thin silicon dioxide layer is formed on the pore walls so as to stabilize them, reducing the drift in effective refractive index by about one order of magnitude respect to the unoxidized samples [18]. Secondly, the thin silicon dioxide layer increases the hydrophilicity of the samples [4] for the liquids in the subsequent sensing experiments.

3. Theory

The optical anisotropy of PSi is a well known property for PSi fabricated (100) surface oriented silicon [17]. In order to simulate the birefringence of mesoporous silicon we used the generalized Bruggeman model [21] which assumes the static field condition, which is satisfied when the wavelength of light is much longer than the transverse pore size. In our case the static field condition is satisfied since pore diameters are in the order of 50 nm and working wavelength is 1500 nm. The generalized Bruggeman model is described by

$$\sum_i f_i \frac{n_i^2(\lambda) - n_{e,o}^2(\lambda)}{n_{e,o}^2(\lambda) + L_{e,o} \cdot \left(n_i^2(\lambda) - n_{e,o}^2(\lambda)\right)} = 0 \tag{1}$$

where f_i is the volume fraction of the different materials that form the PSi membrane, $n_i(\lambda)$ their refractive indices, and $L_{e,o}$ are the depolarization tensor factors. The unknown $n_e(\lambda)$ and $n_o(\lambda)$ are the extraordinary and ordinary refractive and are related to the birefringence by means of $\Delta n(\lambda) = n_e(\lambda) - n_o(\lambda)$. Due to in the present work all the results are obtained for a wavelength of 1500 nm, from now on we will consider the values of $n_{i,e,o}$, as $n_{i,e,o}(\lambda = 1500nm)$. The depolarization tensor factors L_e and L_o describe the screening efficiency of external electromagnetic field inside the pores. For pores grown perpendicular to the surface they have values of $L_e = 0$ and $L_o = 0.5$ [22]. The generalized Bruggeman model has been used in the literature to

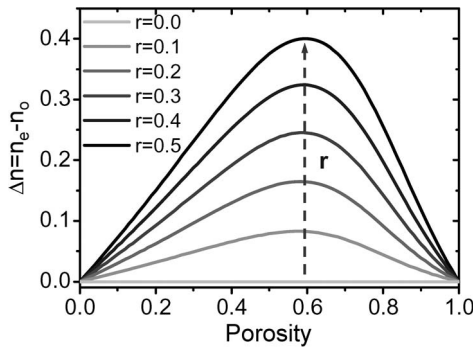

Fig. 2. Simulated birefringence as a function of the porosity for different values of r (r represents the amount of pores in the $\langle 100 \rangle$ direction over the total pores volume).

simulate the birefringence of porous alumina membranes with pore sizes around 50 nm giving good accordance between the measured results and the simulated ones [22]. On the contrary, preliminary results on (100) PSi showed a discrepancy of one order of magnitude between the measured birefringence values and the simulated ones using the Bruggeman model [23]. The main reason of this discrepancy is because in mesoporous silicon fabricated from n-type substrates the pores not only grow in the $\langle 100 \rangle$ direction but also in the $\langle 113 \rangle$ directions [24]. These branches can be clearly seen in Fig. 1(b) and so for a more realistic simulated birefringence values, the pores grown in the $\langle 113 \rangle$ direction must be taken into account. For that we propose a simple method based on modifying the depolarization tensor factors by

$$L_{e,o} = r \cdot L_{e,o_{\langle 100 \rangle}} + (1 - r) \cdot L_{e,o_{\langle 113 \rangle}} \tag{2}$$

where r is a parameter that relates the pore volume in the $\langle 100 \rangle$ direction to that of the total pore volume. According to the data given in the literature [22], the depolarization tensors factors are $L_{e_{\langle 100 \rangle}} = 0.0$ and $L_{o_{\langle 100 \rangle}} = 0.5$ when the pores are modeled as cylinders that grow perpendicular to the sample surface. In accounting for the anisotropy of the pores grown in the $\langle 113 \rangle$ direction, due to the symmetry with respect to the $\langle 100 \rangle$ direction, the depolarization tensor factors were assumed to be $L_{e,o_{\langle 113 \rangle}} = 1/3$. Using the generalized Bruggeman model and the new depolarization tensor factors (1) was solved as a function of the porosity for different values of the r coefficient (Fig. 2).

Birefringence values are related to the phase retardation of the light parallel and perpendicular components by the following equation [17]:

$$\Delta\phi(\alpha) = \frac{2\pi}{\lambda}(d_e(\alpha) \cdot \eta_e(\alpha) - d_o(\alpha) \cdot \eta_o(\alpha)) \tag{3}$$

where λ is the wavelength the light source, d_e, d_o, η_e, η_o are given by the following expressions:

$$d_{e,o}(\alpha) = \frac{d}{\sqrt{1 - \frac{\sin^2\alpha}{n^2_{e,o}(\alpha)}}} \tag{4}$$

$$\eta_e(\alpha) = \frac{1}{\sqrt{\frac{\sin^2\alpha}{n^2_e(\alpha)} + \frac{\cos^2\alpha}{n^2_o(\alpha)}}} \tag{5}$$

$$\eta_o(\alpha) = n_o \tag{6}$$

being d the PSi membrane thickness, α the angle between the light beam and the vector normal to the PSi surface, and n_e, n_o the ordinary and extraordinary refractive index.

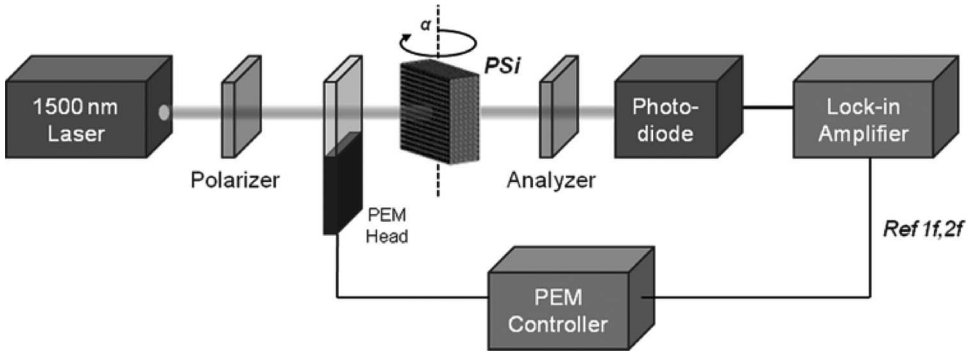

Fig. 3. Setup used for the phase retardation measurement of the fabricated PSi membranes.

4. Experimental

Optical birefringence can be measured by a wide variety of methods; the simplest one is based on the measurement of the transmitted light through a sample when it is placed between crossed polarizers [17]. Although this method is simple to implement, it does not provide highly accurate results and instead a photoelastic modulator (PEM) can be used [25]. In recent years, the use of a PEM has also been proposed to help improve upon the LoD of optical sensors based on surface plasmon resonance (SPR) [26] and plasmonic gratings [27].

For the measurement of phase retardation associated with the birefringence of the PSi samples, the optical setup used is the one depicted in Fig. 3. Specifically, the output light from a stabilized 1500 nm laser (New Focus TLB-6326) is collimated and the light linearly polarized. The continuous light was phase modulated by the PEM through sinusoidal variation of its polarization. The modulated light passes through the PSi sample, which was mounted on a motorized rotation stage (Thorlabs CR1-7Z) which permits changing the sample rotation angle. After passing the PSi sample and a second polarizer the light is detected by an InGaAs photodiode which is connected to a lock-in amplifier (SR-810) in order to perform the synchronous detection and measure the first and second harmonic amplitude of the signal.

The phase retardation is related to the first and second harmonics of the modulated light by [28]

$$\Delta\phi(\alpha) = \arctan\left(\frac{V_{1f}(\alpha)}{V_{2f}(\alpha)} \cdot \frac{J_2(A_0)}{J_1(A_0)}\right) \tag{7}$$

where α is the angle between the light beam and the vector normal to the PSi surface, V_{1f}, V_{2f} are the amplitude of the first and second harmonic and $J_1(A_0)$, $J_2(A_0)$ the first Bessel function of first and second order, being A_0 the amplitude of the modulating signal (in radians).

Before beginning with sample characterization the resolution of the setup was tested by taking multiple measurements of a quartz sample with a known birefringence. The measured values had a Gaussian distribution with a standard deviation equal to 10^{-7} rad. By adopting the convention that the resolution is given by the standard deviation when the values have a Gaussian distribution, we obtain the resolution of our measurement system as 10^{-7} rad.

5. Results and Discussion

Using the optical setup described in Section IV the phase retardation of the fabricated samples was measured as a function of the sample rotation angle. The first measurements were carried out in order to determine the birefringence of the different samples. After that, the phase retardation was measured when different solutions of water and ethanol filled the membranes pores. For this purpose the samples were immersed in a optical cuvette (mounted over the rotation stage) were the different solutions of water and were introduced. The LoD of the system was also obtained and lastly, the effect that temperature variation has over the PSi transducer performance was determined.

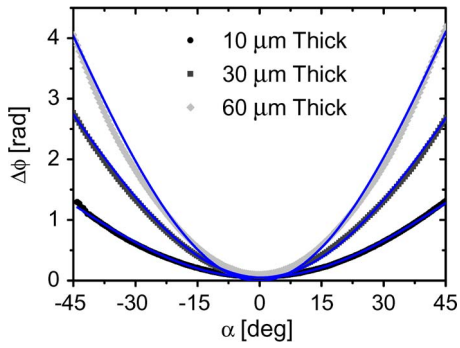

Fig. 4. Phase retardation as a function of the sample rotation angle for samples with thicknesses of 10, 30 and 60 μm. Blue lines represent the theoretical values obtained from the fitting of (7) to experimental ones.

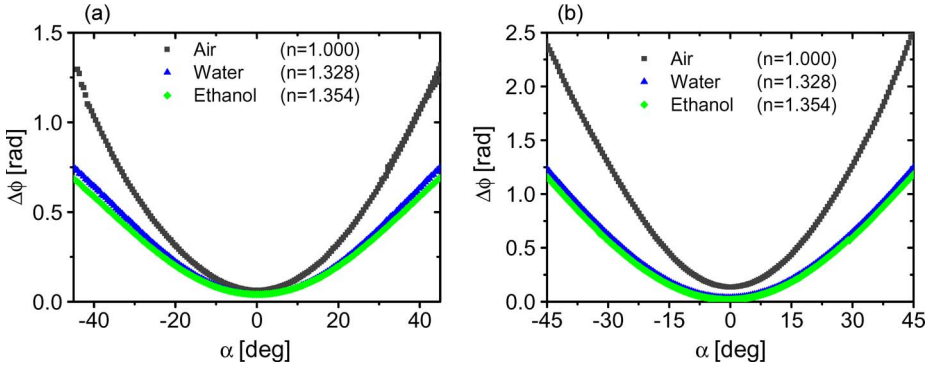

Fig. 5. Phase retardation as a function of the light incidence angle for pores filled with air (gray line), water (blue line) and ethanol (green line) for a 10 μm thick sample (a), and 30 μm thick sample (b).

5.1. Birefringence

The birefringence of the fabricated mesoporous membranes is clearly related to the sensitivity, with membranes being more sensitive when they have greater birefringence. The birefringence of the membranes was obtained by fitting the measured phase retardation values to the theoretical values given by (3). The measured phase retardation values of the fabricated samples are shown in Fig. 4 where blue lines represent the theoretical values obtained from the fitting. Birefringence values of 0.06607, 0.04401 and 0.03712 were obtained for the 10, 30 and 60 μm samples, respectively. A clear decrease in birefringence values when sample thicknesses increase is seen. A SEM inspection of sample cross sections confirmed that this was due to more pores growing in the $\langle 113 \rangle$ directions when the etching time increases.

5.2. Sensitivity

One of the two key figures of merit for an optical transducer is the sensitivity of the optical response to given changes in the refractive index of its environment. In this section the sensitivities of the three membranes are obtained by measuring the samples phase retardations when immersed in liquids with different refractive indices. The liquids employed were water ($n_{Water} = 1.328$) and ethanol ($n_{Ethanol} = 1.354$), as well as solutions of ethanol in water with concentrations of 50:50 and 75:25.

The measurements were carried out by the process explained in the previous section with the only difference being that the samples were immersed in the liquids. Results in air, water and ethanol for the 10 and 30 μm thick samples are shown in Fig. 5. Three clear annotations can be

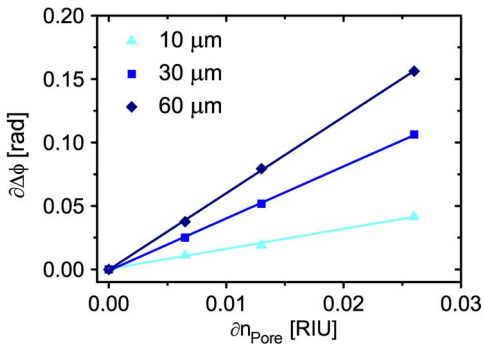

Fig. 6. Phase retardation shifts for samples rotation angle of 45° as a function of the refractive index of the material that fills the pores for samples with thickness 10, 30 and 60 μm (dots). A solid line represents the linear fitting of the experimental data, showing sensitivities of 1.6 rad/RIU, 4 and 6 rad/RIU for the 10, 30 and 60 m thick, respectively.

made: firstly, a reduction in the phase retardation is observed when the refractive index of the liquids that fill the samples increases. Secondly, both phase retardation and its derivative are higher for thicker samples, thus greater sensitivities are also expected. Thirdly, the change in the phase retardation and therefore sensitivity increases with the incidence angle.

Fixing the sample azimuthal rotation angle to 45° the phase retardation was measured when the samples were immersed in a solution of water:ethanol $= 100:0, 25:75, 50:500:100$. Fig. 6 shows the phase retardation change as a function of the solution refractive index showing a linear behavior between the liquids refractive index and the change in the phase retardation value. The phase retardation change was fitted to a linear function showing sensitivities of 1.6, 4 and 6 rad/RIU.

5.3. Limit of Detection

While the sensitivity gives an idea of the optical transducer performance, the usually more important figure of merit is the smallest refractive index change that it can respond to and be resolved, i.e., measure accurately, that is the LoD. The limit of the detection relates the sensitivity of the transducer to the resolution of the readout system by

$$LoD[RIU] = \frac{\sigma[rad]}{\partial\Delta\phi[rad/RIU]} \tag{8}$$

where σ is the measurement system resolution and $\partial\Delta\phi$ is the transducer sensitivity.

As previously reported [18], [29], light scattering in an inhomogeneous medium like PSi generates incoherent light which depolarizes the light thereby deteriorating the system resolution which for our system was measured at 10^{-7} rad for a quartz reference sample. The amount of depolarized light increases with the PSi sample thickness, so the system resolution needs to be tested for PSi samples with different thickness. The resolution of the measurement system was therefore obtained from the standard deviation of the birefringence measured values of the fabricated PSi samples (10, 30 and 60 μm thick) when they were immersed in water. We observed that the resolution decreases dramatically when the thickness of the samples increases: going from 1×10^{-5} to 5×10^{-5} to 5×10^{-4} for 10, 30 and 60 μm, respectively.

Combining the values of the sensitivity obtained in the previous section and the resolution values obtained above, the limits of detection that can be reached with each membrane can be determined from (8). Table 1 shows the sensitivity, resolution and LoD values for all the membranes measured. We can see that although the sensitivity increases with the sample thickness, at the same time the resolution decreases dramatically due to the depolarization. The thinnest fabricated membrane (10 μm) is therefore potentially the most suitable for biosensing purposes due to its smaller LoD.

TABLE 1

Sensitivity, resolution and LoD of the three types of PSi samples measured in aqueous environment.

Thickness $[\mu m]$	Sensitivity $[rad/RIU]$	Resolution $[rad]$	LoD $[RIU]$
10	1.6	$1x10^{-5}$	$6.25x10^{-6}$
30	4.5	$5x10^{-5}$	$1.25x10^{-5}$
60	6	$1x10^{-4}$	$8.33x10^{-5}$

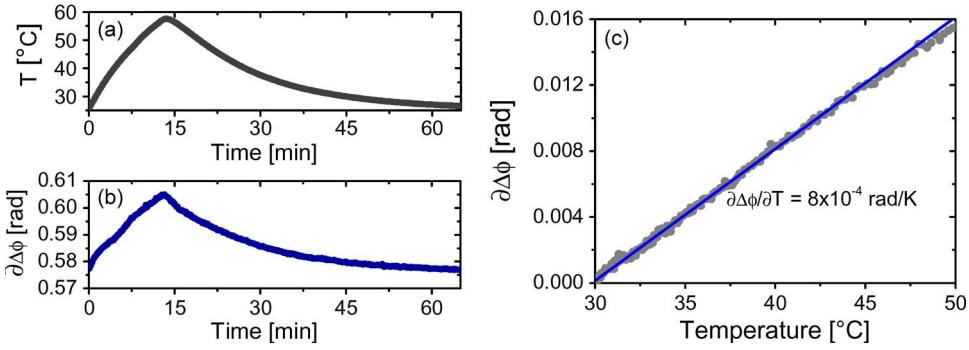

Fig. 7. (a) Sample temperature variation as a function of time. (b) Phase retardation as a function of time. (c) Phase retardation change as a function of the sample temperature.

5.4. Thermal Stability

The refractive index of the materials used to develop photonic or optical sensors, such as semiconductors or glasses is temperature dependent. Due to that, the optical properties of the transducer not only change when the refractive index of the surrounding media does, but it also changes as the temperature of the same media does.

In order to quantify this change for biosensing the thermal stability of a PSi membrane in the same aqueous environment was determined. To do so, the sample holder was placed in a closed chamber where the temperature could be increased from ambient to 50 °C and a platinum temperature sensor placed within it in order to monitor its temperature. As the chamber was heated both the phase retardation as well as the sample temperature were monitored in time during a rising and falling cycle [Fig. 7(a) and (b)]. The phase retardations was plotted against the chamber temperature [Fig. 7(c)] showing a liner dependence with a slope of 8×10^{-4} rad/°C. This value could be used to determine the resolution needed for the thermal stabilization system within an instrument based on such a sensing mechanism. Thus for a resolution in the phase retardation measurement of 10^{-5} rad, a thermal control with a temperature change of 12.5 mK will produce a change in the phase retardation equal to the system resolution. This means that an active thermal control with a setpoint temperature resolution of 1 mK will provide a thermal stability for phase variation one order of magnitude better than that of the overall system phase resolution.

6. Conclusion

A highly sensitive device for biosensing purposes has been presented that is based on the use of a phase retardation readout scheme for the characterization of optical anisotropic of mesoporous silicon membranes. The fabrication of mesoporous free-standing membranes with pore diameters around 50 nm and thickness of 10, 30 and 60 μm were reported, which are suitable for biosensing.

The results of the anisotropy characterization of the fabricated membranes showed that the birefringence decreases with the sample thickness due to the amount of pores that grow in the ⟨113⟩ directions having increased with the etch time. The sensing experiments carried out with the membranes using different solutions of water and ethanol showed that the thinner membranes (10 μm thick) present the lowest LoD, equal to 6.25×10^{-6} RIU. The thicker membranes have a worse LoD due to the increase in depolarization worsening the resolution of the measurement system. In the last section of the work the thermooptic coefficient of a 10 μm thick membrane is measured in aqueous environment at 8×10^{-4} rad/°C.

Acknowledgment

The authors acknowledge Julian Heredero Calero for his design and mechanization of the sample holder and temperature chamber.

References

[1] X. Fan, I. M. White, S. I. Shopova, H. Zhu, J. D. Suter, and Y. Sun, "Sensitive optical biosensors for unlabeled targets: A review," *Anal. Chim. Acta*, vol. 620, no. 1/2, pp. 8–26, Jul. 2008. [Online]. Available: http://www.sciencedirect.com/science/article/pii/S0003267008009343

[2] D. Hill, "Advances in nanophotonic sensing technologies during three international label-free lab-on-chip projects," *BioNanoScience*, vol. 1, pp. 162–172, 2011, DOI:10.1007/s12668-011-0026-1. [Online]. Available: http://dx.doi.org/10.1007/s12668-011-0026-1

[3] F. S. Ligler, "Perspective on optical biosensors and integrated sensor systems," *Anal. Chem.*, vol. 81, no. 2, pp. 519–526, Jan. 2009. [Online]. Available: http://pubs.acs.org/doi/abs/10.1021/ac8016289

[4] K. A. Kilian, T. Bocking, and J. J. Gooding, "The importance of surface chemistry in mesoporous materials: Lessons from porous silicon biosensors," *Chem. Commun.*, vol. 6, pp. 630–640, 2009. [Online]. Available: http://dx.doi.org/10.1039/B815449J

[5] C. Li, R. Orobtchouk, T. Benyattou, A. Belarouci, Y. Chevolot, V. Monnier, E. Souteyrand, E. Gerelli, and C. Jamois, *New concepts of integrated photonic biosensors based on porous silicon, Biosensors—Emerging Materials and Applications*, P. A. Serra, Ed. Rijeka, Croatia: InTech., 2011. [Online]. Available: http://www.intechopen.com/articles/show/title/new-concepts-of-integrate d-photonic-biosensors-based-on-porous-silicon

[6] A. Jane, R. Dronov, A. Hodges, and N. H. Voelcker, "Porous silicon biosensors on the advance," *Trends Biotechnol.*, vol. 27, no. 4, pp. 230–239, Apr. 2009. [Online]. Available: http://www.sciencedirect.com/science/article/B6TCW-4VR0MBX-2/2/c9730bc89c2ee8572fb4decbb1a64ce2

[7] G. Korotcenkov and B. K. Cho, "Porous semiconductors: Advanced material for gas sensor applications," *Crit. Rev. Solid State Mater. Sci.*, vol. 35, no. 1, pp. 1–37, 2010. [Online]. Available: http://www.tandfonline.com/doi/abs/10.1080/10408430903245369

[8] V. S.-Y. Lin, K. Motesharei, K.-P. S. Dancil, M. J. Sailor, and M. R. Ghadiri, "A porous silicon-based optical interferometric biosensor," *Science*, vol. 278, no. 5339, pp. 840–843, Oct. 1997. [Online]. Available: http://www.sciencemag.org/content/278/5339/840.abstract

[9] V. Mulloni and L. Pavesi, "Porous silicon microcavities as optical chemical sensors," *Appl. Phys. Lett.*, vol. 76, no. 18, pp. 2523–2525, May 2000. [Online]. Available: http://link.aip.org/link/?APL/76/2523/1

[10] H. Ouyang, M. Christophersen, R. Viard, B. Miller, and P. Fauchet, "Macroporous silicon microcavities for macromolecule detection," *Adv. Funct. Mater.*, vol. 15, no. 11, pp. 1851–1859, Nov. 2005. [Online]. Available: http://dx.doi.org/10.1002/adfm.200500218

[11] L. M. Bonanno and L. A. DeLouise, "Whole blood optical biosensor," *Biosens. Bioelectron.*, vol. 23, no. 3, pp. 444–448, Oct. 2007. [Online]. Available: http://www.sciencedirect.com/science/article/pii/S0956566307002795

[12] G. Rong, A. Najmaie, J. Sipe, and S. Weiss, "Porous silicon waveguides for DNA detection," in *Proc. 3rd IEEE Int. Conf. Group IV Photon.*, 2006, pp. 13–15.

[13] F. Michelotti, B. Sciacca, L. Dominici, M. Quaglio, E. Descrovi, F. Giorgis, and F. Geobaldo, "Fast optical vapour sensing by Bloch surface waves on porous silicon membranes," *Phys. Chem. Chem. Phys.*, vol. 12, no. 2, pp. 502–506, 2010. [Online]. Available: http://dx.doi.org/10.1039/B914280K

[14] M. Kompan, J. Salonen, and I. Shabanov, "Anomalous birefringence of light in free-standing samples of porous silicon," *J. Exp. Theor. Phys.*, vol. 90, no. 2, pp. 324–329, Feb. 2000, DOI:10.1134/1.559107. [Online]. Available: http://dx.doi.org/10.1134/1.559107

[15] E. Gross, D. Kovalev, N. Künzner, V. Y. Timoshenko, J. Diener, and F. Koch, "Highly sensitive recognition element based on birefringent porous silicon layers," *J. Appl. Phys.*, vol. 90, no. 7, pp. 3529–3532, Oct. 2001. [Online]. Available: http://link.aip.org/link/?JAP/90/3529/1

[16] R. Liu, T. A. Schmedake, Y. Y. Li, M. J. Sailor, and Y. Fainman, "Novel porous silicon vapor sensor based on polarization interferometry," *Sens. Actuators B, Chem.*, vol. 87, no. 1, pp. 58–62, Nov. 2002. [Online]. Available: http://www.sciencedirect.com/science/article/B6THH-46RVCRW-3/2/f3d84c4895e7cee786c4b3a91cf3bc3d

[17] O B.-H., R. Liu, Y. Y. Li, M. Sailor, and Y. Fainman, "Vapor sensor realized in an ultracompact polarization interferometer built of a freestanding porous-silicon form birefringent film," *IEEE Photon. Technol. Lett.*, vol. 15, no. 6, pp. 834–836, Jun. 2003.

[18] J. Álvarez, P. Bettotti, I. Suárez, N. Kumar, D. Hill, V. Chirvony, L. Pavesi, and J. Martínez-Pastor, "Birefringent porous silicon membranes for optical sensing," *Opt. Exp.*, vol. 19, no. 27, pp. 26 106–26 116, Dec. 2011. [Online]. Available: http://www.opticsexpress.org/abstract.cfm?URI=oe-19-27-26106
[19] Z. Gaburro, P. Bettotti, M. Saiani, L. Pavesi, L. Pancheri, C. J. Oton, and N. Capuj, "Role of microstructure in porous silicon gas sensors forNO_2," *Appl. Phys. Lett.*, vol. 85, no. 4, pp. 555–557, Jul. 2004. [Online]. Available: http://link.aip.org/link/?APL/85/555/1
[20] C. J. Oton, M. Ghulinyan, Z. Gaburro, P. Bettotti, L. Pavesi, L. Pancheri, S. Gialanella, and N. E. Capuj, "Scattering rings as a tool for birefringence measurements in porous silicon," *J. Appl. Phys.*, vol. 94, no. 10, pp. 6334–6340, Nov. 2003. [Online]. Available: http://link.aip.org/link/?JAP/94/6334/1
[21] J. E. Spanier and I. P. Herman, "Use of hybrid phenomenological and statistical effective-medium theories of dielectric functions to model the infrared reflectance of porous sic films," *Phys. Rev. B*, vol. 61, no. 15, pp. 10 437–10 450, Apr. 2000. [Online]. Available: http://link.aps.org/doi/10.1103/PhysRevB.61.10437
[22] A. Lutich, M. Danailov, S. Volchek, V. Yakovtseva, V. Sokol, and S. Gaponenko, "Birefringence of nanoporous alumina: Dependence on structure parameters," *Appl. Phys. B, Lasers Opt.*, vol. 84, pp. 327–331, 2006. [Online]. Available: http://dx.doi.org/10.1007/s00340-006-2262-6
[23] J. Alvarez, P. Bettotti, N. Kumar, I. Suarez, D. Hill, and J. Martinez-Pastor, "Highly-sensitive anisotropic porous silicon based optical sensors," in *Proc. SPIE—Frontiers Biol. Detect., Nanosens. Syst. IV*, 2012, vol. 8212, no. 1, p. 821 209. [Online]. Available: http://link.aip.org/link/?PSI/8212/821209/1
[24] S. Rönnebeck, S. Ottow, J. Carstensen, and H. Föll, "Crystal orientation dependence of macropore formation in n-Si with backside-illumination in HF-electrolyte," *J. Porous Mater.*, vol. 7, no. 1–3, pp. 353–356, Jan. 2000, DOI:10.1023/A:1009639105357. [Online]. Available: http://dx.doi.org/10.1023/A:1009639105357
[25] C. F. Wong, "Birefringence measurement using a photoelastic modulator," *Appl. Opt.*, vol. 18, no. 23, pp. 3996–3999, Dec. 1979. [Online]. Available: http://ao.osa.org/abstract.cfm?URI=ao-18-23-3996
[26] D. J. Diner, A. Davis, B. Hancock, G. Gutt, R. A. Chipman, and B. Cairns, "Dual-photoelastic-modulator-based polarimetric imaging concept for aerosol remote sensing," *Appl. Opt.*, vol. 46, no. 35, pp. 8428–8445, Dec. 2007. [Online]. Available: http://ao.osa.org/abstract.cfm?URI=ao-46-35-8428
[27] M. Maisonneuve, O. d'Allivy Kelly, A.-P. Blanchard-Dionne, S. Patskovsky, and M. Meunier, "Phase sensitive sensor on plasmonic nanograting structures," *Opt. Exp.*, vol. 19, no. 27, pp. 26 318–26 324, Dec. 2011. [Online]. Available: http://www.opticsexpress.org/abstract.cfm?URI=oe-19-27-26318
[28] F. Benabid, M. Notcutt, L. Ju, and D. Blair, "Birefringence measurements of sapphire test masses for laser interferometer gravitational wave detector," *Phys. Lett. A*, vol. 237, no. 6, pp. 337–342, Jan. 1998. [Online]. Available: http://www.sciencedirect.com/science/article/pii/S0375960197008189
[29] K. H. Jun and K. S. Lim, "Simulation of the depolarization effect in porous silicon," *Appl. Opt.*, vol. 42, no. 7, pp. 1211–1215, Mar. 2003. [Online]. Available: http://ao.osa.org/abstract.cfm?URI=ao-42-7-1211

4.

Real-time polarimetric optical sensor using macroporous alumina membranes

J. Álvarez, C. Serrano, D. Hill, and J. Martínez-Pastor, Opt. Lett. Vol. 38(7), pp. 1058-1060 (2013)

Real-time polarimetric optical sensor using macroporous alumina membranes

Jesús Álvarez,* Carlos Serrano, Daniel Hill, and Juan Martínez-Pastor

Unit of Optoelectronic Materials and Devices, Materials Science Institute, University of Valencia, Catedrático José Beltran, 2, Paterna (Valencia) 46980, Spain

**Corresponding author: jesus.alvarez@uv.es*

Received February 11, 2013; revised February 25, 2013; accepted February 25, 2013; posted February 26, 2013 (Doc. ID 185202); published March 20, 2013

We report on the demonstration of real-time refractive index sensing within 60 μm thick free-standing macroporous alumina membranes with pore diameters of 200 nm. The free-standing macroporous alumina membranes allow the analytes to flow through the pores for targeted delivery, resulting in fast sensing responses. The polarimetric measurement platform exploits the optical anisotropy of the membranes in monitoring the refractive index variations of the analytes that fill the pores, providing highly sensitive and real-time measurements. The experimental characterization of the membranes' birefringence at wavelengths of 808, 980, and 1500 nm showed a decrease in birefringence for shorter wavelengths caused by the depolarization process that takes place when polarized light passes through a porous medium. Volumetric sensing experiments performed at the same wavelengths demonstrated detection limits of 8.1×10^{-6}, 5.2×10^{-6}, and 6×10^{-6} refractive index units at wavelengths of 808, 980, and 1500 nm, respectively.

OCIS codes: 130.6010, 120.0280, 260.1440, 260.3060, 260.5430, 280.1415.

Refractive index sensing is a powerful technique widely used for real-time monitoring of chemical and biological processes [1]. This technique forms the basis of label-free photonic biosensors, where the refractive index of the biosensor surface is modified by the presence of a target analyte [2]. For the development of photonic biosensors, nanostructured materials, such as porous silicon (PSi) and porous alumina (AAO) have gained special attention, as they have higher surface areas than planar biosensors for capturing analytes, permitting lower detection limits [3]. To date, several label-free photonic biosensors have been successfully developed on both PSi [4,5] and AAO [6,7]. All these works are based on measuring the optical thickness of the porous layer by the reflectometric interference spectroscopy (RIfS) method. The RIfS method involves measuring the reflectance interference pattern that arises from the light reflected from the air-porous and the porous-substrate interfaces. In order to accurately measure the optical thickness change due to presence of the target analyte, the interference fringes need to be well resolved, which limits the porous layer to just the top layer of the substrate, and the pore diameters need to be less than 100 nm in order to avoid light scattering [8]. With that structure, the delivery of analytes into the pores is mainly governed by the stationary flux produced by electrostatic interactions resulting in long sensing response times.

In this Letter, we present an approach that overcomes those limitations, obtaining fast and highly sensitive results, through a combination of polarimetry and a 60 μm thick free-standing macroporous AAO membrane with pore diameters of 200 nm. The macroporous free-standing membranes allow the analytes to flow through the pores for targeted delivery of the analyte to the sensor surface, breaking the mass transport limitations and so delivering faster response times [9,10]. The birefringence of the macroporous AAO membrane produced by its pores being perpendicular to its planar surface can be used for sensing applications, as its value is highly dependent on the refractive index of the material within the pores [11].

Building on our previous demonstration of highly sensitive optical sensing with a mesoporous PSi membrane [12], we extended the polarimetric approach to macroporous AAO membranes within a flow cell for real-time sensing. To do so, the birefringence of the macroporous AAO membranes was measured at different wavelengths and compared to those reported in the literature for AAO membranes with pore diameters below 40 nm [13]. Thereafter, real-time volumetric sensing experiments were carried out at the same wavelengths in order to determine the sensitivity of the macroporous AAO membranes and therefore the detection limit of the overall polarimetric system.

The polarimetric measurement platform used for measuring the optical anisotropy of the free-standing macroporous AAO membrane is depicted in Fig. 1.

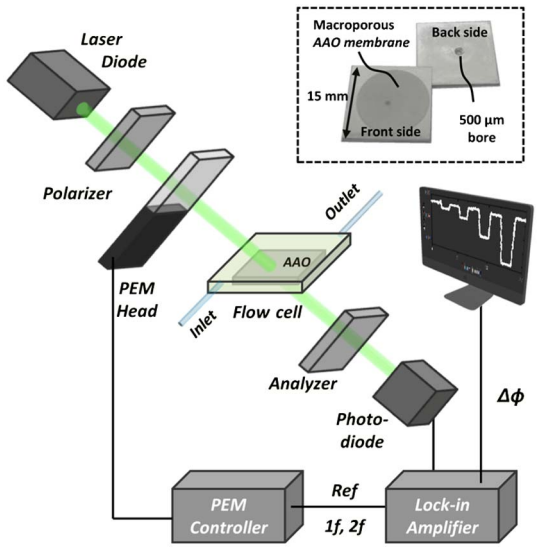

Fig. 1. (Color online) Polarimetric setup used for optical anisotropy characterization of the free-standing macroporous AAO membranes. The inset shows a picture of a macroporous AAO membrane mounted on an aluminum substrate.

The output light from a laser diode is collimated and directed to a first linear polarizer. The linearly polarized light from the polarizer arrives at a photoelastic modulator (PEM; Hinds Instruments PEM-100) that modulates the light polarization. The modulated light is incident at 45° to the alumina membrane, which is mounted on a flow cell. The light exiting the membrane, after passing a second polarizer, is detected by a photodiode that is connected to a lock-in amplifier. The lock-in amplifier (SR-830) demodulates the detected signal, extracting the amplitudes of its first and second harmonics, which are related to the phase retardation $\Delta\phi$ between the ordinary and extraordinary components of the polarized light by [12]

$$\Delta\phi = \arctan\left(\frac{V_{1f}}{V_{2f}} \cdot \frac{J_2(A_0)}{J_1(A_0)}\right), \quad (1)$$

where V_{1f} and V_{2f} are the amplitudes of the first and second harmonics of the modulated signal, $J_1(A_0)$ and $J_2(A_0)$ are the Bessel functions of first- and second-order, respectively, and A_0 is the amplitude of the modulating signal (in radians).

The polarimetric measurement platform offers several advantages over other photonic platforms relying on the vertical interrogation mechanism that avoids a complex coupling system constituting a robust sensing platform, minimizing the alignment requirements for light coupling.

The free-standing AAO membranes used for this work were acquired from Whatman (Anodisc membranes) and had thicknesses of 60 μm, pore diameters of 200 nm, and a porosity of 0.5. The free-standing membranes were mounted on 250 μm thick aluminum supports using a 1 μm thick layer of Poly(methyl methacrylate) resist as the adhesion layer. A hole of 500 μm diameter was drilled in each aluminum substrate before mounting the membrane in order for the laser light and analytes to access the AAO. The mounted membranes were then placed in a glass flow cell whose inlet port was connected to a fluid dispensing system that provides a constant flow rate of 10 μL/min.

Before running the volumetric sensing experiments, the birefringence of the macroporous AAO membranes was measured at the three different wavelengths of 808, 980, and 1500 nm, respectively. The birefringence values were obtained by measuring the phase retardation between the main components of light as a function of the light incidence angle over the AAO membrane, which was mounted on a rotation stage [12]. The measured birefringence values were 0.020, 0.034, and 0.042 at wavelengths of 808, 980, and 1500 nm, respectively. These values are comparable to the birefringence value of 0.062 reported in [13] for nanoporous alumina membranes with pores sizes below 40 nm. The birefringence of the macroporous AAO membranes decreases for shorter wavelengths due to the depolarization process that takes place when a polarized light passes through a scattering medium such as the macroporous membrane [14]. Light scattering is higher at shorter wavelengths, increasing the depolarization of light and so decreasing the birefringence.

After characterizing the wavelength-dependent birefringence of the AAO membranes, a real-time refractive index sensing experiment was carried out in order to determine the bulk refractive index sensitivity of the AAO membrane as well as the detection limit of the whole polarimetric sensing system. To do so during 3 min, we flowed through the AAO membrane different solutions of NaCl in deionized water (DIW) whose mass concentrations ranged from 0.2% to 2%. After each NaCl solution injection, DIW was pumped through the membrane in order to prove that phase retardation had returned to its initial value and so the sensing system was reversible. The phase retardation as a function of time is shown in Fig. 2 for the three wavelengths of 808, 980, and 1500 nm. Immediately after switching, a transitory response of about 1 min is produced by the new solution replacing the old one inside the pores. Furthermore, when the concentration of NaCl in the solution increases, the phase retardation decreases, as it is proportional to the index contrast between the alumina and the material filling the pores.

The refractive index change of the different NaCl solutions at room temperature is $\Delta n_{\mathrm{NaCl:DIW}} = 0.001747\mathrm{RIU}/\%$. This relation was obtained from measurements of different solutions of NaCl in DIW using dual polarization interferometry [15]. Although this relation was obtained at a wavelength of 632 nm, the formula is valid for the three wavelengths studied in this work because the dispersion coefficients of DIW and NaCl solutions are likely to be similar. The phase retardation changes for the different solutions of NaCl at the three different wavelengths are plotted in Fig. 3 as a function of the refractive index of the NaCl solutions used.

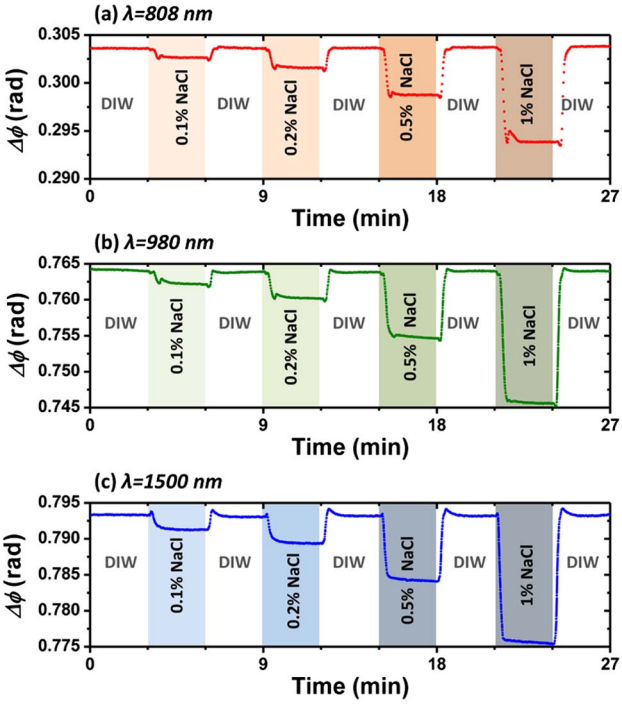

Fig. 2. (Color online) Sensorgram showing the signal response due to flowing through the macroporous AAO membrane different solutions of NaCl in DIW when using laser diodes with wavelengths of (a) 808 nm, (b) 980 nm, and (c) 1500 nm.

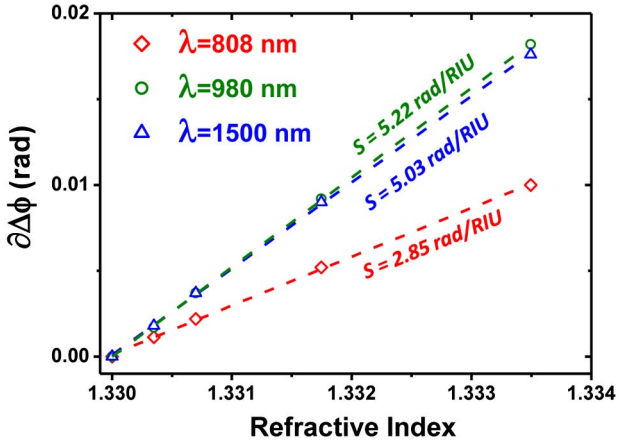

Fig. 3. (Color online) Phase retardation change as a function of the refractive index of the NaCl solutions flowing through the macroporous AAO membrane.

The bulk refractive index sensitivity S of the macroporous AAO membrane was obtained from the slope of the curves $\partial\Delta\phi$ versus refractive index. Linear fits to the curves provide values of 2.85, 5.22, and 5.03 rad/RIU at wavelengths of 808, 980, and 1500 nm, respectively, with correlation coefficients $R^2 = 0.999$. The highest sensitivity arises at 980 nm from a compromise between the light wavelength and the membrane birefringence, which itself is wavelength dependent. This can be seen from the relation between the phase retardation, the wavelength, and the birefringence given by

$$\Delta\phi = \frac{2\pi}{\lambda} d \cdot \Delta n, \tag{2}$$

where λ is the light wavelength, d is the membrane thickness, and Δn is its birefringence. Higher phase retardation and therefore more sensitivity will be obtained for shorter wavelengths and higher birefringence.

The detection limit of the whole sensing system relates the sensitivity of the membrane S with the resolution of the measurement system σ by

$$\mathrm{DL[RIU]} = \sigma[\mathrm{rad}]/S[\mathrm{rad/RIU}]. \tag{3}$$

The resolution of the measurement system is considered to be equal to the standard deviation of the measured phase retardation, i.e., 2.3×10^{-5}, 2.7×10^{-5}, and 3×10^{-5} rad at wavelengths of 808, 980, and 1500 nm, respectively. The detection limits were calculated as 8.1×10^{-6}, 5.2×10^{-6}, and 6×10^{-6} refractive index units at wavelengths of 808, 980, and 1500 nm. The lowest detection limit occurs at 980 nm, which enables a future low-cost multiplexed device using silicon CCD detectors whose price is considerably cheaper than the CCD detectors used in the 1500 nm range.

We have demonstrated refractive index sensing by using free-standing macroporous AAO membranes with flow-through properties. From measuring the birefringence of the macroporous membranes at different wavelengths, we found that the birefringence decreases for shorter wavelengths due to the depolarization process that takes place in porous materials. Besides, the refractive index sensing experiments showed that the lowest detection limit was 5.2×10^{-6} refractive index units obtained at 980 nm, which enables the development of a future low-cost multiplexed device using a silicon CCD detector.

This work was carried out within the FP7-ICT-257401-POSITIVE project, funded by the European Commission. Authors acknowledge $\Delta n_{\mathrm{NaCl:DIW}}$ data provided by POSITIVE consortium partners Marcus Swann and Paul Coffey (Farfield Group) from measurements using dual polarization interferometry.

References

1. D. Hill, BioNanoScience **1**, 162 (2011).
2. M. Estevez, M. Alvarez, and L. Lechuga, Laser Photon. Rev. **6**, 463 (2012).
3. T. Lazzara, I. Mey, C. Steinem, and A. Janshoff, Anal. Chem. **83**, 5624 (2011).
4. M. M. Orosco, C. Pacholski, and M. J. Sailor, Nat. Nanotechnol. **4**, 255 (2009).
5. C. K. Tsang, T. L. Kelly, M. J. Sailor, and Y. Y. Li, ACS Nano **6**, 10546 (2012).
6. S. D. Alvarez, C. Li, C. Chiang, I. K. Schuller, and M. J. Sailor, ACS Nano **3**, 3301 (2009).
7. T. Kumeria, M. D. Kurkuri, K. R. Diener, L. Parkinson, and D. Losic, Biosens. Bioelectron. **35**, 167 (2012).
8. T. Kumeria and D. Losic, Nanoscale Res. Lett. **7**, 88 (2012).
9. A. Yanik, M. Huang, A. Artar, T. Chang, and H. Altug, Appl. Phys. Lett. **96**, 021101 (2010).
10. Y. Guo, H. Li, K. Reddy, H. S. Shelar, V. R. Nittoor, and X. Fan, Appl. Phys. Lett. **98**, 041104 (2011).
11. J. Álvarez, P. Bettotti, N. Kumar, I. Suarez, D. Hill, and J. Martínez-Pastor, Proc. SPIE **8212**, 821209 (2012).
12. J. Álvarez, N. Kumar, P. Bettotti, D. Hill, and J. Martinez-Pastor, IEEE Photon. J. **4**, 986 (2012).
13. A. Lutich, M. Danailov, S. Volchek, V. Yakovtseva, V. Sokol, and S. Gaponenko, Appl. Phys. B **84**, 327 (2006).
14. J. Álvarez, P. Bettotti, I. Suárez, N. Kumar, D. Hill, V. Chirvony, L. Pavesi, and J. Martínez-Pastor, Opt. Express **19**, 26106 (2011).
15. H. Cross, A. Reeves, S. Brand, M. Swann, L. L. Peel, N. J. Freeman, and J. R. Lu, J. Phys. D **37**, 74 (2004).

5.

Real-time polarimetric biosensing using macroporous alumina membranes

J. Álvarez, L. Sola, G. Platt, M. Cretich, M. Swann, M. Chiari, D. Hill, J. Martínez-Pastor, Proc. SPIE Vol. 8765, Bio-MEMS and Medical Microdevices, pp. 87650 (2013)

Real-time polarimetric biosensing using macroporous alumina membranes

Jesús Álvarez[*a], Laura Sola[b], Geoff Platt[c], Marina Cretich[b], Marcus Swann[c], Marcella Chiari[b], Daniel Hill[a] and Juan Martínez-Pastor[a]

[a]Unit of Optoelectronic Materials and Devices, Materials Science Institute, University of Valencia, Catedrático José Beltrán 2, 46980 Paterna, Valencia, Spain

[b]Istituto di Chimica del Riconoscimento Molecolare, Consiglio Nazionale delle Ricerche, Via Mario Blanco, 9, 20146 Milano, Italy

[c]Farfield Group Ltd, Voyager West Wing, Level 7, Chicago Avenue, Manchester Airport, Manchester, M90 3DQ, UK

ABSTRACT

We report the first demonstration of real-time biosensing in free standing macroporous alumina membranes. The membranes with their 200 nm diameter pores are ideal candidates for biosensing applications where fast response times for small sample volumes are needed as they allow analytes to flow through the pores close to the bioreceptors immobilized on the pores walls. A bulk refractive index sensitivity of 5.2×10^{-6} refractive index units was obtained from signal responses to different concentrations of NaCl solutions flowing through the pores. Finally, after functionalizing the alumina pore surfaces with an epoxysilane and then spotting it with β-Lactoglobulin protein, the interactions between the β-lactoglobulin and rabbit anti-β-lactoglobulin, as well as the interaction between the rabbit anti-β-lactoglobulin and a secondary antibody anti-rabbit Immunoglobulin G were monitored in real-time.

Keywords: Porous alumina, Form birefringence, Polarimetry, Optical sensing and sensors, Biological sensing and sensors.

1. INTRODUCTION

Refractive index (RI) sensing is a powerful technique widely used for real-time monitoring of chemical and biological process [1]. This technique forms the basis of many label-free photonic biosensors, where the refractive index of the biosensor surface is modified by the presence of a target analyte [2]. For the development of photonic biosensors nanostructured materials like porous silicon (PSi) or porous alumina (AAO) have gained special attention as they have higher surface areas than planar biosensors for capturing analytes permitting lower detection limits [3]. To date, several label-free photonic biosensors have been successfully developed on both PSi [4, 5] and AAO [6, 7] and are exclusively based on measuring the optical thickness of the porous layer by reflectometric interference spectroscopy (RIfS). The RIfS method involves measuring the reflectance interference pattern that arises from the light reflected from the air-porous and the porous-substrate interfaces. In order to accurately measure the optical thickness change due to presence of the target analyte the interference fringes need to be well resolved, which limits the porous layer to just the top layer of the substrate, and the pore diameters to less than 100 nm in order to avoid light scattering [8]. With that structure, the delivery of the analytes into the pores is therefore mainly governed by the stationary flux produced by electrostatic interactions resulting in slow responses and so long sensing times.

To overcome those limitations we propose an approach that employs free standing macroporous AAO membranes with pore diameters of 200 nm. The membranes allow the analytes to flow-through the pores no more than 100 nm from the sensor surface, breaking the mass transport limitations and so effectively targeting the delivery of the analyte to the sensor surfaces, for fast sensor response [9, 10]. With the pores of the macroporous AAO membranes being perpendicular to their planar surface they can be used for sensing applications as their birefringence is highly dependent on the refractive index of the material within the pores [11, 12].

*jesus.alvarez@uv.es; phone +34 96 35 43268; fax +34 96 35 43633; www.uv.es/umdo/

Bio-MEMS and Medical Microdevices, edited by Angeliki Tserepi, Manuel Delgado-Restituto, Eleni Makarona
Proc. of SPIE Vol. 8765, 87650I · © 2013 SPIE · CCC code: 1605-7422/13/$18 · doi: 10.1117/12.2017432

2. MATERIALS AND METHODS

2.1 Materials

The free-standing macroporous alumina membranes were acquired from Whatman (Anodisc™ membranes, 13 mm diameter, 200 nm pores, 60 μm thickness and 0.5 porosity). BSA (Bovine serum albumin), Tween 20, PBS (Phosphate buffered saline) tablets, toluene, epoxysilane compound (3-glycidoxypropyl)trimethoxysilane were acquired from Aldrich (St. Louis, MO, USA). The primary antibody used, rabbit anti-β-lactoglobulin, was purchased from Bethyl Laboratories (Montgomery, TX, USA) and both the β-lactoglobulin B protein and secondary antibody, anti-rabbit IgG, from Aldrich (St. Louis, MO, USA). Strepavidin coated CdSe quantum dots (Qdot® 800 Streptavidin Conjugate) were supplied by Invitrogen (Life technologies, NY, USA).

2.2 Epoxysilane surface functionalization

A self-assembled epoxysilane monolayer was chemisorbed on the porous alumina pore walls through a reaction of alumina hydroxyl groups with the silane groups so that later receptors biomolecules could be attached.

In doing so, first the hydroxyl groups of the alumina membranes surface were activated by an oxygen plasma and then the alumina membranes were immersed into a 1% solution (in volume) of (3-glycidoxypropyl) trimethoxy silane in dry toluene over night at room temperature. This was followed by a curing step at 80°C under vacuum to ensure a high degree of coverage of the surface. Finally the membranes were rinsed with toluene and ethanol and dried under a stream of nitrogen in order to remove any physisorbed silane groups.

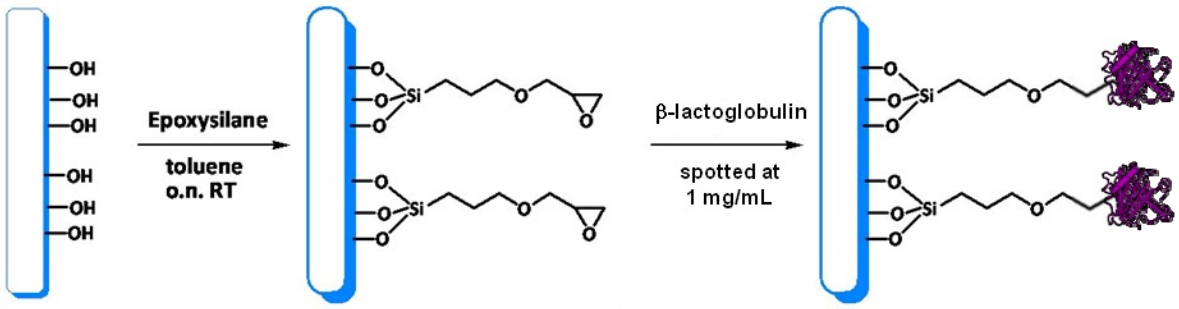

Figure 1. Formation of the epoxysilane monolayer on the alumina surface by (3-glycidoxypropyl)trimethoxysilane and the following immobilization of β-lactoglobulin protein onto the resulting monolayer.

2.3 Membranes transfer to silicon supports

In order to provide mechanical stability to the free-standing alumina membranes they were transferred to silicon substrates after the epoxysilane functionalization. This was done by mounting the alumina membranes onto silicon supports using a 1 μm thick layer of PMMA (Poly(methyl methacrylate)) resist as the adhesion layer. The silicon substrates used were 500 μm thick single side polished square pieces of 15 by 15 millimeters with a CO_2 laser cut 750 μm hole for the laser diode light and the analytes to pass through the membranes.

2.4 Bioreceptor immobilization

Once the free standing membranes had been functionalized and transferred to the silicon supports the β-lactoglobulin protein bioreceptors were immobilized on the silanized surface, via spotting, through the linkage to the active surface epoxy groups. For this purpose a piezoelectric spotter SciFlexArrayer S5 from Scienion was used to spot ten microliters of β-lactoglobulin B protein at 1 mg/mL concentration on the functionalized alumina membrane. Thereafter the spotted membranes were incubated at room temperature in a moisture chamber overnight and rinsed with PBS solution to remove unbound protein. The spotted membranes were then blocked by a BSA solution at 0.1 μg/mL concentration, washed again with PBS and dried under a nitrogen stream.

2.5 Polarimetric readout platform

The polarimetric readout platform for measuring the optical anisotropy of the free standing macroporous AAO membrane is depicted in Fig. 1 (a). Output light from a laser diode is first collimated and then directed to a linear polarizer with the resulting linearly polarized light then enters a photoelastic modulator (PEM; Hinds Instruments PEM-

100). The modulated light exiting the PEM is then incident at 45º to the planar surface of the alumina membrane, which is mounted within a flow-cell. The light exiting the membrane, after passing a second polarizer, is detected by a photodiode which is connected to a lock-in amplifier (SR-830). The lock-in amplifier demodulates the detected signal extracting the amplitudes of its first and second harmonics, which are related to the phase retardation $\Delta\phi$ between the ordinary and extraordinary components of the polarized light traversing the membrane by [13]:

$$\Delta\phi = \arctan\left(\frac{V_{1f}}{V_{2f}} \cdot \frac{J_2(A_0)}{J_1(A_0)}\right) \tag{1}$$

where V_{1f} and V_{2f} are the amplitudes of the first and second harmonics of the modulated signal, $J_1(A_0)$ and $J_2(A_0)$ are the Bessel functions of first and second order respectively, and A_0 is the amplitude of the modulating signal (in radians).

A layout of the flow-cell used for the flow-through sensing is depicted in Fig. 2 (b). The silicon chip mounted alumina membrane is placed between two glass windows with inlet and an outlet ports. The inlet port is connected to a syringe pressure source which operating at 15 psi deliver a constant flow rate of 100 μL/min.

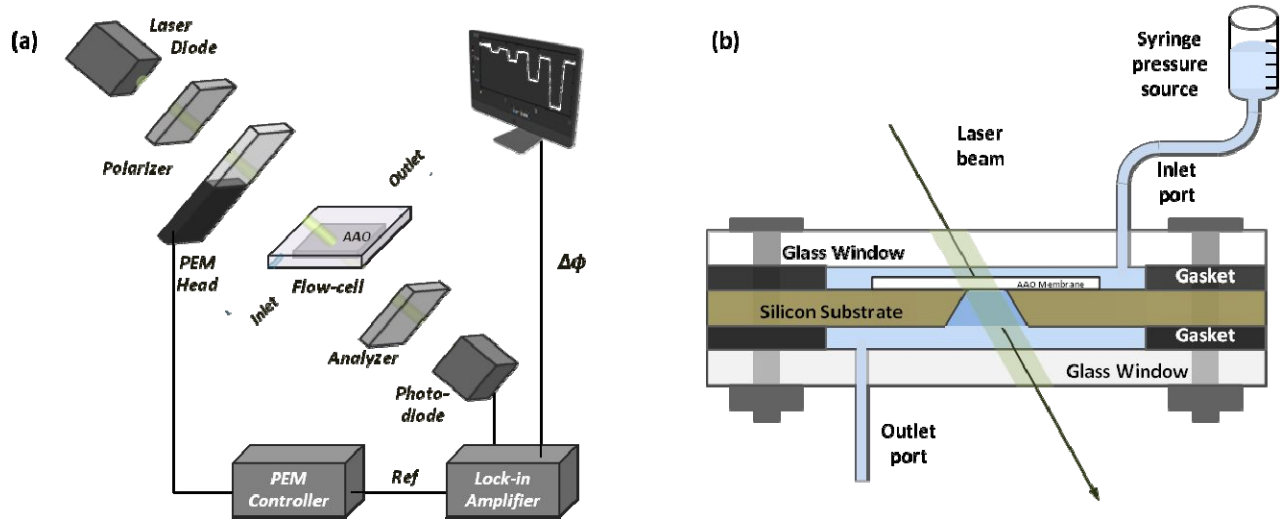

Figure 2. (a) Polarimetric readout platform used for the optical anisotropy measurement of a macroporous free-standing alumina membrane. (b) Detail of the silicon chip mounted free-standing alumina membrane within the flow cell.

3. RESULTS AND DISCUSSION

3.1 Bulk refractive index sensitivity

Real-time sensing experiments were carried out for several epoxysilane coated membranes in order to determine the bulk refractive index sensitivity of the AAO membranes as well as the reproducibility of the sensor device and the measurement platform. To do so different concentrations of NaCl in deionized water (DIW) solutions whose mass concentrations ranged from 0.2% to 2% were flowed during three minutes through the AAO membranes. After each NaCl solution injection DIW was pumped through the membrane in order to prove that phase retardation had returned to its initial value and so the sensing system was reversible [14]. The phase retardation change as a function of time for one such membrane is shown in Fig. 2 (a) where a transitory response of about one minute can be seen immediately after switching, produced by the new solution replacing the old one inside the pores. Fig 2 (b) shows phase retardation changes as a function of the refractive index change for different solutions of NaCl used for ten different membranes. The mean sensitivity is 5.36 rad/RIU (refractive index units) and has a standard deviation of 0.1 rad/RIU and a correlation coefficient up to 0.999.

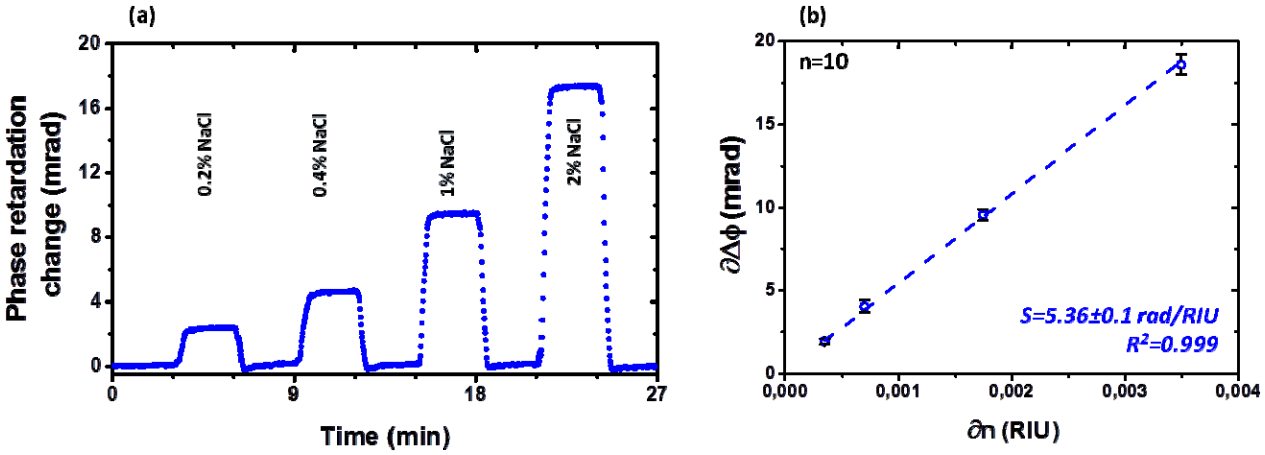

Figure 3 (a) Sensorgram showing the signal response due to flowing several solutions of NaCl in deionized water through a macroporous AAO membrane. (b) Phase retardation change as a function of refractive index change for different NaCl solutions.

From knowing the sensitivity of the alumina membranes, the detection limit of the whole sensing system could then be obtained from the relationship between the sensitivity of the membranes and the resolution of the polarimetric measurement platform:

$$DL[RIU] = \sigma[rad] / S[rad/RIU] \qquad (2)$$

The resolution of the measurement platform was considered to be equal to the standard deviation of the measured phase retardation values, or 2.7×10^{-5} rad, resulting in a detection limit of 5.2×10^{-6} refractive index units.

3.2 Real-time biosensing

After characterizing the reproducibility and the bulk refractive index sensitivity of the coated alumina membranes the immunoassay represented in Fig. 4 (a) was carried out. First a base line for the sensing system was obtained by flowing PBS solution during 10 minutes through a spotted and functionalized membrane. On achieving a stable base line a 1 µg/mL concentration of primary antibody was flown through the membrane to bind specifically to the immobilized β-lactoglobulin protein. A secondary antibody (biotinilated anti-rabbit IgG) and a signal enhancer (strepavidin coated CdSe quantum dots) were used to increase the response produced by the binding between the first antibody and the b-lactoglobulin. Fig. 4 (b) shows the real-time response produced by the binding between the primary and secondary antibodies as well as the signal enhancement produced by the quantum dots.

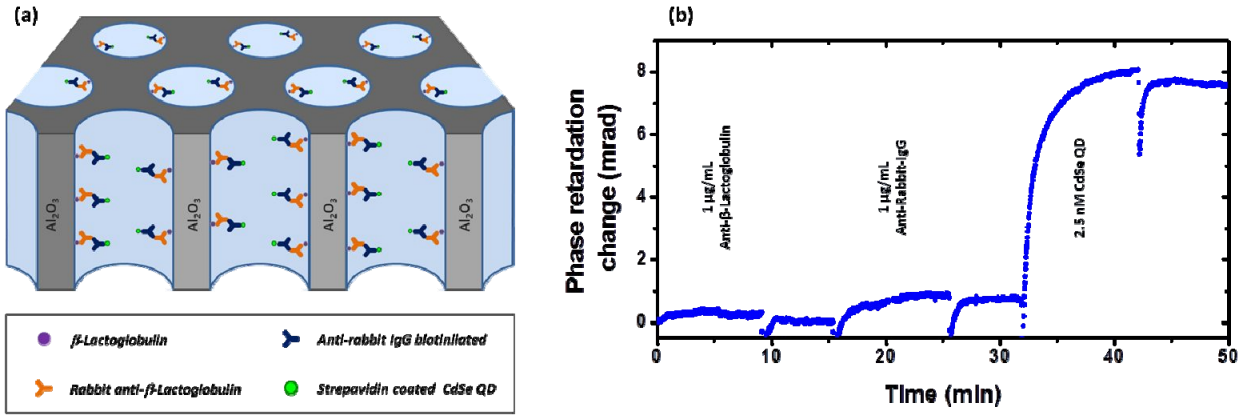

Figure 4 (a) A schematic representation of the immunoassay carried out in a macroporous alumina membrane. β–lactoglobulin protein was used as the immobilized antigen for the detection of rabbit anti-β-lactoglobulin. Secondary antibody biotinilated anti-rabbit-IgG and strepavidin coated CdSe quantum dots were used to increase the signal produced by the primary antibody. (b) A sensorgram showing the signal response due to the binding of the first and secondary antibodies as well as the enhancement produced by the strepavidin coated CdSe quantum dots.

3.3 Control assays

Two control assays were carried out in order to demonstrate that the signal responses shown in Fig. 4 (b) are due to specific antigen-antibody interactions having taken place. The results of a first control assay run on an unspotted membrane shows the absence of a binding response when the β-lactoglobulin protein is not immobilized on the functionalized pores surface (Fig. 5 (a)). A second experiment run on a β-lactoglobulin spotted membrane shows the absence of a binding response when the first antibody (rabbit anti-b-lactoglobulin) is not present, demonstrating that the response enhancement produced by the secondary antibody (anti-rabbit IgG biotinilated) as well as the enhancement produced by the strepavidin coated quantum dots are due to the presence of the first antibody.

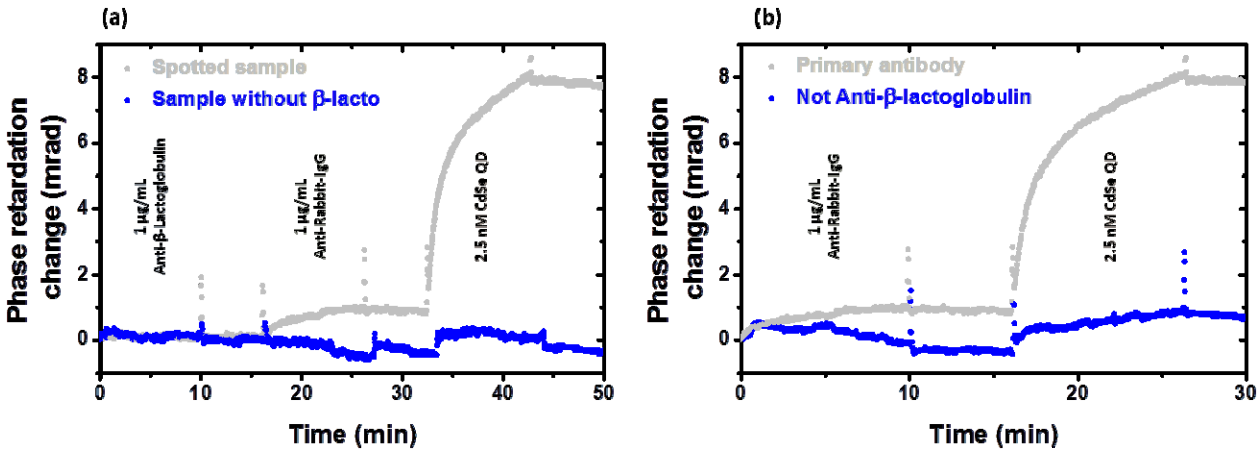

Figure 5. (a) Sensorgram showing a comparison between the responses of a membrane with β-lactoglobulin immobilized on its surface (gray line) and a membrane containing no β-lactoglobulin immobilized (blue line). (b) Sensorgram showing a comparison between the responses produced by the secondary antibody and the quantum dots on a membrane with the anti-β-lactoglobulin (gray line) and a membrane without the anti-β-lactoglobulin (blue line).

4. CONCLUSIONS

In summary, we have presented a biosensing device based on a free standing macroporous alumina membrane with flow-through properties that allows analytes to be targeted delivered for fast sensing response time and therefore real-time measurements for small sample volumes as it is. The interrogation mechanism of the system is based on a polarimetric readout setup for the measurement of the optical anisotropy of a macroporous alumina membrane, whose birefringence is highly sensitive to the refractive index of the material that fills its pores. A bulk refractive index sensing experiment using several solutions of NaCl in deionized water showed a volumetric detection limit below 5.2×10^{-6} refractive index units. Biosensing experiments carried out using β-lactoglobulin as an immobilized antigen provided a specific binding response between the rabbit anti-β-lactoglobulin and the antigen as well as a response from the recognition between the secondary antibody anti-rabbit IgG and the primary antibody rabbit anti-β-lactoglobulin.

ACKNOWLEDGMENTS

Authors acknowledge the contributions from POSITIVE collaborators Tormod Volden and Siegfried Graf (Centre Suisse d' Electronique et de Microtechnique) for the design and fabrication of the flow-cell. This work was carried out within the FP7-ICT-257401-POSITIVE project, funded by the European Commission.

REFERENCES

[1] D. Hill, "Advances in Nanophotonic Sensing Technologies During Three International Label-Free Lab-On-Chip Projects" BioNanoScience-Springer New York, **1**, 162 (2011).

[2] M.C. Estevez, M. Alvarez, L.M. Lechuga "Integrated optical devices for lab-on-a-chip biosensing applications" Laser Photonics Rev, **6**(4), 463 (2012).
[3] T.D. Lazzara, I. Mey, C. Steinem, A. Janshoff, "Benefits and limitations of porous substrates as biosensors for protein adsorption" Analytical chemistry, **83**(14), 5624 (2011).
[4] M.M. Orosco, C. Pacholski, M.J. Sailor "Real-time monitoring of enzyme activity in a mesoporous silicon double layer", Nature Nanotechnology, **4**, 255 (2009).
[5] C.K. Tsang, T.L. Kelly, M.J. Sailor, Y.Y. Li, "Highly Stable Porous Silicon–Carbon Composites as Label-Free Optical Biosensors" ACS Nano, **6**, 10546 (2012).
[6] S.D. Alvarez, C.P. Li, C.E. Chiang, I.K. Schuller, M.J. Sailor, "A Label-Free Porous Alumina Interferometric Immunosensor" ACS Nano, **3**, 3301 (2009).
[7] T. Kumeria, M.D. Kurkuri, K.R. Diener, L. Parkinson, D. Losic, "Label-free reflectometric interference microchip biosensor based on nanoporous alumina for detection of circulating tumour cells" Biosensors and Bioelectronics, **35**(1), 167 (2012).
[8] T. Kumeria, D. Losic, "Controlling interferometric properties of nanoporous anodic aluminium oxide" Nanoscale Research Letters, **7**(88), 1 (2012).
[9] A.A. Yanik, M. Huang, A. Artar, T.Y. Chang, H. Altug, "Integrated nanoplasmonic-nanofluidic biosensors with targeted delivery of analytes" Applied Physics Letters, **96**(2), 021101 (2010).
[10] Y. Guo, H. Li, K. Reddy, H.S. Shelar, V.R. Nittoor, X. Fan, "Optofluidic Fabry-Perot cavity biosensor with integrated flow-through micro-/nanochannels" Applied Physics Letters, **98**(4), 041104 (2011).
[11] J. Álvarez, P. Bettotti, N. Kumar, I. Suarez, D. Hill, J Martínez-Pastor, "Highly-sensitive anisotropic porous silicon based optical sensors" Proc. SPIE, **8212**(1), 821209, (2012).
[12] J. Álvarez, P. Bettotti, I. Suárez, N. Kumar, D. Hill, V. Chirvony, L. Pavesi, J. Martínez-Pastor, "Birefringent porous silicon membranes for optical sensing" Opt. Express, **19**(27), 26106 (2011).
[13] J. Álvarez, N. Kumar, P. Bettotti, D. Hill, J. Martínez-Pastor, "Phase-Sensitive Detection for Optical Sensing With Porous Silicon" IEEE Photonics Journal, **4**(3), 986 (2012).
[14] J. Álvarez, C. Serrano, D. Hill, and J. Martínez-Pastor, "Real-time polarimetric optical sensor using macroporous alumina membranes," Opt. Lett. **38**(7), 1058 (2013).